Aus dem Max-Planck-Institut für Kolloid- und Grenzflächenforschung

Synthese und Kolloidale Eigenschaften neuartiger Blockcopolymere mit β-Dicarbonyl Einheiten

Synthesis and Colloidal Properties of a Novel Type of Block Copolymers bearing β-Dicarbonyl Residues

Dissertation

Zur Erlangung des akademischen Grades
Doktor der Naturwissenschaften
(Dr. rer. nat.)
in der Wissenschaftsdisziplin Physikalische Chemie

eingereicht an der Mathematisch-Naturwissenschaftlichen Fakultät
der Universität Potsdam

von
Theodora Krasia
aus Nikosia, Zypern

Golm, im April 2003

Die vorliegende Arbeit entstand in der Zeit von October 2000 bis April 2003 am Max-Planck-Institut für Kolloid- und Grenzflächenforschung, Golm.

Gutachter:

- Prof. Dr. M. Antonietti
- Dr. habil. H. Cölfen
- Prof. Dr. U. S. Schubert

Tag der mündlichen Prüfung: 10.06.2003

“Vorstellungskraft ist wichtiger als Wissen”.
“The power of imagination is more important than knowledge”.

Albert Einstein, Wissenschaftler, 1879-1955

To my family in Cyprus and here in Germany...

Table of Contents

CHAPTER 1

Abstract

The present work is dealing with the first synthesis and characterisation of amphiphilic diblock copolymers bearing β-dicarbonyl (acetoacetoxy) chelating residues. Polymers were obtained by Group Transfer Polymerisation (GTP)/acetoacetylation and controlled radical polymerisation techniques (RAFT).

Different micellar morphologies of *poly*(*n*-butyl methacrylate)-*block*-*poly*[2-(acetoacetoxy)ethyl methacrylate] (pBuMA-*b*-pAEMA) were observed in cyclohexane as a selective solvent. Depending on the block length ratio, either spherical, elliptical, or cylindrical micelles were formed. The density of the polymer chains at the core/corona interface is considerably higher as compared to any other strongly segregating system reported in the literature. It is demonstrated that there are H-bond interactions existing between acetoacetoxy groups, which increase the incompatibility between block segments. In addition, such interactions lead to the formation of secondary structures (such as β-sheets or globular structures) and larger superstructures in the micrometer length scale.

Block copolymers were also used to solubilise metal ion salts of different geometries and oxidation states in organic media, in which are otherwise insoluble. Sterically stabilised colloidal hybrid materials are formed, i.e. monodisperse micelles having the metal ion salt incorporated in their core upon complexation with the ligating pAEMA block, whereas pBuMA forms the solvating corona responsible for stabilisation in solution. Systematic studies show that the aggregation behaviour is dependent on different factors, such as the tautomeric form of the β-dicarbonyl ligand (keto/enol) as well as the nature and amount of added metal ion salt.

CHAPTER 2

Introduction

2.1 Block copolymers

Block copolymers are macromolecules consisting of at least two blocks of constitutionally and/or configurationally different monomeric units, for example A_m-B_n, A_m-B_n-A_m etc. The different blocks are connected together *via* covalent bonds[1]. Unlike other copolymers, they retain many of the physical characteristics of the "homopolymer" sections. According to the number of different blocks incorporated in a block copolymer, these materials are classified in di-, tri-, or multi- block copolymers.

Usually, the different blocks are thermodynamically immiscible due to their different polarity. A special class of block copolymers in which hydrophobic and hydrophilic segments are incorporated, similar to low molecular weight surfactant molecules is the so called "Amphiphilic Block Copolymers". The word derives from the greek *αμφι* [amphi = both] and *φιλος* [Philos = friend]. This amphiphilic character causes a *microphase separation*, a phenomenon in which similar blocks of different block copolymer molecules aggregate and form different morphologies (see 2.2). The latter are mainly governed by the relative spatial requirements of the blocks[1]. Two examples are presented in Figure 2.1. Lamellae structures, where a layer of one block faces another layer of the same type[1] and spherical domains of one block in a matrix of another can be formed. Such separation occurs not only at a water/oil interface but also at interfaces such as polymer/polymer (blends) metal/polymer and others[2].

Figure 2.1: *Arrangement of A blocks (•) and B blocks (•) in diblock and triblock copolymers: (a) Formation of spherical domains of A-blocks in a continuous matrix of B blocks in an ABA triblock copolymer and (b) Lamellar structure of AB diblock copolymers with equal block volumes*[1].

Depending on the nature of the monomers, the number and lengths of the block segments, as well as the chain architecture (linear, branched, graft, stars etc.), block copolymers can exhibit a wide range of interesting properties. Additionally, their ability to solubilise in different solvents and the presence of functional groups, make them versatile in many industrial applications.

Block copolymers can be synthesised either *via* coupling reactions occurring between different homopolymer segments with functional end-groups[3], or sequential polymerisation of different monomers[4]. To the latter and most commonly used, belong different living, controlled polymerisation techniques such as anionic[5], cationic[6,7,8,9], radical[10,11] and coordination polymerisation[12,13].

2.2 Phase separation behaviour of block copolymers

Mixing two polymers most commonly results in total phase separation on a macroscopic level. This phenomenon can be qualitatively explained in terms of the reduced combined mixing entropy of two different types of polymer chains[14]. In a block copolymer, due to the presence of a covalent bond between the two blocks, microphase separation occurs. The formation of microdomains is attributed to the fact that one block resides in one phase, whereas the second one in the neighbouring phase. The covalent bond between the two blocks plays the role of the interface in this microphase-separated system[15]. The self-assembly behaviour of amphiphilic block copolymers in organic and aqueous media depends on the chemical composition and block lengths, as well as temperature, concentration, and interfacial energy. Hence, a number of different structures and morphologies can be obtained such as micelles of different shapes (spherical, cylindrical, etc., see 2.3), ordered continuous morphologies (lamellae, ordered cylinders) or bicontinuous structures[2]. An overview of the most common structures formed by diblock copolymers is presented in Figure 2.2[2].

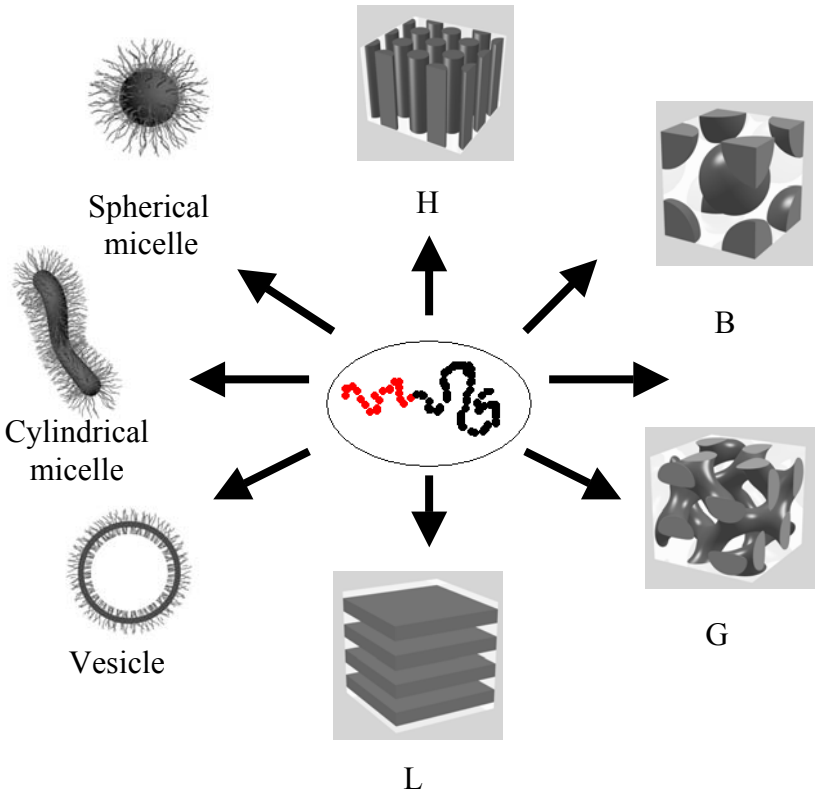

Figure 2.2: *Common morphologies of microphase-separated block copolymers: Body centred cubic packed spheres (B), hexagonally ordered cylinders (H) gyroid (G), lamellar (L), cylindrical micelles, vesicles, spherical micelles etc*[2].

There are three basic parameters which determine the size (usually 10-100 nm) and shape of the microdomains formed by an AB diblock copolymer[2]:

(i) The degree of polymerisation (N) which is equal to the sum of *DPs* of the two blocks,

(ii) The composition of each block, i.e. $f_A = N_A/N$ and $f_B = N_B/N$ and

(iii) The Flory - Huggins interaction parameter $\chi_{AB,}$ which characterises polymer/polymer interactions. (in bulk).

The Flory – Huggins parameter depends on temperature. This dependence is approximately given by:

$$\chi \approx A + B/T \qquad (2.1)$$

A and B are constants which differ from system to system[1].

In bulk, the tendency for microphase separation depends on the term χN, in which enthalpic and entropic contributions are included[16]. Small values of this parameter (≈ 10), describe a non-ordered system in which the polymer blocks are highly miscible with each other, i.e the interface between them is large. This is known as the *Weak Segregation Limit (WSL)*[17]. The second regime of phase behaviour is referred to as the *Strong Segregation Limit (SSL)* when $\chi N>10$. In this case, mixing of the different blocks is energetically unfavourable, leading to the development of small interfaces between the different blocks, thus phase separation. It is in this region where well known morphologies such as lamellae, body centred cubic packed spheres (BCC) and hexagonally ordered cylinders (HEX) are stable[2]. Furthermore, Khoklov *et al.*[18] have named a new *regime Super Strong Segregation Limit (SSSL)* in the cases where $\chi N>>10$.

The various bulk block copolymer morphologies can be presented on a phase diagram of χN versus the composition of a specific block, *f*. An example of such a diagram derived from theoretical calculations by Matsen and Bates[19, 20] is presented in Figure 2.3.

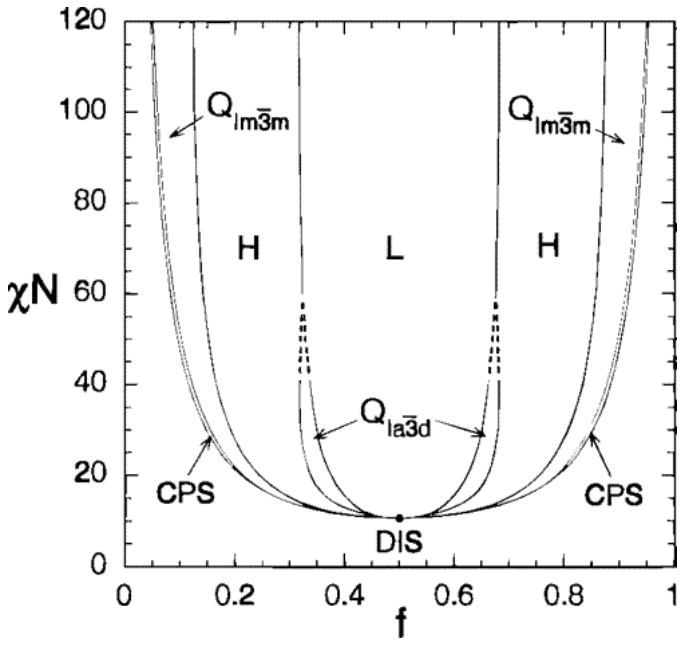

Figure 2.3: *Calculated phase diagram for block copolymers: L: Lamellae; H: Hexagonally ordered cylinders; Q_{Im3m}: Body centred cubic packed spheres; Q_{Ia3d}: Gyroid; CPS: Cubic packed spheres; DIS: Disordered phase*[19,20].

2.3 Micellisation

The phenomenon of micellisation of block copolymers, received much attention in the last decades and up to date, numerous experimental and theoretical investigations have been reported on this subject[21,22]. Several reviews on micellisation phenomena of non-ionic block copolymers in non-aqueous[23] and aqueous[24,25] media as well as on ionic block copolymer micelles[26,27] have been published. In selective solvents, amphiphilic block copolymers form aggregates consisting of rather dense cores of the insoluble blocks, surrounded by diffuse outer shells (coronas) of the soluble ones[28] (Figure 2.4).

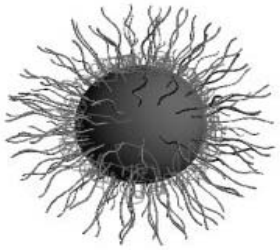

Figure 2.4: *Schematic representation of a spherical block copolymer micelle showing a dense core and a diffuse corona.*

Even though polymeric and low molecular weight amphiphilic systems resemble each other in many aspects, such as the formation of different micellar structures (spherical, cylindrical, etc.), polymeric amphiphiles can generate microphases which are thermodynamically and kinetically more stable. Due to this high stability, such systems can be used in a wide range of applications such as emulsion polymerisation, colloid stabilisation, drug delivery, or as microreactors[17].

Micelle formation of block copolymer systems is determined by three main parameters: The respective block lengths N_A and N_B and the Flory – Huggins parameter, χ. Unlike in bulk, here χ considers both polymer/polymer and polymer/solvent interactions. Further parameters of interest are the statistical segment length, l_k and the monomer volume, v_o.

Assuming that the micellar core is mostly constructed of A blocks and the corona is rich in B blocks, three types of micellar structures can exist, depending on the relative block lengths of N_A and N_B[17]:

- if $N_A << N_B$, meaning that the corona is much larger than the core, then the size of the corona is approximately equal to the size of the micelle. This type is called "*hairy micelle*" (Figure 2.5(a)).
- In the opposite situation, where $N_A >> N_B$, the core is much larger than the corona and a "*crew cut micelle*" is formed. (Figure 2.5 b).

(a) **(b)**

Figure 2.5: *Schematic representation of (a) a hairy micelle and (b) a crew cut micelle.*

The third class of micelles is called "*amphiphilic micelles*". The main characteristic of this micellar type is the large interaction parameter χ. As already mentioned in 2.2, the term χN can be used to describe the tendency for microphase separation in bulk. In solution, if the interaction parameter χ_{AB} (corresponding to interactions between the two blocks), is approximately equal to the one which describes the polymer/solvent interactions of the one block (χ_{AS}) and these are much larger than that of the polymer/solvent interactions of the second block, (χ_{BS}), then χN can serve as a parameter for characterising the thermodynamic state[17]. In the SSSL regime ($\chi N >> 10$), the core consists basically of A blocks, the corona consisting of B domains is swollen with solvent, whereas in the solvent phase no block copolymers are present[17]. In conclusion, in the term "*Amphiphilic micelles*" both types of micelles, (hairy and crew cut) can be included as long as strong segregation is involved.
The three different micellar types exhibit characteristic scaling relations with the aggregation number Z, (i.e the number of individual block copolymer chains per micelle) and the radius R[17]:

Hairy Micelle	$Z \sim N_A^{4/5}$
$N_A << N_B$	$R \sim N_A^{3/5}$
Crew cut Micelle	$Z \sim N_A^{1}$
$N_A >> N_B$	$R \sim N_A^{2/3}$
Amphiphilic Micelle	$Z \sim N_A^{2}$
large χ	$R \sim N_A^{1}$

Förster and co-workers[17] have prepared a series of non-ionic amphiphilic diblock copolymers of the type *poly*(styrene)-*b*-*poly*(4-vinylpyridine). These form micelles in toluene, a selective solvent for the pS block, the size and shape of which were characterised by light scattering and electron microscopy. They have shown that for these systems, *Z* exhibits a scaling relation with *N*, the polymerisation degree for each block:

$$Z \propto N_{P4VP}^{2} N_{PS}^{-0.8} \tag{2.2}$$

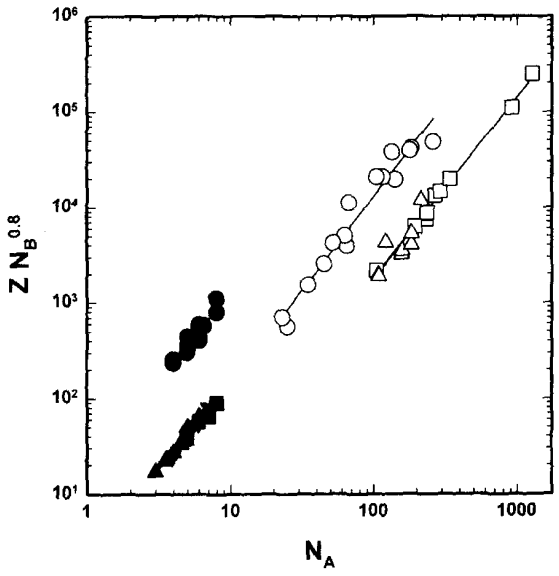

Figure 2.6: *Aggregation numbers Z as a function of N_A and N_B for diblock and triblock copolymer systems[17,29] (empty data points) as well as ionic and non-ionic surfactants (solid data points)[30].*

As shown in the above figure, this behaviour is comparable to that of strongly segregated block copolymer systems as well as low molecular weight ionic and non-ionic surfactants.

2.4 "Living"/Controlled Polymerisation

One of the most important aims of synthetic polymer chemistry is the achievement of control, not only on molecular weights (MW) and molecular weight distributions (MWD) of the polymer chains, but also on their compositions and architectures. "Living" polymerisation appears to be the most suitable and convenient method for this purpose, since it proceeds in the absence of chain transfer or irreversible termination reactions[5]. Most of the chain ends are in a dormant inactive form found in rapid equilibrium with the active species. Usually, initiation and exchange equilibrium reactions between active/inactive species are fast compared to propagation, thus resulting in polymers with controlled molecular weights and narrow molecular weight distributions (Poisson). Molecular weights can be theoretically determined by the molar ratio of monomer to initiator[5].

Anionic and Group Transfer Polymerisation (GTP) are two important examples for "living" polymerisation methods of methacrylates. Another controlled polymerisation technique is the radical Reversible Addition-Fragmentation Chain-Transfer Polymerisation (RAFT). Here, the controlled character is conferred by the presence of dithiocarbonyl compounds, which serve as chain transfer agents (CTA)[31]. These three polymerisation processes were used in the synthesis of homo and block copolymers reported in this work.

2.4.1 Anionic Polymerisation

In 1956, Szwarc[32] first described living anionic polymerisation. In such systems, stable active anionic chain ends are generated *via* the addition of the initiator across the double bond of a monomer. These can be used for synthesising functionalised, block, star and graft copolymers. Additionally, anionic polymerisation ensures control over molecular weights and molecular weight distributions and provides the possibility for controlling stereoselectivity.

The degree of polymerisation, *DP*, is determined from the ratio of monomer concentration, $[M]_o$ to the concentration of active species, *[P*]*, and it is proportional to the percentage of monomer consumption, x. The concentration of active species depends on the initiator efficiency, f_i and the initial concentration of the initiator, $[I]_o$. Therefore, *DP* can be expressed as:

$$\mathrm{DP} = \frac{x[M]_o}{[P^*]_0} = \frac{x[M]_o}{f_i[I]_o} \tag{2.3}$$

$$\mathrm{x} = 1 - \frac{[M]}{[M]_o} \tag{2.4}$$

where $[M]_o$ corresponds to the initial and $[M]$ to the final monomer concentration. For an ideal living polymerisation process, all chains are initiated essentially at the same moment and all of them grow at the same rate until all monomer is consumed[33]. In such case, MWD is very narrow and follows a Poisson-distribution as depicted in Figure 2.7. n_x corresponds to the number of chains with $DP = x$ and N to the total number of chains.

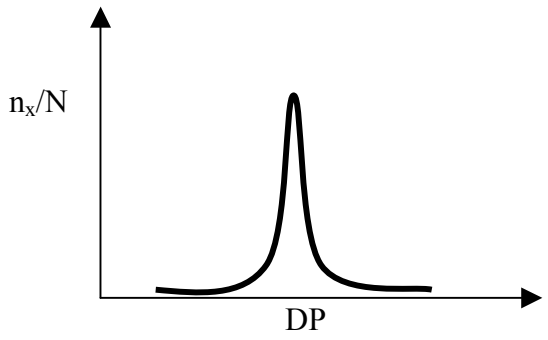

Figure 2.7: *Poisson distribution of simultaneously initiated and propagated polymer chains in an ideal living polymerisation process.*

The polydispersity index, (PDI), is determined from equation 2.5 as:

$$\mathrm{PDI} = \frac{M_w}{M_n} = 1 + \frac{DP}{(DP+1)^2} \approx 1 + \frac{1}{DP}, \text{ for DP >>1} \tag{2.5}$$

In order for living anionic polymerisation to proceed without termination, inert atmosphere or vacuum techniques are required to exclude moisture, oxygen and carbon dioxide[5]. Furthermore, factors such as the proper choice of initiator, solvent, temperature, counterion and additives can affect the way in which anionic polymerisation of a particular monomer proceeds[5]. Alkali-metal suspensions, alkyl or aryllithium reagents, organic radical ions or Grignard reagents are usually used as initiators. Typical monomers that can be polymerised

anionically are styrene, (meth)acrylates, 1,3-dienes, vinylpyridine, oxiranes, lactones and cyclic siloxanes.

2.4.2 Group Transfer Polymerisation (GTP)

In 1983, Webster and co-workers introduced a silicon-mediated polymerisation of acrylic esters[34], which was named Group Transfer Polymerisation (GTP). This new polymerisation process displayed features characteristic of a "living" polymerisation at room temperature[35]. The monomers used in this polymerisation method are vinyl monomers containing carbonyl or cyano groups in the side chain. Methacrylates are considered to be the most appropriate monomer type for GTP. As catalysts, difluoro ions, F_2^-, or oxyanions, COO^-, are used. In the present work tetrabutylammonium bibenzoate (TBABB) served as the catalyst, and a silyl ketene acetal, 1-methoxy-1-trimethylsiloxy-2-methylprop-1-ene (MTS) was used as the initiator. GTP involves a sequential Mukiyama-Michael addition of silyl ketene acetal with alkyl (meth)acrylate in the presence of a small amount of a nucleophilic or Lewis acid catalyst[36]. The name "Group Transfer Polymerisation" was suggested because early studies on the reaction mechanism indicated that the trimethylsilyl group coordinated with a pentacoordinated siliconate anionic catalyst, was transferred from the initiator or propagating chain-end to the carbonyl oxygen of the incoming monomer (Figure 2.8)[37].

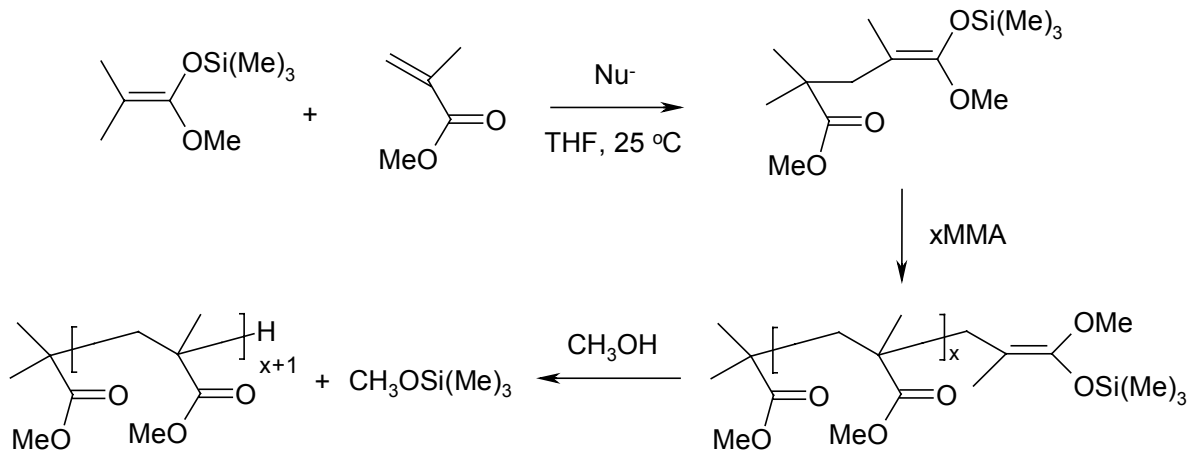

Figure 2.8: *Nucleophile assisted GTP of MMA*[38].

The way in which a nucleophilic and a Lewis acid catalyst participate in the polymerisation process is different. Many proposals concerning GTP polymerisation mechanism, depending on the type of catalyst used were reported. As already mentioned, Webster and Sogah

proposed that during propagation, an intramolecular transfer of pentacoordinated siliconate from a chain-end to the carbonyl group of an incoming monomer takes place *via* an eight membered-transition state (associative-intramolecular GTP mechanism). However, Mai and Müller[39,40] proposed a modified associative mechanism based on kinetic studies. This involved two steps: At first, the monomer adds to the α–carbon of the pentacoordinated siliconate chain-end. Subsequently, the silyl group migrates to the carbonyl oxygen of the monomer.

A dissociative GTP mechanism in which pentacoordinated siliconate dissociates to the ester enolate anion was also proposed[41]. The latter reacts with monomer and forms reversibly a silyl ketene acetal end-group. It is believed that the propagating ester enolate anions undergo a faster silicon exchange between propagating chain ends. In this case, control over molecular weights is ensured by the ratio of monomer to initiator rather than monomer to catalyst[38]. The proposed associative and dissociative GTP mechanisms are presented in Figure 2.9.

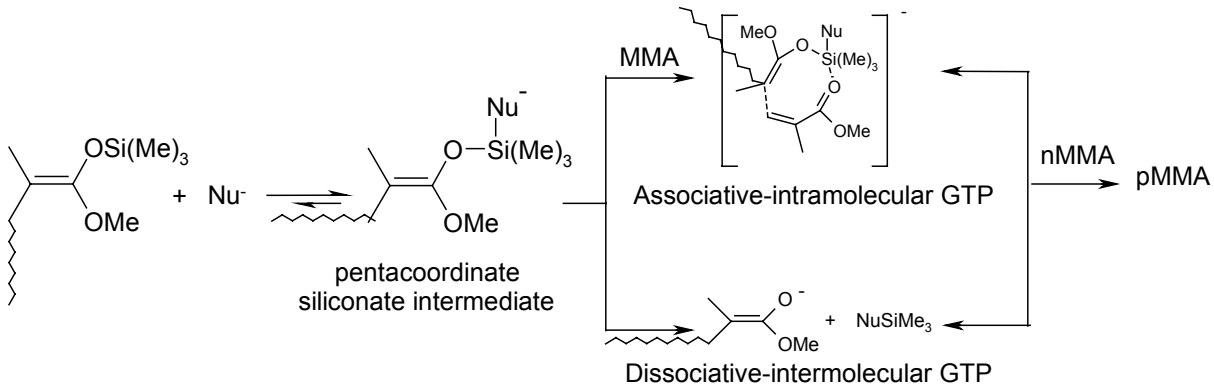

Figure 2.9: *Associative and dissociative transfer mechanisms of MMA in GTP[38].*

Group Transfer Polymerisation has many advantages. Firstly, it proceeds rapidly and provides quantitative polymer yields. As mentioned before, it provides good control over the molecular weights and molecular weight distributions. Furthermore, in contrast to other polymerisation methods, which take place at very low temperatures, GTP occurs at ambient temperature. This point is quite important, since no special experimental techniques for temperature control during polymerisation are required[42]. The polymerisation degree, as in anionic polymerisation, is determined from the molar ratio of monomer to initiator. In addition to the synthesis of homopolymers, it can be also used to produce block, stars and network copolymer architectures. However, GTP has some disadvantages. With this method,

molecular weights over 50,000 g/mol cannot be obtained. This explains the broad molecular weight distributions observed for high molecular weight polymers and also the lack of quantitative polymerisation yields. A second disadvantage is that a wide range of monomers is excluded from the list of those capable of being polymerised by GTP.

2.4.3 Reversible Addition-Fragmentation Chain-Transfer Polymerisation (RAFT)

RAFT represents a new versatile polymerisation technique, which allows for the preparation of well-defined polymers with functionalised end-groups[11,43, 44]. The process shows many of the characteristics of controlled polymerisations such as:

- narrow molecular weight distributions (usually <1.2; sometimes <1.1)[11]
- linear molecular weight conversion profile
- preparation of block copolymers and other complex architectures such as stars, branched or block copolymer networks by the addition of a second monomer[45, 46, 47, 48]
- control over the molecular weight. The DP can be easily derived using equation 2.6:

$$x*[M]_o/[CTA]_o \qquad (2.6)$$

where x is the monomer conversion, $[M]_o$ the initial monomer concentration and $[CTA]_o$ the initial concentration of the chain transfer agent.

- compatibility with a wide range of monomers (including functional monomers containing for example acid, acid salt, hydroxy or tertiary amino groups) and reaction conditions (no particular limitations on solvent or reaction temperature)[11].
- polymerisations can be performed in bulk, solution, emulsion or suspension.

The controlled character of this free radical polymerisation method is attributed to the presence of dithiocarbonyl compounds (Figure 2.10), which mediate the polymerisation *via* a reversible chain transfer process[49]. Usually, azo or peroxy initiators are employed.

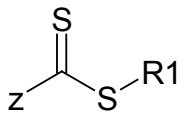

Figure 2.10: *General chemical structure of dithiocarbonyl compounds used as CTA in RAFT.*

For the achievement of high chain transfer constants, group *Z* should be able to activate the C=S double bond. Aryl and alkyl groups are suitable for this purpose, whereas dialkylamino and alkoxy groups according to Rizzardo and co-workers are less adequate[31]. Additionally, R_1 should be a good free radical leaving group compared to the propagating radicals, and capable to re-initiate free radical polymerisation. Groups like CH_2-Ar, CH_2-C=C, CH_2-C=O, CH_2-CCN and others, in conjugation to the radical, are appropriate to stabilise for mesomeric reasons, whereas stabilisation due to inductive effects can be achieved by the use of alkyl groups[50]. In Figure 2.11 the proposed mechanism for RAFT polymerisation is presented[11].

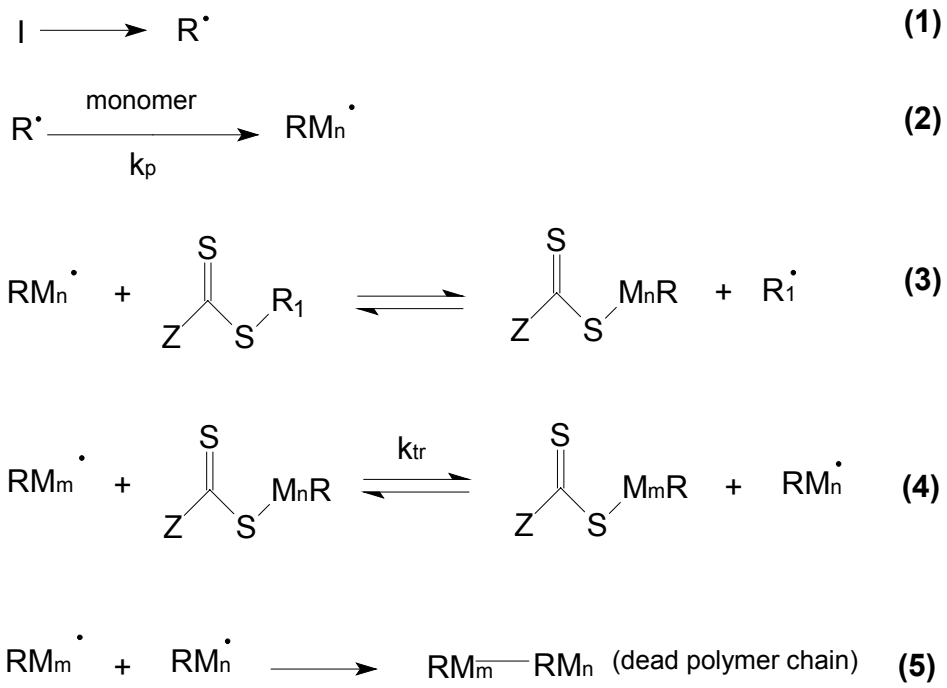

Figure 2.11: *Proposed mechanism for the Reversible Addition-Fragmentation chain Transfer polymerisation.*

As shown above, polymerisation process initiates by the radicals formed due to decomposition of the initiator I (**step 1**). Subsequently, the propagating radicals (**step 2**) react with CTA molecules resulting to the formation of dormant chains (transferred chains) and radical leaving groups $R_1^{\bullet}$ (**step 3**). The latter are capable of initiating another chain. Hence, the amount of radicals remains constant during the whole process.

2.5 Functionalised polymers with metal complexing segments

Over the past three decades many examples appeared in the literature, where macromolecular science seems to be strongly oriented towards the field of organic-inorganic hybrid materials[2,51,52]. A combination of potential applications of metal compounds with the special properties of polymers can lead to the formation of nanometer-scale structured materials with for example good mechanical performance and electrosteric stabilisation of colloids[53].

Coordination polymers with O-, S-, and N-containing ligands and their ability to form polymer-metal complexes with different metal ions have been extensively investigated. Antonietti and co-workers[54] have synthesised novel amphiphilic block copolymers with nitrogen, sulfur and phosphonate moieties, which make them suitable for complexation and solubilisation of different transition-metal ions in organic media. More precisely, they have shown that the functionalised block copolymers form micelles in organic solvents. Those micellar solutions are used for solubilising diverse transition-metal salts such as $Cu(ClO_4)_2$, $Pd(CH_3COO)_2$, $ZnCl_2$, $Rh(CH_3COO)_2$ etc. which are otherwise insoluble. Furthermore, addition of a reducing agent in the solutions of metal salt-containing micelles, leads to the formation of well-defined noble metal colloids.

Chernyshov *et al.*[55] have prepared a new type of a chelating block copolymer with triphenylphosphine groups (Figure 2.12). Those groups are well known for their widespread use in coordination chemistry and catalysis[56].

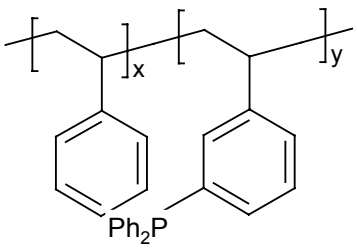

Figure 2.12: *Polystyrene-block-poly-m-vinyltriphenylphosphine (pS-b-pPH).*

Complexation of these polymers with palladium compounds results in the formation of spherical aggregates, presumably uni- and multi-lamellar vesicles and disk-like micelles. Additionally, block copolymer-stabilised Pd nanoparticles were prepared by reduction of the

Pd-containing pS-*b*-pPH block copolymer micellar aggregates using different reducing reagents.

Schubert and co-workers have a number of publications on functionalised polymers with metal-complexing segments such as bi- and terpyridine. One example is the synthesis of linear oligomers and polymers with two terpyridine end-groups[57]. Complexation with transition-metal ions results in the formation of non-covalent coordination polymers (Figure 2.13).

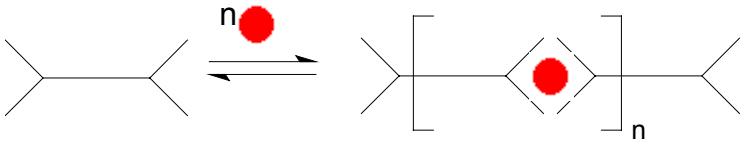

Figure 2.13: *Schematic representation of the proposed non-covalent polymerisation induced by complexation of terpyridine functionalised telechelics with transition metal ions*[57].

In another publication, they reported the introduction of mono- and difunctionalised 6,6´-dimethyl-2,2`-bipyridines into polyesters, aiming to design polymeric biodegradable architectures with specific metal binding units[58]. Furthermore, they have developed a new strategy, giving rise to metallo-supramolecular block copolymers. In such polymers, a metal/ligand complex serves as a supramolecular linker between the hydrophobic and hydrophilic blocks of the amphiphilic block copolymers. For example, a metallo-supramolecular *poly*(styrene)-*block*-*poly*(ethylene oxide) was prepared *via* self-organisation of the α-methoxy-ω-(2,2`:6`,2``-terpyridinyl)oxypoly(ethylene oxide)ruthenium(III) complex and $\omega$-(2,2`:6`,2``-terpyridine)oxypoly(styrene) (*pS-[Ru]pEO*)[59]. This polymer has the ability to form micelles in water with a PS core surrounded by bis(2,2`:6`,2``-terpyridine)ruthenium(II) complexes and a pEO corona. The same principle was applied for the synthesis of metallo-supramolecular graft copolymers[60].

The well-known strong affinity of bidentate β-dicarbonyl moieties to multivalent cations[61] prompted some groups to synthesise polymers with β-dicarbonyl repeating units (Figure 2.14). So far, such polymers have been obtained by free radical polymerisation of methacroylacetone[62], ethyl (meth)acrylolylacetate[63] and 2-(acetoacetoxy)ethyl methacrylate[64] or by the controlled oxidation of poly(vinyl alcohol)[65].

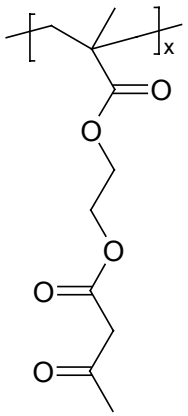

Figure 2.14: *Molecular structure of poly[(2-acetoacetoxy)ethyl methacrylate] (pAEMA), a polymer containing β-dicarbonyl ligating moieties in the side chain.*

Hanabusa *et al.*[66] have reported the synthesis and properties of liquid-crystalline side-chain homopolymers containing *β*-diketonato transition metal complexes of Cu^{2+}, Ni^{2+} and Co^{3+}. Moreover, Mastrorilli and co-workers have synthesised new supported metal complexes *via* thermal copolymerisation of the metal complex precursors (cod)Rh(AEMA) and $Pd(AEMA)_2$[67]. These insoluble rhodium/palladium polymeric resins proved to be active catalysts for the hydrogenation of 1-heptene under mild conditions. The same group reported the catalytic activity of a cross-linked polymer obtained by the reaction of $Pd(AEMA)_2$ and suitable acrylates as comonomers towards hydrogenation reactions[68].

Procedures for a controlled synthesis of block copolymers from acetoacetyl- or ketal-functional monomers have not been reported until now. We first employed two different routes for the preparation of well-defined coordinating block copolymers with *β*-dicarbonyl ligands[53,69]. Systematic studies have shown that these ligating amphiphilic diblock copolymers exhibit strong segregation behaviour in selective organic media. Furthermore, they have the ability to complex and solubilise inorganic metal salts in organic and aqueous media yielding sterically stabilised colloidal hybrid materials.

CHAPTER 3

Characterisation Methods

3.1 Gel Permeation Chromatography (GPC)

Gel Permeation Chromatography (GPC), also known as Size Exclusion Chromatography (SEC), is considered to be one of the most important methods for the determination of molecular weights (MW) and molecular weight distributions (MWD) of polymers. During this process macromolecules are fractionated according to their hydrodynamic volume. A dilute polymer solution containing a broad molecular-weight distribution of polymer chains, oligomers or even unreacted monomer is allowed to flow through a column packed with finely divided solid particles. These can be either microporous glass beads or swollen, polymer gel. Smaller molecules can penetrate the pores and hence spend some time in the column before their elution, whereas the larger ones, unable to do the same, are eluted first out of the column[33]. The separation process is illustrated in Figure 3.1.

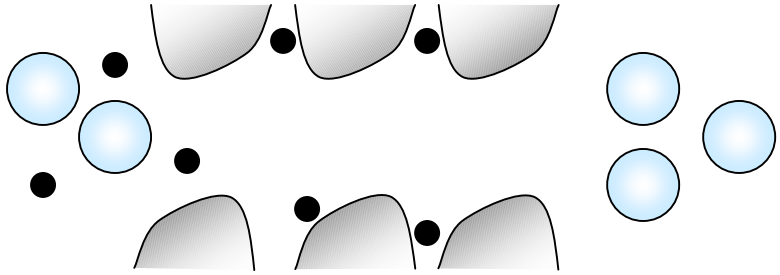

Figure 3.1: *Schematic representation of the fractionation process occurring for a dilute polymer solution in GPC.*

The polymer concentration in the analyte is measured as a function of time or elution volume (V_e). The latter is defined as:

$$V_e = V_o + k_{GPC}V_i \tag{3.1}$$

V_o is the exclusion volume, V_i the volume inside the pores and k_{GPC} the distribution coefficient. Differential Refractometer (DRI) and/or Ultraviolet/visible (UV-*Vis*) absorption systems are the most commonly employed GPC detectors. According to the first method, the

difference in the refractive index between the eluted solution and the pure solvent is proportional to the concentration of the polymer chains. In the case where a UV-*Vis* detector is used, and the polymer is consisted of UV-active monomer units, then by setting the spectrometer to a specific wavelength (e.g to the aromatic absorption region of a polymer with phenyl rings) the signal will be proportional to the mass. When a polymer chain carries a UV-active end-group, a signal proportional to this group will be detected.

GPC is a relative method for determining molecular weights. This can be achieved only after calibrating the system in terms of the elution volume. Calibration is performed using fractions of a particular polymer which have been previously well characterised in terms of molecular weights, using absolute methods such as Osmometry and Light Scattering. These samples are known as polymer "standards". The measured elution volumes are plotted as a function of the molecular weight ($logM = f(V_e)$). A typical calibration curve, using *poly*(*n*-butyl methacrylate) standards is presented in Figure 3.2.

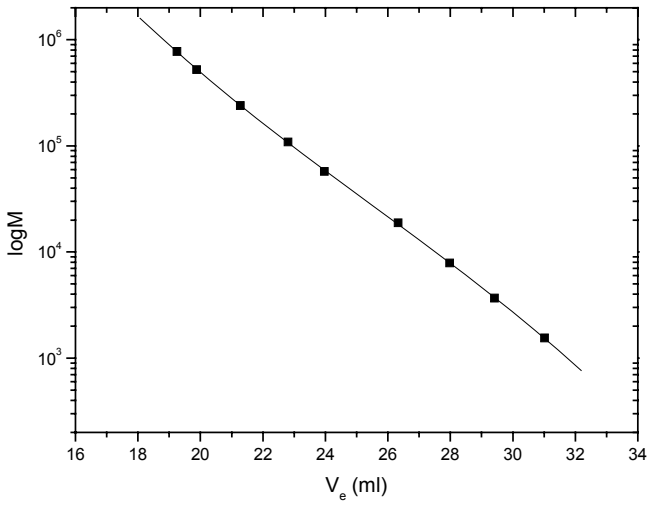

Figure 3.2: *GPC calibration curve using well-defined poly(BuMA) standards.*

As mentioned previously, usually the signal intensity (I_{RI}) in any slice *i* of a GPC chromatogram is proportional to the concentration of the eluting chains, c_i:

$$c_i \sim \frac{(I_{RI})_i}{\sum_j (I_{RI})_j} \tag{3.2}$$

The expression in the denominator corresponds to the total area of the chromatogram.

The molecular weight corresponding to each chromatographic fraction can be determined *via* the calibration curve. Thus, from the obtained data, number- and weight-average molecular weights[70] (M_n, M_w respectively) can be calculated among others (equations 3.3 and 3.4) and with them the polydispersity index (PDI = M_w/M_n).

M_w/M_n takes values from $1 \rightarrow \infty$. If this ratio is equal to 1 then a situation where all molecules have exactly the same molecular weight (i.e monodisperse) is achieved.

$$\bar{M}_n \equiv \frac{\sum_i c_i}{\sum_i c_i / M_i} \tag{3.3}$$

$$\bar{M}_w \equiv \frac{\sum_i c_i M_i}{\sum_i c_i} \tag{3.4}$$

For block copolymers, calculated GPC values of M_n, M_w and PDI are only apparent, since the measured UV and RI traces of copolymer samples are not a direct measure of the concentration of the eluting chains, and a suitable calibration is usually not available. To obtain absolute molecular weights, corrections with respect to the comonomer-specific detector response must be made, and on-line molar-mass-sensitive detectors are required, such as differential viscosity and multi-angle laser light scattering, which are expensive and require special knowledge for data evaluation[71].

The classical way for determining absolute M_n for diblock copolymer systems used in the present work, combines GPC with ^{1}H NMR. From GPC we were able to determine absolute M_n, M_w and PDI values for one of the blocks (pMMA, pBuMA) for which calibration curves were available, using equations 3.3 and 3.4. Thus, knowing the molecular weight of the block copolymer "precursor" and calculating the copolymer compositions using ^{1}H NMR (comparing the peak integrals assigned to the different comonomers), we were able to determine the DP of the two blocks within the copolymer.

3.2 Scattering Methods

Dynamic and Static Light Scattering

Light Scattering is extensively used for characterising polymers or colloidal particles in dilute solutions in terms of size and aggregation behaviour[72]. In general, a molecule, which interacts with an electromagnetic radiation, absorbs and scatters the radiation. Scattering is attributed to the fact that the electrons within molecules interact with the oscillating electric field of radiation, inducing a dipole, which oscillates with the electric field. As this oscillating dipole is an electromagnetic radiation source, the molecules emit light, what is called *Scattered Light*. This has almost the same wavelength as the incident light and it is produced from elastic (or Rayleigh) scattering.

3.2.1 Dynamic Light Scattering (DLS)

DLS is considered to be one of the quickest and most convenient methods for the determination of the hydrodynamic radii and polydispersity of colloidal systems. In DLS, monochromatic light with intensity I_o, passes through the sample - a dilute solution of suspended particles - and the latter scatters light in all directions relative to the incident beam. The major portion of the scattered light has almost the same wavelength as the incident radiation. The intensity of the scattered light $I(\theta)$ is detected at angle θ to the incident beam direction and at distance r from the centre of the system as shown in Figure 3.3[33].

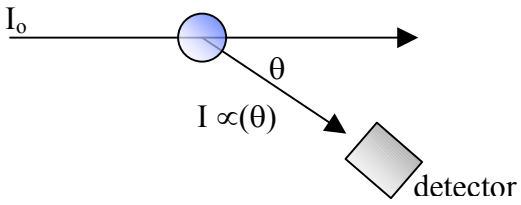

Figure 3.3*: Scattering of monochromatic light by a dilute sample solution and detection of the scattered beam at a specific scattering angle.*

The scattered light coming from each particle has a specific amplitude and phase. At the detector, all these small scattered light amplitudes interfere and add up to a different sum, which depends on the relative phases of the moving particles. The faster the particles move around, the faster the signal changes. The above process is dynamic and therefore the

scattering is called Dynamic Light Scattering. The variation in the intensity of the scattered light $I(\omega)$ over a frequency range from - ∞ to + ∞ is given by:

$$I(\omega)= \frac{1}{2\pi}\int_{-\infty}^{\infty} g_1(t)\exp(-i\omega t)dt \qquad (3.5)$$

where ω is the difference between the angular frequency of the scattered and that of the incident light and $g_1(t)$ is the electric field autocorrelation function. In Dynamic Light Scattering the output from the photomultiplier tube is the unormalised intensity autocorrelation function, $G_2(t)$[73] which is given as:

$$G_2(t) = A + [Bg_1(t)]^2 \qquad (3.6)$$

A is a constant background intensity to which the correlation function decays after a suitably long delay time t, and B is a constant close to unity[73]. The scattering intensity is analysed by an Avalanche Photodiode and it appears to fluctuate randomly as shown in Figure 3.4:

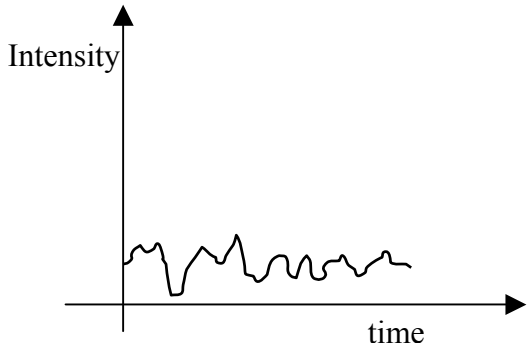

Figure 3.4: *Random fluctuation of the scattering intensity analysed using an Avalanche Photodiode with time.*

If the polymer system is monodisperse and only concentration relaxation processes exist, then:

$$g_1(t) = \exp(-\Gamma t) \qquad (3.7)$$

$$\Gamma = Dq^2 \tag{3.8}$$

Γ^1 is the relaxation time of the diffusive process of the polymer, D is the translational diffusion coefficient, and q is the scattering vector. The latter is expressed as:

$$q = \frac{4\pi n \sin(\theta/2)}{\lambda_o} \tag{3.9}$$

where n is the refractive index, θ the scattering angle and λ_o the laser's wavelength.
In polymer solutions D is concentration dependent as shown in equation 3.10. D_o corresponds to the diffusion coefficient value at infinite dilution and c is the polymer concentration. k_D is a term in which thermodynamic as well as frictional parameters of a polymer in a specific solvent are included.

$$D = D_o (1 + k_D c) \tag{3.10}$$

Assuming that molecules obey Brownian motion[74] (as they can move freely in the solvent colliding randomly with solvent molecules) and considering R_H to be the radius of a sphere with equivalent friction, by using Stoke's Equation the hydrodynamic radius R_H can be calculated. k_B is the Boltzmann`s constant, T the absolute temperature and η_o the viscosity of the solvent.

$$R_H = \frac{k_B T}{6\pi n_o D_\tau} \tag{3.11}$$

In real systems, intermolecular interactions have an influence on the diffusion processes of the particles. The influence of the concentration c and the scattering vector q on the apparent diffusion coefficient can be described in a way similarly to Static Light Scattering:

$$D_{app}(q) = D (1 + C_{app} R_g^2 q^2 + ...) \cdot (1 + k_D c \ ...) \tag{3.12}$$

Simultaneous extrapolation to c = 0 and q = 0 leads to the determination of the diffusion coefficient. Due to the fact that polymer systems are often polydisperse, each different

relaxation time will contribute to the observed average Γ and hence influence the shape of the correlation function. In this case $g_1(t)$ will derive from a superimposition of different diffusing processes[4]:

$$g_1(t) = \left\langle e^{-\Gamma t} \right\rangle = \int_0^\infty e^{\Gamma t} G(\Gamma) d\Gamma \tag{3.13}$$

The average diffusion coefficient can only be determined, when $G(\Gamma)$ is known. Analysis of this term is possible by applying an inverse Laplace transformation using the program FASTORT.EXE.

3.2.2 Static Light Scattering (SLS)

Static Light Scattering is a well-established technique used for the characterisation of macromolecules. The technique is based on the polarisability generated within the molecules when an electromagnetic wave interacts with their electrons, inducing a dipole moment. In contrast with X-ray scattering, here scattering centres are not individual electrons but molecules or groups of molecules. The ratio of the light scattered I_s, to the incident light I_o per scattering centre is described *via*[75]:

$$b^2(\theta) = \frac{16\pi a^2 \cos^2(\theta)}{\lambda^4 R^2} \tag{3.14}$$

where λ is the wavelength of the light, θ is the angle of observation in respect to the polarisation plane, R is the distance from the scattering centre to the detector and a the polarisability. For vertically polarised light, the term $cos^2(\theta)$ equals to 1.

Over 100 years ago, Lord Rayleigh considered light scattering in terms of the optical properties of individual molecules in a dilute gas[76]. Light Scattering was first utilised to determine molecular weights of polymers by Smoluchowski[77,78] and Einstein[79], who described fluctuations of the refractive index in liquids. Later on, Debye[80] and Zimm[81] developed the equations used nowadays. In those, the observed light scattering intensity is related to the osmotic pressure of the polymer as[14]:

$$\frac{Kc}{R(\theta)} = \frac{1}{RT}\left(\frac{\partial \pi}{\partial c}\right)_T \tag{3.15}$$

The term $R(\theta)$ is called Rayleigh's ratio and equals to:

$$\mathrm{R}(\theta) = \frac{I(\theta) r^2}{I_o V_s} \tag{3.16}$$

$I(\theta)$ is the light intensity observed at angle θ, scattered by a volume V_s. r corresponds to the distance from the source and I_o is the intensity of the incident light. In equation (3.15), K represents an optical constant, particular for each polymer/solvent system, which is given as:

$$\mathrm{K} = \frac{2\pi_1^2 n_o^2 (dn/dc)^2}{N_A \lambda^4} \tag{3.17}$$

where π_1 equals to 3.14, n_o is the refractive index at wavelength λ and N_A is Avogadro's number. The basic equation of light scattering applied to polymer solutions is given in (3.18). A_2 is the second virial coefficient.

$$\frac{Kc}{R(\theta) - R(solvent)} = \frac{1}{M_w P(\theta)} + 2A_2 c \tag{3.18}$$

If the particles are very small compared to the wavelength of the incident radiation, $P(\theta)$, the so called single chain form factor, equals to one. $P(\theta)$ describes the angular scattering arising from the conformation of an individual chain. If now the particles are larger than the 1/20 of λ, $P(\theta)$ differs from unity and it becomes independent the particles` shape as θ approaches zero. The region at very small angles is known as the Guinier region[80]. In this region, $P(\theta)$ becomes a measure of the radius of gyration, R_g. For a random coil, $P(\theta)$ can be expressed by:

$$\mathrm{P}(\theta) = \frac{2}{R_g^2 q^4}\left\{R_g^2 q^2 - \left[1 - \exp\left(-R_g^2 q^2\right)\right]\right\} \tag{3.19}$$

According to Zimm[81] the equations in which the light scattering intensity is related to the z-average radius of gyration R_g, the weight average molecular weight M_w and the second virial coefficient A_2 at the limit of zero angle and zero concentration are:

$$\left(K\frac{c}{R(\theta)}\right)_{\theta=0} = \frac{1}{M_w} + 2A_2c + \ldots \tag{3.20}$$

$$\left(K\frac{c}{R(\theta)}\right)_{c=0} = \frac{1}{M_w}\left[1 + \frac{1}{3}\left(\frac{4\pi_1}{\lambda'}\right)R_g^2 \sin^2(\theta/2) + \ldots\right] \tag{3.21}$$

λ` is the wavelength of the light in solution. For the construction of a typical Zimm plot illustrated in Figure 3.5, the two above equations must be combined.

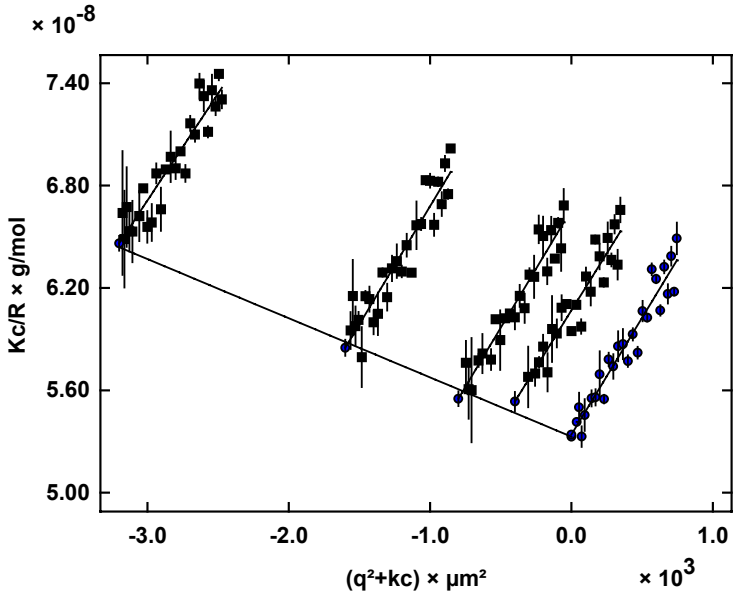

Figure 3.5: *Experimental Zimm Plot for $pBuMA_{342}$-b-$pAEMA_{39}$ ligating block copolymer complexed with Fe(III) (metal/ligand = 0.45) in cyclohexane solution (results obtained in the present work).*

Thus, by plotting *K[c/R(θ)] versus* a function of both, angle and concentration [*(q^2 + kc); q*: scattering vector, see eq.(3.9)] simultaneous calculation of M_w, R_g and A_2 is enabled.

3.3 Microscopy Techniques

3.3.1 Atomic Force Microscopy (AFM)

Atomic Force Microscopy, a three-dimensional imaging technique invented in 1986 by Binnig, Quate and Gerber[82], has been extensively used for providing information on atomic and molecular scale interactions as well as nanoscale adhesive and elastic response. It is considered to be a very powerful tool for resolving processing and material problems in areas such as electronics, telecommunications, biology, chemistry and many others. In Figure 3.6, a simple schematic diagram of an Atomic Force Microscope is illustrated.

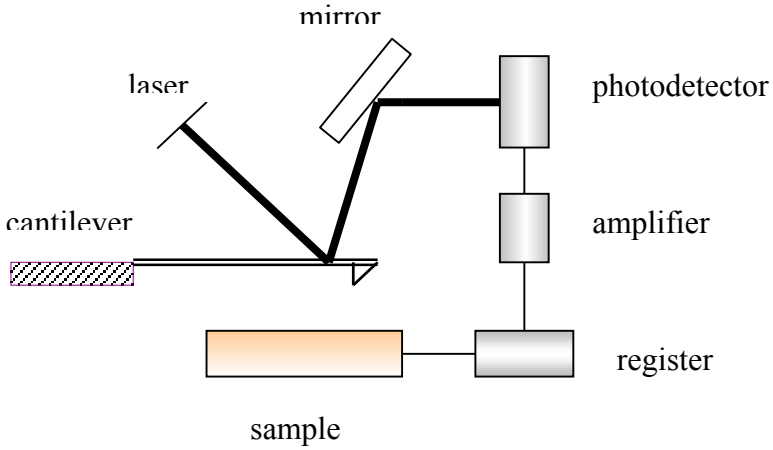

Figure 3.6: *Schematic representation of an Atomic Force Microscope*.

A sharp tip is scanned automatically over the sample surface in a way that enables the piezo-electric scanners to maintain the tip at a constant force (obtaining height information) or height (obtaining force information) above the surface of the sample. As shown in Figure 3.6, an optical detection system is employed, by having the tip attached to the underside of a reflective cantilever. Furthermore, a laser beam strikes the backside of the cantilever, and as the tip scans the sample surface moving up and down, the laser beam is deflected off the attached cantilever into a dual element photodiode. The difference in light intensities between the upper and lower photodetectors is measured and converted into voltage.

There are three common modes used in AFM: The *Contact***,** the *non-Contact* and the *Tapping Mode.* In the contact mode, the tip makes physical contact with the sample. As the tip moves across the sample, the contact force causes the cantilever to bend according to changes in the topography. In contrast, in the non-contact mode, the cantilever is vibrated near the surface of the sample. This is advantageous since the tip has little or no contact with the sample.

Finally, tapping mode is the most common AFM mode and the one used extensively in the present work. With it, high resolution topographic imaging of "problematic" sample surfaces can be achieved, surfaces which can be easily damaged and are held weakly to their substrate or are difficult to visualise with other AFM techniques. Additionally, by tapping mode problems associated with friction, adhesion or electrostatic forces are overcomed. In this last AFM mode, the tip is alternately placed in contact with a surface and then is lifted off the surface to avoid dragging it across. Tapping Mode imaging is implemented in ambient air by oscillating the cantilever assembly at, or near its resonance frequency using a piezoelectric crystal. The piezo-motion causes the oscillation of the cantilever usually with amplitude greater than 20nm when the tip is not touching the surface. The oscillating tip is then moved slowly towards the surface and begins to tap it lightly. When the cantilever touches the surface, its oscillation amplitude is reduced due to the loss in energy. It is this reduction that is used for measuring the characteristics of a surface.

There are some advantages in using tapping mode instead of the other AFM mode techniques. Firstly, the tip of the cantilever does not stick to the sample surface causing its damage. Therefore it is the best mode for imaging soft and fragile samples such as polymers[83] and biological objects[84]. In Figure 3.7(i) a 3-D AFM amplitude image of red blood cells from a human blood sample[85] *(μm scale)* is presented. This image was constructed by recording the cantilevel motion in z direction as a function of the sample's x and y position. Figure 3.7(ii) illustrates an amplitude image of polymeric monodisperse micelles produced in the present work *(nm scale)*.

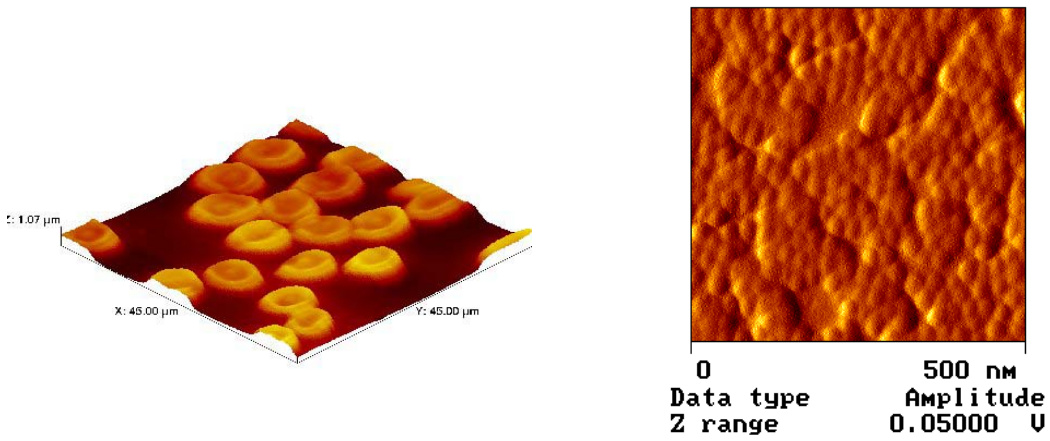

Figure 3.7: *AFM amplitude images of (i) human blood cells and (ii) micelles of poly(n-BuMA)$_{80}$-b-poly[2-(acetoacetoxy)ethyl methacrylate]$_{22}$ (spin coated from a cyclohexane solution on a mica surface).*

Additionally, compared to the contact and non-contact modes, the amplitude of the tip contacting the surface is sufficient to overcome any adhesion forces between the tip and the sample. Moreover, the surface material is not pulled sideways by shear forces due to the fact that the applied force is always vertical. Finally, tapping mode operates in a large, linear range allowing reproducibility of a measurement.

3.3.2 Scanning Electron Microscopy (SEM)

SEM constitutes one of the oldest and most widely used methods for surface analysis. Due to the fact that it provides a three-dimensional visual image, qualitative analysis is relatively straightforward. In SEM, scanning a focused electron beam along the specimen of interest creates an image. The beam interacts with a thin layer (few micrometers) at the surface of the specimen. This interaction causes the production of secondary electrons, which are emitted from the sample surface, are detected and used to modulate the brightness of a synchronously scanned cathode ray tube (CRT). Hence these electrons are responsible for the formation of a TV-type of image[14]. X-rays, characteristic of that part of the specimen probed by the electron beam, allow both a qualitative and quantitative determination of the elements present in the selected region[86]. High energy back-scattered electrons can be separated and also used for image formation. Since the back-scattering efficiency is a function of the atomic weight, this image reveals compositional variations due to average atomic number. An example of a SEM microgram is presented in Figure 3.8.

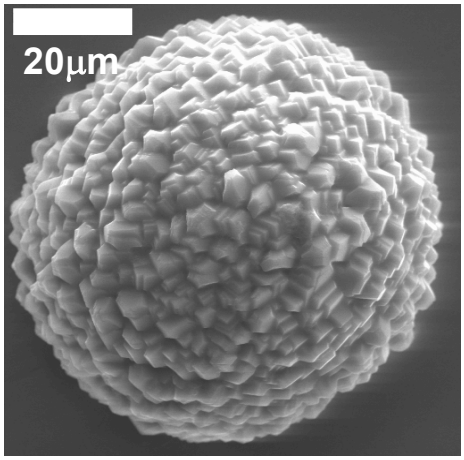

Figure 3.8: *SEM image of a large spherule $CaCO_3$ particle grown in the presence of poly(ethylene glycol)-b-poly(methacrylic acid)*[87].

Furthermore, additional information can be obtained by SEM concerning:

- Surface topography, if low energy secondary electrons are collected,
- Atomic number or orientation if higher energy back-scattered electrons are used for imaging,
- Differentiation between surface roughness, porosity etc.
- Critical dimension measurements due to high sensitivity and resolution down to 1-2 nm.

3.4 Analytical Ultracentrifugation (AUC)[88, 89]

AUC, invented in the 1920`s by Thé Svedberg, is a very powerful and valuable method for the investigation of the physicochemical properties of macromolecules and colloids. The various techniques used in AUC lead to direct determination of molar masses, molecular weight distributions, shapes, particle sizes, interaction constants, sedimentation and diffusion coefficients etc.

When a gravitational field is applied on a solute particle suspended in a solvent, then three different forces act on the particle as illustrated in Figure 3.9.

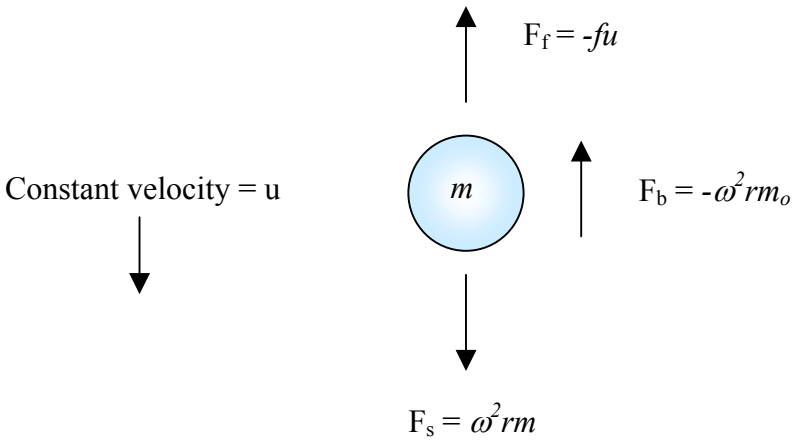

Figure 3.9: *Forces acting on a solute particle subjected to a gravitational field.*

F_s corresponds to the gravitational force and it is proportional to the mass of the particle and acceleration. The latter is determined by the distance of the particle from the rotational axis, r, and the square of the angular velocity, ω, in a spinning rotor.

$$F_s = m\omega^2 r = \frac{M\omega^2 r}{N_A} \qquad (3.22)$$

m is the mass of a single particle, *M* the molecular weight of the solute, and N_A Avogadro`s number. $F_b$, is the buoyant force. From Archimedes` principle this equals to:

$$F_b = - m_o\omega^2 r \tag{3.23}$$

where m_o is the mass of the fluid displaced by the particle. Furthermore, m_o can be written as:

$$m_o = m\bar{v}\rho = M\bar{v}\rho/N_A \tag{3.24}$$

$\bar{v}$ is the partial specific volume of the solute and ρ the density of the solvent. If the density of the particle is greater than that of the solvent, the particle will begin to sediment. As it moves towards the cell bottom, its velocity will increase due to an increase in the radial distance. The particle will then experience a frictional force F_f:

$$F_f = -fu \tag{3.25}$$

f is the frictional coefficient and depends on the size and shape of the particle.
Within a short period of time, these three forces come into balance:

$$F_s + F_b + F_f = 0 \tag{3.26}$$

Combination of equations 3.24-3.26 gives:

$$M (1 - \bar{v}\rho)/N_A f = u/\omega^2 r \equiv s \tag{3.27}$$

The velocity of the particle per unit gravitational acceleration ($u/\omega^2 r$) is called *sedimentation coefficient, s.* The above equation is known as *Svedberg`s equation.* The frictional coefficient is related to the diffusion coefficient *D via* STOKES-EINSTEIN equation:

$$f = RT/N_A D \tag{3.28}$$

Where *R* is the gas constant and *T* the absolute temperature. Determination of *D* is possible using Light Scattering or specific AUC experiments. The ratio of the sedimentation to diffusion coefficient gives the molecular weight:

$$M = s^{o}RT/D^{o}(1 - \bar{v}\rho) \tag{3.29}$$

s^{o} and D^{o} correspond to the extrapolated to zero concentration values to exclude any interaction effects between the particles during motion.

In the present work AUC was utilised in the investigation of hybrid colloidal systems of polymers and inorganic matter and proved to be very useful in understanding their solution behaviour.

3.5 Double – Jet Method (DJ)

The Double-Jet Method is one of the most important techniques used in biomineralisation, for investigating the efficiency of various synthetic block copolymers to control the crystallisation process of minerals. It was initially employed for producing different inorganic particles used in the photographic industry[90]. The advantage of DJ is that monodisperse nanocrystals can be produced since fast crystallisation of a constant number of particles is promoted. In Figure 3.10 a schematic representation of a Double-Jet reactor is illustrated.

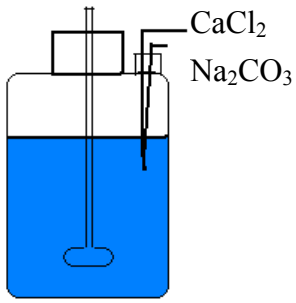

Figure 3.10: *Double – Jet reactor.*

The chemical equation involved in DJ is:

$$CaCl_2 + Na_2CO_3 \rightarrow CaCO_3 + 2NaCl\downarrow$$

The two reactants are continuously injected *via* capillaries into the reactor during vigorous stirring, to avoid heterogeneous nucleation. The ends of the two capillaries are joined together to achieve high local reactant concentrations and thus extreme supersaturation at the moment where the two reactants leave the capillaries[5]. In this manner, $CaCO_3$ nuclei are simultaneously formed and transported to regions of lower $CaCO_3$ concentration where they can further grow. The point at which crystal formation occurs can be easily detected since it is accompanied by a sudden increase in the turbidity of the solution. The end of the crystallisation process is defined at the time where macroscopic crystals are observed.

Equation 3.29 defines the efficiency of different block copolymers to control crystallisation growth. S_m represents the ratio between the polymer mass capable of keeping a defined mass of $CaCO_3$ in colloidal solution[91]. The smaller this ratio is, the better a stabilisator the polymeric material is,

$$S_m = \frac{m_{pol}}{m_{CaCO_3}} \tag{3.30}$$

CHAPTER 4

Results and Discussion

4.1 Synthesis and Characterisation of Amphiphilic Block Copolymers with β-Dicarbonyl Segments

Coordination polymers with β-dicarbonyl moieties have up to now only been available as homopolymers, random copolymers and resins. As already mentioned in paragraph 2.5, homopolymers bearing these functionalities were obtained *via* radical polymerisation techniques[62,63,64,65]. The advantage of such processes is that they can tolerate most functional groups, thus polymerisation of a wide range of monomers can be achieved. However, such reactions often yield chemically disperse products, which are not suitable for accurate systematic studies on phase behaviour and material properties[53]. Procedures for a controlled synthesis of homo and block copolymers using acetoacetyl- or ketal-functionalised monomers have not been reported until now. We first introduced two alternative routes for the synthesis of well-defined homopolymers and amphiphilic block copolymers with β-dicarbonyl segments. The first one involves two main steps: Initially, well-defined block copolymers are synthesised employing "living"/controlled polymerisation techniques (*Anionic and Group Transfer Polymerisation*). Subsequent transformation reactions are applied, resulting in functional amphiphilic block copolymers[53]. More precisely, the hydrophobic block copolymers *poly*(*n*-butyl methacrylate)-*b*-*poly[*(2-trimethylsilyloxy)ethyl methacrylate)] (pBuMA-*b*-pTMSHEMA) synthesised by GTP, were treated with dilute aqueous HCl solution. By acidic hydrolysis at room temperature, the protecting trimethylsilyl groups of the pTMSHEMA block could be quantitatively removed. A subsequent transesterification reaction of the hydroxylated block copolymer "precursors" (pBuMA-*b*-pHEMA) with *tert*-butyl acetoacetate, resulted in the incorporation of β-dicarbonyl segments into the polymers. Similarly, hydrophilic block copolymers of *poly*[2-(acetoacetoxy)ethyl ethylene]-*b*-*poly*(ethylene oxide) (pAEE-*b*-pEO), were obtained in a two-step transformation procedure: (1) A hydroboration/oxidation reaction of the *poly*(1,2 butadiene) block (pB) in pB-*b*-pEO (synthesised anionically), followed by (2) modification of the hydroxylated block copolymer

segment in *poly*[2-(hydroxyethyl) ethylene]-*b*-*poly*(ethylene oxide) (pHEE-*b*-pEO) with *tert*-butyl acetoacetate.

The above synthetic methodology was quite convenient and efficient, since the modification steps involved proceeded quantitatively. However, a procedure that could directly yield narrow-dispersed homopolymers and block copolymers without any intermediate modification steps involved would have been ideal for our purposes. Therefore we proceeded, introducing *Reversible Addition-Fragmentation Chain-Transfer Polymerisation (RAFT)*, a controlled free radical polymerisation technique recently developed by Rizzardo and co-workers[31]. This was the first reported use of RAFT for the polymerisation of AEMA and preparation of not only homopolymers, but also block copolymers from a wide range of monomers such as methacrylates, acrylates and acrylamides[69]. This distinguishes RAFT from other controlled polymerisation methods such as Anionic or Group Transfer Polymerisation since direct polymerisation of AEMA is not possible by the latter methods.

In the sub-chapters that follow, the synthesis and molecular characterisation of homopolymers and block copolymers based on AEMA will be presented and discussed in detail.

4.1.1 Hydrophobic Block Copolymers with β-Dicarbonyl Segments by GTP

As mentioned in 4.1, GTP was the polymerisation method used in the synthesis of a series of block copolymers of the type pBuMA-*b*-pTMSHEMA. TMSHEMA was chosen to be one of the blocks, because of the ease of quantitative removal of the trimethylsilyl protecting groups by acidic hydrolysis, resulting in block copolymers with hydroxy functionalities. Polymerisation took place at ambient temperature in tetrahydrofuran. The initiator used was MTS whereas TBABB served as polymerisation catalyst (Figure 4.1).

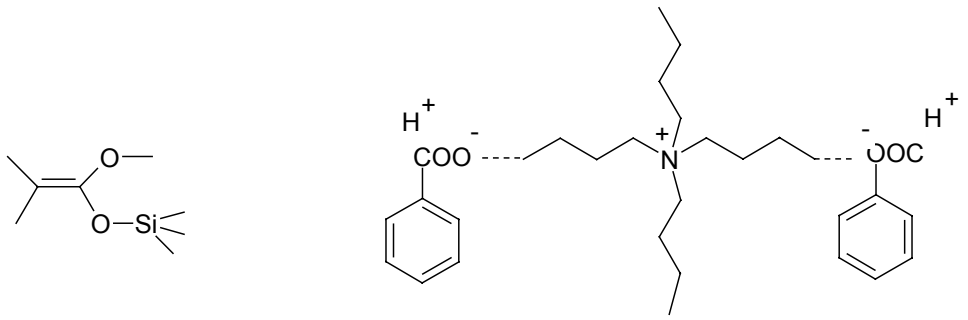

(a) **(b)**

Figure 4.1: *(a) 1-methoxy-1-trimethylsiloxy-2-methyl-prop-1-ene (MTS), (b) tetrabutylammonium bibenzoate, (TBABB).*

A general reaction scheme for the synthesis of pBuMA-*b*-pTMSHEMA block copolymers is presented in Figure 4.2.

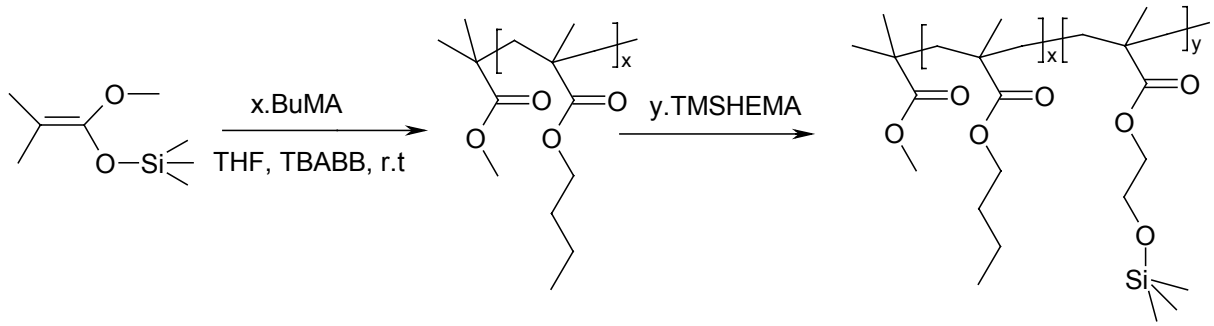

Figure 4.2: *Sequential GTP for the synthesis of pBuMA-b-pTMSHEMA.*

The above polymerisation proceeds also with reverse monomer addition, i.e. TMSHEMA can be polymerised first. This is attributed to the fact that both monomers have similar structural characteristics (both are methacrylates) and hence, similar electron affinities and reactivities[33]. On the contrary, as will be discussed in 4.1.2, for the synthesis of the pB-*b*-pEO block copolymers, the butadiene block must be polymerised first.

Molecular weights (MWs) and polydispersity indices (PDI), for all pBuMA-*b*-pTMSHEMA copolymers were determined by GPC in THF using pBuMA calibration standards. Copolymer compositions were calculated by ^{1}H NMR spectroscopy by comparing peak integrals assigned to the different comonomers. For example, the peak integral corresponding to the -OCH_2 protons in BuMA residues appearing at $\delta = 3.8 – 4.0$ ppm was set in ratio to that of the–Si(CH_3)$_3$ protons in TMSHEMA appearing at 0.1 ppm.

In Table 4.1, molecular weights, PDIs and copolymer compositions for pBuMA-*b*-pTMSHEMA copolymers are summarised. *S* is used to indicate that the polymers are protected with silyl groups.

Table 4.1: *MWs, PDIs and copolymer compositions as determined by GPC and ^{1}H NMR for pBuMA-b-pTMSHEMA copolymers and precursors.*

Polymer ID	x[#]	y[+]	$f_{TMSHEMA}$*	PDI[#]
A-1 precursor	80	-	-	1.07
A-1S	80	22	0.22	1.03
A-2 precursor	342	-	-	1.14
A-2S	342	39	0.10	1.05
A-3 precursor	74	-	-	1.04
A-3S	74	60	0.45	1.09
A-4 precursor	58	-	-	1.04
A-4S	58	10	0.15	1.07

[#] GPC (THF, pBuMA calibration), * molar fraction of TMSHEMA in the copolymer determined by ^{1}H NMR.

[+] $y = x\frac{f_{TMSHEMA}}{1 - f_{TMSHEMA}}$

Witzeman and Nottingham have reported the transesterification reaction of *tert*-butyl acetoacetate with alcohols or primary and secondary amine groups[92]. This method proceeds quantitatively and it is free of side reactions. Those two parameters are of great importance when performing organic reactions on polymers. Therefore, we decided to use this method for incorporating *β*-dicarbonyl segments into block copolymers. The hydroxylated block in pBuMA-*b*-pHEMA was reacted with *tert*-butyl acetoacetate forming a new ester bond, while at the same time *tert*-butyl alcohol was released as a side product. In Figure 4.3 the sequential steps applied for transforming pBuMA-*b*-pTMSHEMA into pBuMA-*b*-pAEMA are presented.

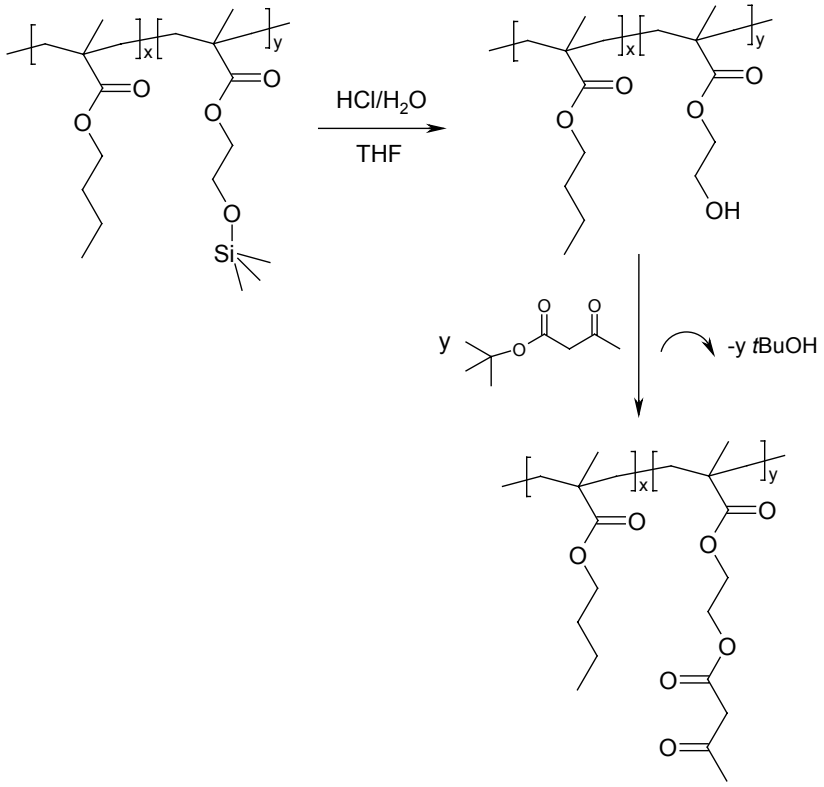

Figure 4.3: *Acidic hydrolysis followed by a transesterification reaction: two-step modification procedure for obtaining pBuMA-b-pAEMA starting from pBuMA-b-pTMSHEMA.*

Transesterifications are equilibrium reactions and in order to achieve optimal yields of the desired esters, the released *tert*-butyl alcohol should be removed.

Witzeman and Nottingham performed the reaction in toluene or xylene at 120 ^{o}C. The released alcohol was distilled off from the reaction mixture resulting in reaction yields from 69 to 97%. However, we developed another, more convenient procedure, in which the removal of *tert*-butyl alcohol is achieved with the formation of a ternary azeotrope with benzene and water[53]. The azeotrope has a b.p. of 67.3 ^{o}C. The hydroxylated block copolymer "precursor" is left to react with *tert*-butyl acetoacetate in benzene at moderate temperature (see Chapter 6 for details). Subsequent water addition causes the formation of the ternary azeotrope and while the dispersion is heated to reflux, the aqueous phase (water + *t*-BuOH) is removed from the reaction flask using a Dean-Stark apparatus. What is then left in the reaction flask is a solution of the final product in benzene, free of any side-products. All acetoacetylated block copolymers obtained were characterised by GPC, ^{1}H NMR and FT-IR (see Chapter 6 for detailed spectroscopic data). The degree of acetoacetylation was determined by comparing the peak areas in ^{1}H NMR corresponding to the signals of -OCH_2-

protons of pBuMA with the -CH_3 and -CH_2 signals in pAEMA and was found to exceed 95% in all cases. This proves that this new alternative modification route indeed leads to maximum yields of the desired product in the absence of any side reactions.

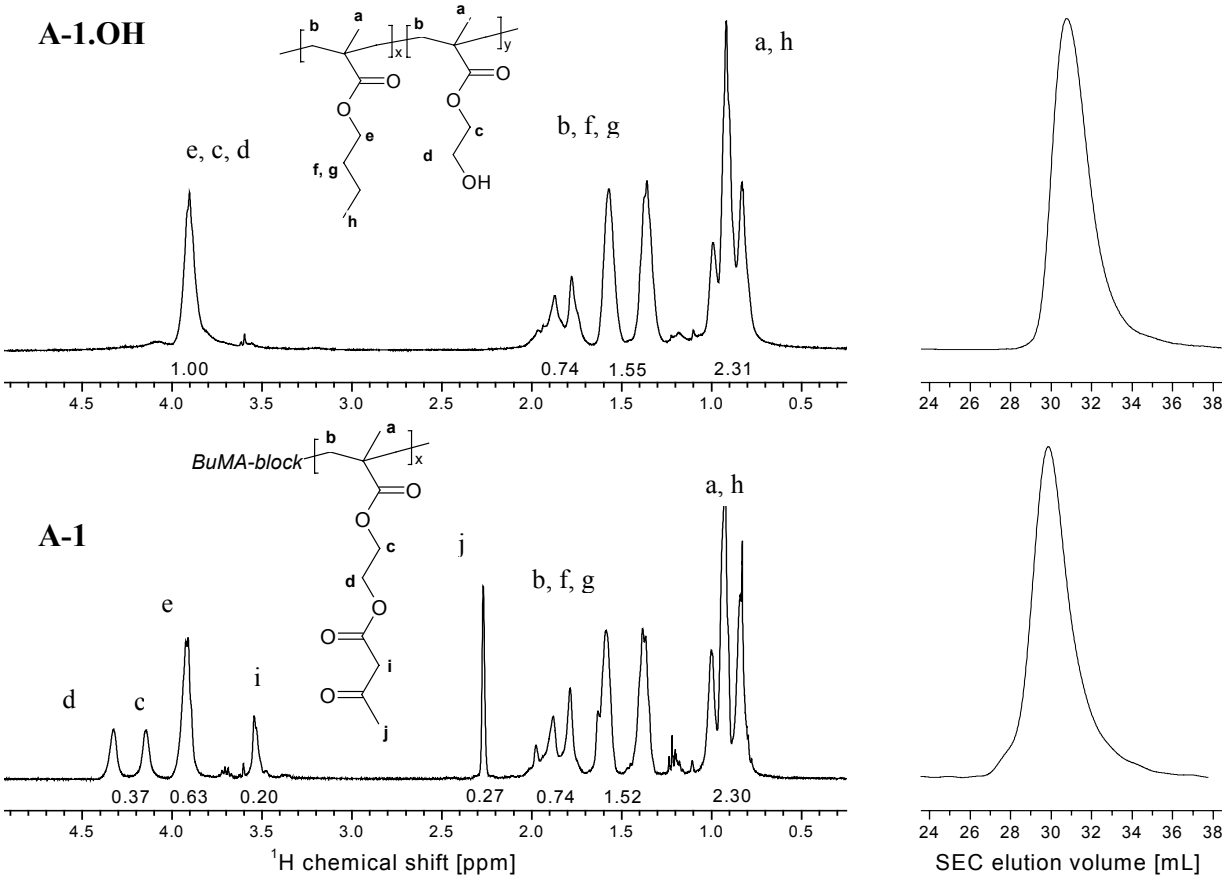

Figure 4.4: *^{1}H NMR spectra ($CDCl_3$) (left) and SEC chromatograms (DMA, DRI detector signal) (right) of the hydroxylated block copolymer precursor, A-1.OH and the corresponding acetoacetylated product A-1.*

In Figure 4.4, ^{1}H NMR spectra and SEC chromatograms of pBuMA-*b*-pHEMA (**A-1.OH**) and pBuMA-*b*-pAEMA (**A-1**) are presented. Comparing the two, several interesting observations can be made. First of all, the signals corresponding to the -CH_2 groups next to the hydroxy group in *A-1.OH* (*c, d*) shift downfields upon modification. This is a reasonable effect, since they are now located in a different chemical environment, which is influenced by the polar carbonyl groups introduced. Comparing the ^{1}H NMR spectrum of *A-1* with that of pAEMA synthesised by RAFT we observe exactly the same chemical shifts (see 4.1.3.1, Figure 4.7). This confirms two earlier suggestions: the success of the transformation reaction as well as

the effect of the introduction of the β-dicarbonyl moiety on the chemical environment of the -CH_2 groups found in its proximity. *A-1.OH* and *A-1* are identical in terms of molecular weight distributions, as indicated by the SEC chromatograms depicted in Figure 4.4. Hence, transformation occurs quantitatively and is free of side reactions. The fact that the acetoacetylated samples elute faster in the SEC mode than the hydroxylated block copolymer "precursors" could be attributed to a larger hydrodynamic volume of the derivatised functional β-dicarbonyl segment in comparison to the hydroxyl group.

4.1.2 Hydrophilic Block Copolymers with β-Dicarbonyl Segments by Anionic Polymerisation

Water-soluble block copolymers with functional groups able to bind onto metal ions are of great importance. Such polymers can be used in a wide range of applications such as biomineralisation processes, waste-water treatment, catalysis and hydrometallurgy[53]. Since β-dicarbonyl moieties are strong bidentate ligands for many multivalent cations[61], we decided to introduce this functionality in water-soluble block copolymers using similar experimental techniques described in 4.1.1. Sequential anionic polymerisation of 1,3-butadiene and ethylene oxide in THF was applied for the synthesis of pB-*b*-pEO as shown in Figure 4.5. The initiator used was *sec*-butyllithium/*t*-BuP_4.

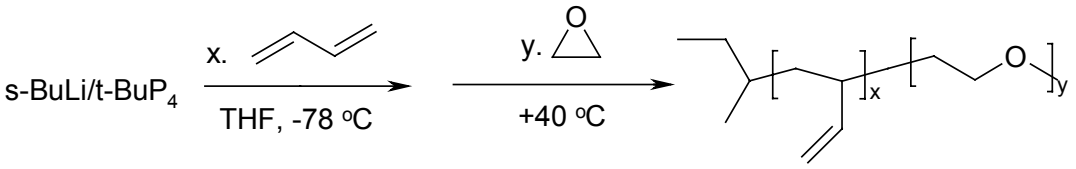

Figure 4.5: *Synthesis of pB-b-pEO block copolymers via sequential anionic polymerisation.*

It has to be mentioned that even though polymerisation of the 1,3 butadiene yielded almost quantitatively poly(1,2-butadiene), a small percentage of poly(1,4-butadiene) (~ 5%) was formed as proved by ^{1}H NMR. The *poly*(1,2-butadiene) units were then hydroxylated in 90% yield *via* a hydroboration/oxidation process using 9-BBN and H_2O_2[93] leading to the block copolymer "precursor" pHEE-*b*-pEO (Figure 4.6).

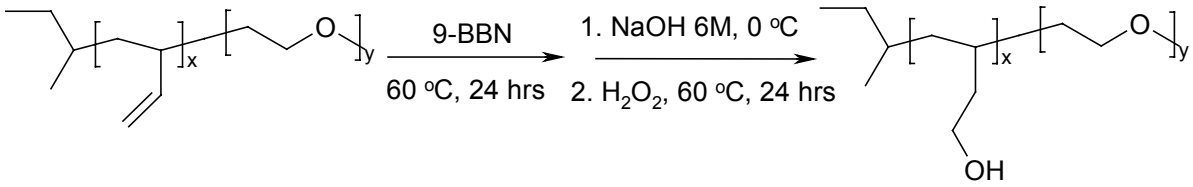

Figure 4.6: *Hydroboration/oxidation reaction of pB-b-pEO copolymers: Synthesis of pHEE-b-pEO block copolymers.*

A transacetoacetylation reaction was again employed for transforming pHEE-*b*-pEO to the desired hydrophilic block copolymers with *β*-dicarbonyl segments. The resulting polymers, (pAEE-*b*-pEO) were characterised by GPC, ^{1}H NMR and FT-IR (see Chapter 6 for spectroscopic data). Analytical data have shown that modification over the two steps proceeded in yields of more than 70%. Side reactions were absent and therefore the narrow molecular weight distribution of the block copolymer "precursors" was maintained after modification.

4.1.3 Homo and Block Copolymers with β-Dicarbonyl Segments by Reversible Addition-Fragmentation Chain-Transfer (RAFT)

Up to now, we described an indirect route for the synthesis of well-defined block copolymers with *β*-dicarbonyl moieties, in which sequential modification steps were involved. Even though this route does not suffer from the usual drawbacks of multistep reactions, such as low modification yields or side reactions, it is time-consuming, since several synthetic steps are required, and fails to give AEMA homopolymers due to solubility problems of the hydroxylated pHEMA "precursor" in benzene. The wish of finding a direct synthetic procedure for obtaining these block copolymers prompted us to look for a convenient polymerisation method which would allow for: (1) controlled polymerisation of AEMA for the preparation of functionalised homopolymers and (2) its sequential polymerisation with other monomers to obtain well-defined block copolymers. To reach this goal, we considered employing controlled radical polymerisation techniques such as Stable Free Radical Polymerisation (SFRP), Atom Transfer Radical Polymerisation (ATRP) and Reversible Addition-Fragmentation chain-Transfer polymerisation (RAFT). For our purpose, RAFT was chosen since it promotes a controlled polymerisation of (meth)acrylates and other monomers and can tolerate many functional groups incorporated into the monomer (like in the case of

AEMA). Furthermore, unlike ATRP, it does not involve any kind of metal-ion complex catalyst, which might interfere with the *β*-dicarbonyl group of AEMA.

4.1.3.1 Synthesis of well-defined pAEMAs

Following a standard procedure as described in the literature[31] a series of well-defined homopolymers of AEMA was successfully synthesised *via* RAFT. As chain transfer agents, either 2-cyano- or 2-phenyl-prop-2-yl dithiobenzoate were used and 2,2'-azobis(isobutyronitrile) (AIBN) served as the radical source. Polymerisations were carried out in ethyl acetate at 60 ^{o}C. The products were characterised by means of SEC and ^{1}H NMR. The latter confirmed the expected chemical structure as depicted in Figure 4.7.

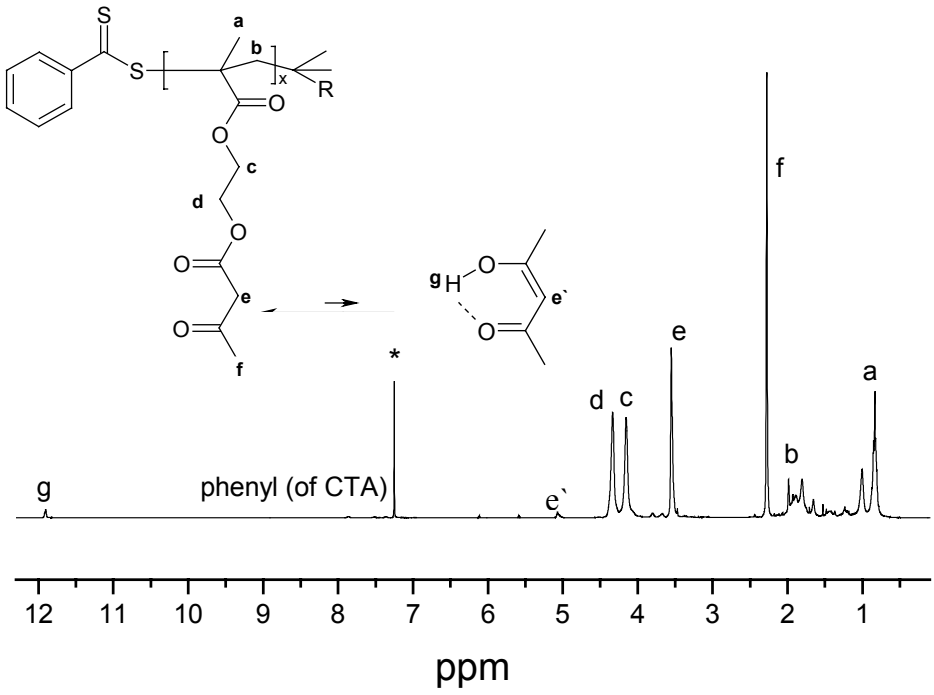

Figure 4.7: *Chemical structure of pAEMA (R = CN or C_6H_5) produced by RAFT radical polymerisation and the corresponding ^{1}H NMR spectrum (*: $CDCl_3$).*

From the above spectrum we were able to calculate the percentage of the enolate tautomer of *β*-dicarbonyl side chains found in equilibrium with the dominant keto tautomer in $CDCl_3$. This was done by comparing the signal of the proton corresponding to the enolate =C*H* proton (**e`**) with the –CH_2 (**e**) of the keto form and it was found very low, 6-8%. Furthermore, information on the polymer tacticity was obtained by observing the CH_3 (**a**) signals of the polymer backbone. The peak appearing around 0.8 ppm corresponds to syndiotactic

configuration (rr, 60%) whereas those at 1.0 and 1.2 ppm to heterotactic (mr, 27%) and isotactic (mm, 13%) respectively. SEC in THF illustrates that all polymers have a monomodal and narrow molecular weight distribution (< 1.2). Additionally, polymerisation of AEMA follows first-order kinetics with k_{app} of $(3.37 \pm 0.11)*10^{-2}$ hr^{-1} (Figure 4.8 a). The apparent number-average molecular weights (M_n, determined by GPC) of polymers appeared to increase linearly with conversion (Figure 4.8 b) indicating control over molecular weights. However, these apparent experimental values were systematically higher than the theoretical ones calculated from the ratio $[AEMA]_o/[CTA]$ x conversion, presumably due to partial CTA deactivation. Considering the real Mn values (calculated from NMR) CTA efficiency varied from 35-70%.

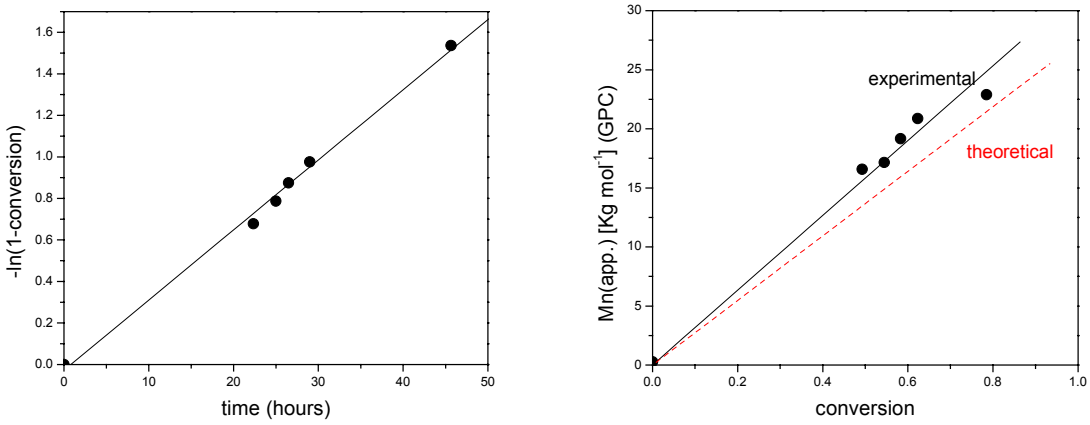

(a) **(b)**

Figure 4.8: *Homopolymerisation of AEMA with RAFT: (a) linear fit of –ln(1-conversion) versus time showing first-order kinetics and (b) linear fit of apparent M_n (GPC) versus conversion indicating control over molecular weights.*
Experimental conditions: $[AEMA]_o$ =2.6M , [CPDB]=0.0214M , $[AIBN]_o$ =0.0041M solvent: EA, temperature: 60 °C, yield: 85%.

As known from the literature, ATRP is another versatile controlled radical polymerisation technique for preparing a wide range of homopolymers and block copolymers with different architectures and compositions[94]. However, we assumed that for this specific monomer ATRP is not an appropriate method. These assumptions were based on the fact that the β-dicarbonyl moiety of AEMA could possibly interfere with the metal-ion complex catalyst. In other words, the strong affinity of the β-dicarbonyl group for metal ions might cause a structural change of the metal/ligand catalyst complex by competing with the conventional

ligating moiety used in ATRP (for example 4,4'-dinonyl-2,2'-bipyridine (dNbipy) or tris[2-(dimethylamino)ethyl]amine (Me_6TREN)), resulting in a non-controlled polymerisation process. To confirm this, we investigated ATRP of AEMA using *tert*-butyl α-bromoisobutyrate as the initiator and CuBr/dNbipy as the catalyst complex in methyl ethyl ketone at 90 ^{o}C. Indeed, at very early stages of polymerisation, the colour of the reaction mixture turned from red-brown to yellow. This indicated that the growing multidentate AEMA chains had most probably exchanged the dNbipy ligand. The bimodal and fairly broad molecular weight distribution of the product confirmed that indeed ATRP could not be applied for the polymerisation of AEMA. Furthermore, by using Me_6TREN, another common ATRP ligand, an insoluble polymer gel was obtained. A possible explanation for this might be that this ligand is a sufficiently strong base to abstract the -$OCH_2COCH_2COCH_3$ acidic protons from AEMA, thus promoting an aldol-type cross-linking of the polymer chains. In Figure 4.9 SEC chromatograms of pAEMA obtained by RAFT (*A*), Atom Transfer (*B*) and Free Radical polymerisation (*C*) are presented. (Note: It is already known from the literature that a free radical polymerisation of AEMA leads to polydisperse products[51]. In order to compare the three techniques we repeated this experiment under similar experimental conditions used in the RAFT polymerization).

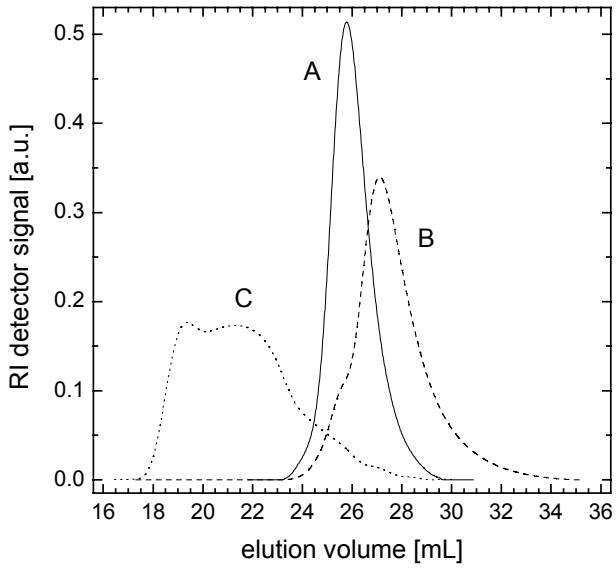

Figure 4.9: *SEC chromatograms (THF) of pAEMA obtained by RAFT (A), atom transfer (B) and free radical polymerisation (C). Experimental conditions: (A): $[AEMA]_0$ = 5.2 M, $[PPDB]_0$ = 0.0264 M, $[AIBN]_0$ = 4.87 mM, EA, 60 ^{0}C, 18 hr. (B): $[AEMA]_0$ = 2.1 M, $[\alpha BiB]_0$ = 10.5 M, $[CuBr]_0$ = 7.4 mM, $[CuBr_2]_0$ = 0.4 mM, $[dNbpy]_0$ = 14.7 mM solvent: MEK, 90 ^{0}C, 80 min. (C): $[AEMA]_0$ = 2.1 M, $[AIBN]_0$ = 10.0 mM, EA, 60 ^{0}C, 20 hr.*

In conclusion, RAFT appears to be the most appropriate controlled radical polymerisation technique for the synthesis of well-defined pAEMAs. ATRP fails because the β-dicarbonyl group of AEMA interferes with the mechanism involved in the polymerisation process, which uses a metal/ligand complex as a catalyst. pAEMA dissolves readily in chloroform, dioxane, methyl ethyl ketone, tetrahydrofuran, acetone, ethyl acetate, trifluoro acetic acid (TFA), dimethyl formamide (DMF) and dimethyl sulfoxide (DMSO) but it is insoluble in cyclohexane, benzene, methanol or water. Its specific density, measured for a sample with a molecular weight of 6.6 Kg mol^{-1}, was found to be 1.2632 $g.ml^{-1}$. DSC measurements showed for pAEMA a glass transition temperature (T_g) of +3.0 ^oC (ΔC_p = 0.269 J. g^{-1} K^{-1}). T_g values around 1 ^oC obtained by dielectric relaxation spectroscopy (DRS) (see APPENDIX I) agreed with DSC results. Furthermore, thermogravimetric analysis has shown that pAEMA is thermally resistant against elimination up to ~ 200 ^oC.

4.1.3.2 Synthesis of well-defined block copolymers based on AEMA

As mentioned in Chapter 2, one of the main advantages of RAFT is its versatility for preparing a large number of polymers with complex architectures such as block, stars, or graft copolymers[45-48]. The synthesis of a well-defined homopolymer based on AEMA already provided important information, since we were able to determine many of its physical characteristics and investigate its behaviour and solubility in different solvent systems. In addition to that, we were able to synthesise well-defined linear amphiphilic block copolymers with β-dicarbonyl moieties[69] with fairly narrow polydispersities (<1.3). As second monomers, methyl methacrylate (MMA), *n*-butyl (meth)acrylate, (BuMA and BA) and *N*-isopropylacrylamide (NiPAM) were used. In Table 4.2 a list of block copolymers of AEMA obtained *via* RAFT is presented.

Table 4.2: *Block copolymers based on AEMA prepared by RAFT radical polymerisation.*

Sample	M_n [Kg/mol]*	f_{AEMA}*	PDI#	Yield [%]a
*p*AEMA-*b*-*p*MMA	12.9	0.56	1.20	38
*p*MMA-*b*-*p*AEMA	15.1	0.29	1.12	95
*p*AEMA-*b*-*p*BuMA	34.8	0.13	1.15	84
*p*AEMA-*b*-*p*BuA	14.9	0.51	1.22	49
*p*AEMA-*b*-*p*NiPAM	12.3	0.4	1.17	56

* Determined by ^{1}H NMR; # determined by GPC (BuMA, MMA calibrations); a gravimetric analysis

4.2 Investigation of the Aggregation Behaviour of Hydrophobic Block Copolymers with β-Dicarbonyl Segments in Organic Media

Self-organisation of block copolymers in solution is a spontaneous association process resulting from interaction energies and entropic contributions between the individual chains and the solvent. The size, shape and basic nature of the associated structure are controlled by a complex series of factors. As already mentioned in Chapter 2, parameters such as the polymerisation degree of each individual block, the solvent system, the FLORY-HUGGINS interaction parameter between one of the blocks and the solvent and the relative volume fraction of each component can be crucial for inducing microphase separation in solution.

Numerous publications dealing with the aggregation behaviour of a wide range of amphiphilic block copolymers in solution appear in the literature[28,95,96,97]. Since amphiphilic block copolymers bearing β-dicarbonyl segments are completely new systems, we were interested in examining their behaviour in selective solvents.

The aggregation behaviour of these block copolymers, might be also affected by hydrogen-bonding interactions that, according to the literature[98,99] can take place between β-dicarbonyl moieties.

In addition to that, incorporation of these strong bidentate β-dicarbonyl ligands in block copolymers facilitates coordination and solubilisation of inorganic metal salts in organic media, in which they are otherwise completely insoluble. We were therefore aiming to: (1) investigate the aggregation behaviour of these block copolymer systems upon complexation, (2) how aggregation behaviour is affected by changing the nature of the metal ion (i.e using metal ion salts with different geometries and oxidation states) or (3) nature of the ligand (keto-tautomer or enolate anion) (see Chapter 4.4).

Investigations were carried out in cyclohexane and DMSO. In cyclohexane (a selective solvent for the pBuMA block), the formation of micelles consisting of a pBuMA solvating corona and a pAEMA core is favoured. In DMSO (a good solvent for the pAEMA block) the reverse is observed, i.e. pAEMA chains are located at the exterior and pBuMA at the interior of the micellar aggregates. ^{1}H NMR, Light Scattering (LS), analytical ultracentrifugation (AUC) and atomic force microscopy (AFM) were the methods used throughout this investigation.

4.2.1 Micellisation behaviour in selective solvents

Förster and co-workers have extensively investigated the micellisation behaviour of a series of diblock copolymers of the type *poly*(styrene)-*b*-*poly*(4-vinylpyridine) (pS-*b*-p4VP) in toluene[17]. They illustrated that this system exhibits aggregation behaviour resembling that of strongly segregated diblock and triblock copolymer systems and low molecular weight ionic and non ionic surfactants. In those systems, aggregation number *Z* is related to the different block lengths within the block copolymer as:

$$Z \propto N_A^2 N_B^{-0.8} \tag{4.1}$$

N_A corresponds to the length of the inner block forming the core and N_B to that of the outer block which forms the micellar corona. Systematic studies on the aggregation behaviour of pBuMA-*b*-pAEMA copolymers were carried out in cyclohexane aiming to find out to which extent it was comparable to strongly segregated amphiphilic block copolymer systems. Based on group considerations, a value of χ~0.8 was calculated for the BuMA/AEMA bulk system[100] (see APPENDIX III). Considering this value, we expect that these two monomer units are highly incompatible, thus strongly segregating. In Table 4.3, molecular weights and polydispersities corresponding to all pBuMA-*b*-pAEMAs investigated in this study are presented.

Table 4.3: *MWs, PDIs and copolymer compositions as determined by GPC and ^{1}H NMR for a series of pBuMA-b-pAEMA copolymers.*

Polymer ID	Mn [Kg/mol]$^{\#}$	$N_B^{\#}$	N_A^{+}	f_{AEMA}*	PDI$^{\#}$
A-2	56.99	342	39	0.10	1.05
A-5	35.72	206	30	0.13	1.15
A-4	9.96	58	10	0.15	1.07
A-1	16.01	80	22	0.22	1.03
A-3	23.38	74	60	0.45	1.09

*determined by ^{1}H NMR; $^{\#}$ GPC (THF, pBuMA calibration); $^{+}$ $N_A = N_B * f_{AEMA}/1\text{-}f_{AEMA}$

Numerous reports appear in the literature where NMR spectroscopy was used to study micellisation phenomena in cationic[101,102], anionic[103,104] and amphiphilic systems[96,24 ,105]. For example, Davis and co-workers[106] have combined liquid-state ^{1}H NMR together with solid-state ^{13}C NMR to obtain information on the structure of nanoparticles formed by a series of *poly*(lactic acid)-*b*-*poly*(ethylene oxide) block copolymers. Furthermore, Pan *et al.*[107] have reported among others, the synthesis of *poly*(styrene)-*b*-*poly*(p-nitrophenyl methacrylate) (pS-*b*-pNPM) and studied their micellisation behaviour in selective solvents using NMR. They showed that micelles consisting of a pS corona and a pNPM core were formed in chloroform, whereas in DMSO "reverse" micellar structures were observed.

^{1}H NMR spectroscopy was one of the techniques used in the present work, to study micellisation of pBuMA-*b*-pAEMA copolymers in selective solvents. In Figure 4.10, ^{1}H NMR spectra of $pBuMA_{74}$-*b*-$pAEMA_{60}$ in $CDCl_3$, cyclohexane-d_6 (CH-d_6) and DMSO-d_6 are presented.

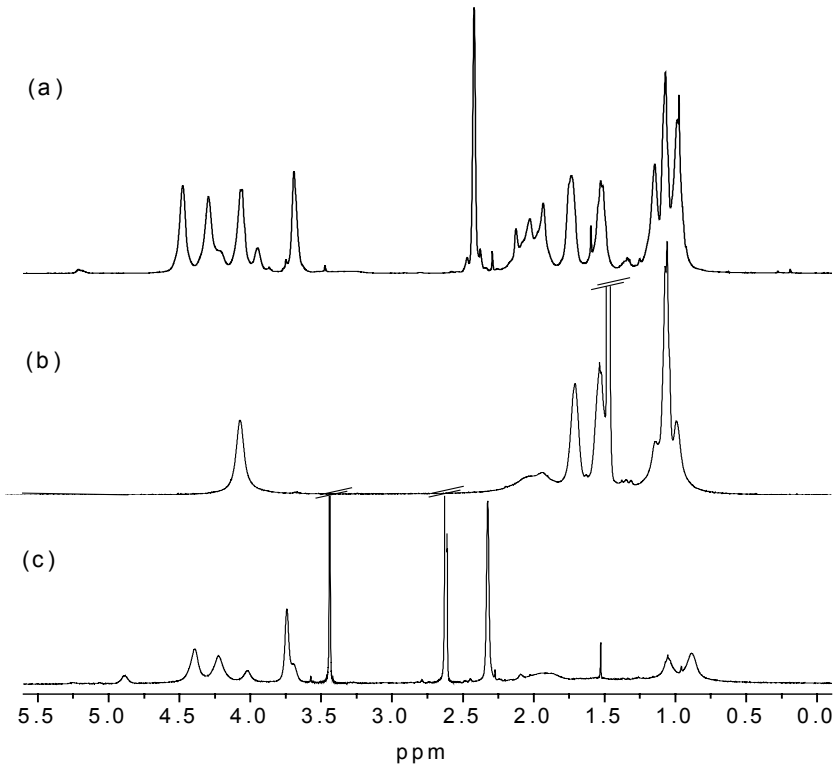

Figure 4.10: *Study of the micellisation behaviour of $pBuMA_{74}$-b-$pAEMA_{60}$ by ^{1}H NMR: (a) $CDCl_3$: no micelle formation; (b) CH-d_6: micelles in which the pBuMA block forms the micellar corona; (c) DMSO-d_6: "reverse" micelles in which the pAEMA block forms the micellar corona. // solvent.*

In $CDCl_3$, a good solvent for both blocks, no micellisation occurs and only unimers are present in solution. For this reason, relatively sharp and well-distinguished signals corresponding to the protons of both blocks can be visualised (*spectrum a*). However, in CH-d_6 the proton signals of the pAEMA block disappear whereas the remaining ones (of pBuMA) become broader. This indicates the formation of micelles with pBuMA chains being located on the outside and pAEMA on the inside of the micellar aggregates (*spectrum b*). The broadening of the signals might be attributed to the fact that *via* micelle formation, the mobility of the chains decreases and consequently the relaxation time is decreased. In DMSO-d_6 the situation is reversed, i.e. only the signals of the pAEMA block can be visualised (*spectrum c*). This proves the formation of micellar structures with pAEMA being the solvating block and pBuMA being located at the interior of the micelle.

An effort to calculate cmc values for these systems in cyclohexane employing light scattering techniques was unsuccessful (too low scattering intensities for very diluted solutions). Even at very low solution concentrations (range of 0.00125 – 0.1wt%, depending on each polymer), at which scattering intensities were still measurable, micelles were still present in solution, indicating that these block copolymer systems are characterised by very low cmc values.

In *spectrum c*, an interesting phenomenon observed is the appearance of additional signals in the region between 3.5 and 4.7 ppm. For this phenomenon two explanations could be possible: The first is that the –OC*H*$_2$ protons of pBuMA located at the interface can be visualised (small signal appearing around 4 ppm in spectrum c) in contrary to those that are well-separated from the polar region. Similarly, Davis *et al.*[106], during their investigations on the micellisation of pLA-*b*-pEO using NMR, have reported that even though the hydrophobic core of the micelle consisting of pLA blocks is not to be seen in D_2O and only the signals of the solvating pEO corona are observed, the methyl protons of the pLA block at the interface between the two regions are visible. Secondly, visualisation of new signals may be also attributed to shifting or splitting caused by specific interactions taking place between adjacent β-dicarbonyl groups (H-bonding).

Dynamic and Static Light Scattering were introduced to determine the basic characteristics of these micelles. DLS was used to determine the hydrodynamic radii (R_H). An independence of R_H on the measuring angle and solution concentration indicated the presence of monodisperse micelles. By SLS, the radii of gyration (R_g), second virial coefficients (A_2) and aggregation numbers (Z) were calculated using Zimm plots (Figure 4.11). In Table 4.4, all results obtained by DLS and SLS concerning micellisation of **A-1 – A-5** in cyclohexane are summarised.

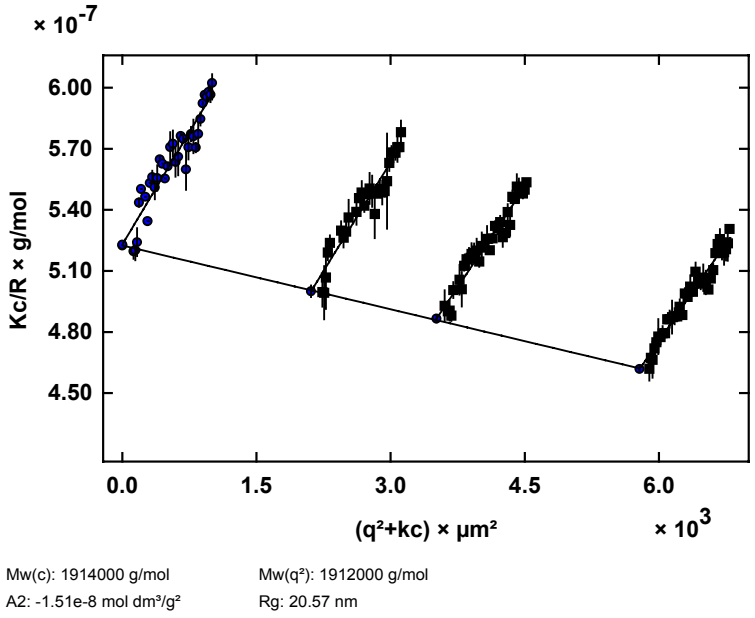

Figure 4.11: *Experimental Zimm plot for $pBuMA_{80}$-b-$pAEMA_{22}$ in cyclohexane.*

Table 4.4. *Experimental results obtained by DLS and SLS for a series of pBuMA-b-pAEMA block copolymer micelles formed in cyclohexane.*

Polymer ID	R_g (nm)	R_H (nm)	R_g/R_H	A_2*10^{-8} (mol mL/g^2)	Z
A-2	26	32	0.8	0.15	342
A-5	24	31	0.8	0.12	311
A-4	9	11	0.8	0.14	93
A-1	21	12	1.7	-1.51	120
A-3	54	49	1.1	-99.4	1025

Already from these results, the R_g/R_H ratios (~ 0.775, characteristic value for hard spheres) corresponding to the first three block copolymers indicate the presence of spherical micelles. The negative values of the second virial coefficients indicate that A-3 forms aggregates, which strongly attract each other. Therefore, in order to be able to measure LS for this system we had to go down to very low concentrations (0.005%), since at higher concentrations these aggregates coagulate and precipitate.

As previously mentioned, equation 4.1 describes the relation between aggregation number and polymerisation degrees of the inner (N_A) and the outer (N_B) block in a micelle, which applies for micellar systems with strong tendency for segregation. Considering the high χ value (0.8) calculated for the BuMA/AEMA bulk system, we expect that these systems will exhibit strong segregation behaviour in selective solvents, since the two blocks are highly incompatible. Indeed, compensating the N_B dependence by the factor $ZN_B^{0.8}$ and plotting it against N_A, all of our data points collapse on a straight line with a slope of 2 (Figure 4.12). In the same plot, data corresponding to other amphiphilic block copolymer systems exhibiting similar micellisation behaviour are presented. Surprisingly, this novel type of amphiphilic block copolymers is able to form micelles where the density of the individual polymer chains is even more increased along the micellar surface compared to other strongly segregated systems in solution.

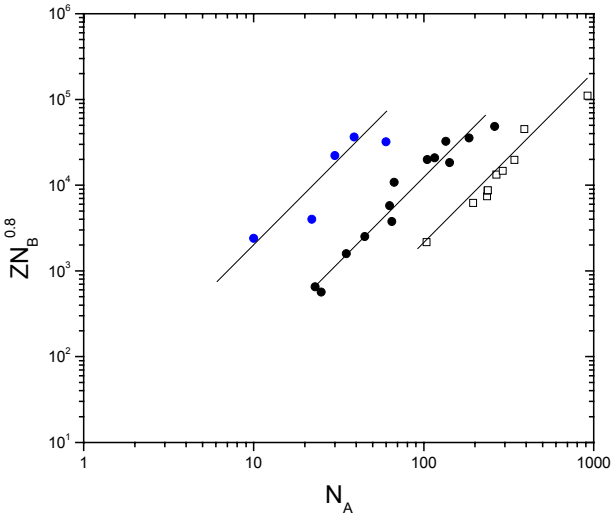

Figure 4.12: *Aggregation numbers Z as a function of N_A and N_B for different amphiphilic block copolymer systems: pBuMA-b-pAEMA in cyclohexane (blue circles), pS-b-p4VP in toluene (black circles)[17], pS-b-pMAc[29] in dioxane/water 80:20, (empty rectangles). Slope of lines = 2.*

So far we have obtained some information on the micellar aggregates of pBuMA-*b*-pAEMA formed in cyclohexane (Table 4.4). However, determination of other characteristics such as the core radius, R_c, the dimensions of the micellar corona (D_h) or the interchain distance b between neighbouring chains in the core/corona interface requires knowledge of the geometric characteristics of these micelles. SLS and AFM were the techniques employed for this purpose.

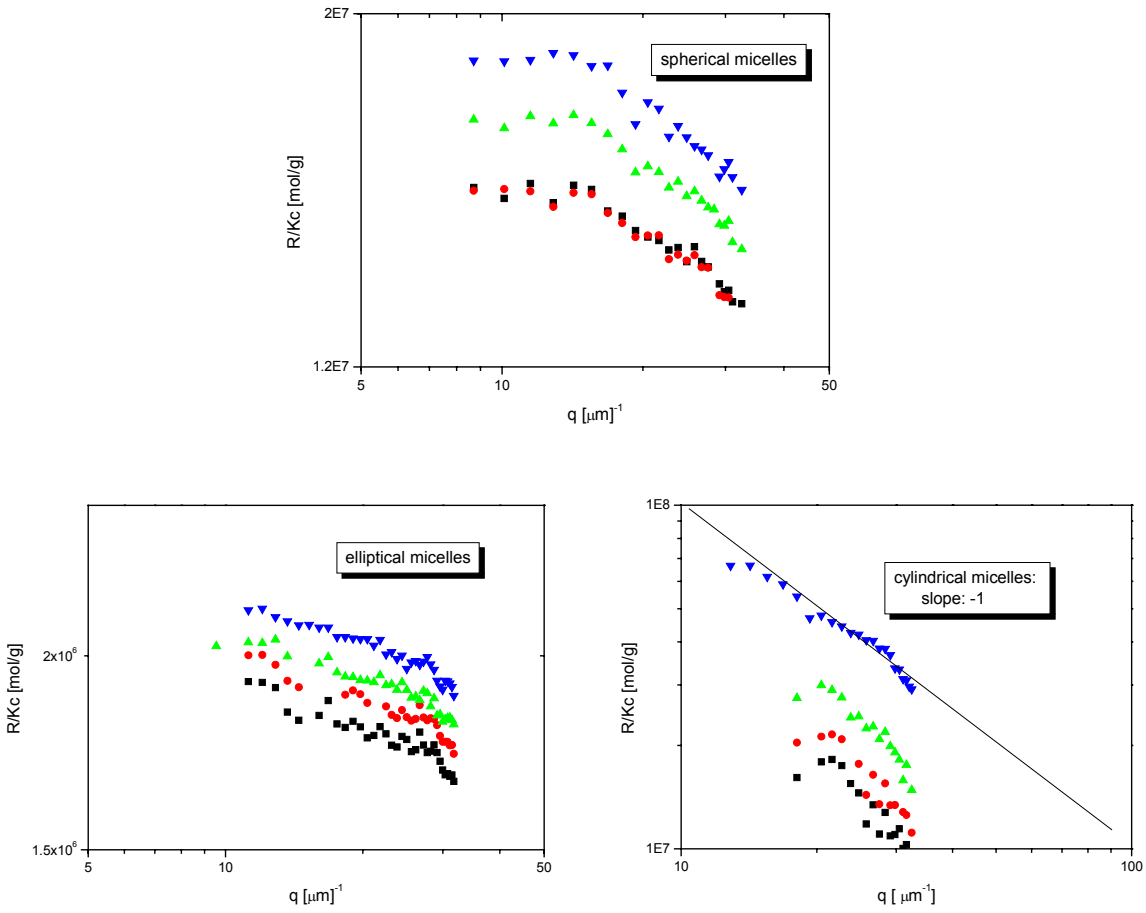

Figure 4.13: *SLS data corresponding to three different solution concentrations as well as the extrapolated ones (black squares). (a)* ***spherical micelles*** *of A-2; (b)* ***elliptical micelles*** *of A-1 and (c)* ***cylindrical micelles*** *of A-3 formed in cyclohexane.*

From SLS it is possible to extract information concerning the shape of the micellar aggregates. It is known from the literature that a logarithmic plot of the scattering intensity *R/Kc versus* the scattering vector q, presenting a slope of –1 indicates the presence of cylindrical micelles[108]. In Figure 4.13 such plots are presented for three different block copolymers: $pBuMA_{342}$-*b*-$pAEMA_{39}$ **(A-2)** $pBuMA_{80}$-*b*-$pAEMA_{22}$ **(A-1)** and $pBuMA_{74}$-*b*-

$pAEMA_{60}$ **(A-3)**. Figure 4.13 (c) clearly indicates that A-3 forms cylindrical micelles in cyclohexane, since all plots corresponding to three different solution concentrations as well as the extrapolated one give linear fits with a slope of –1. By SLS it was also possible to calculate the length of the A-3 cylindrical micelles. In Figure 4.14, *R*q/Kc* is plotted against *q*. The intercept of the extrapolated curve directly gives a value which corresponds to M_w/l. Since the molecular weight of the micellar aggregates M_w was known from the Zimm plot, the length of the cylindrical micelles *l* was calculated to be 190-240 nm. From AFM, (Figure 4.15 b) the thickness of the cylinders was calculated to be approximately 75 nm.

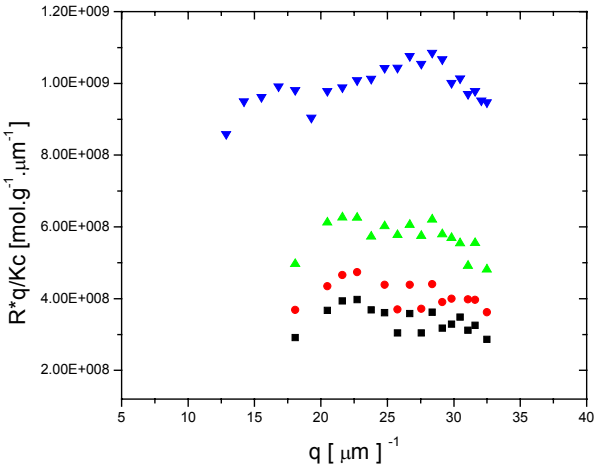

Figure 4.14: *Determination of the length of the cylindrical micelles formed by A-3 in cyclohexane by LS. The intercept of the extrapolated plot (black squares) directly gives Mw/l* ($1.016*10^8$ *g* mol^{-1} μm^{-1}).

The different micellar morphologies were visualised by AFM, which confirmed the results obtained by LS. In Figure 4.15 AFM micrographs of spherical micelles formed by A-2 and cylindrical micelles formed by A-3 in cyclohexane are presented.

(a)

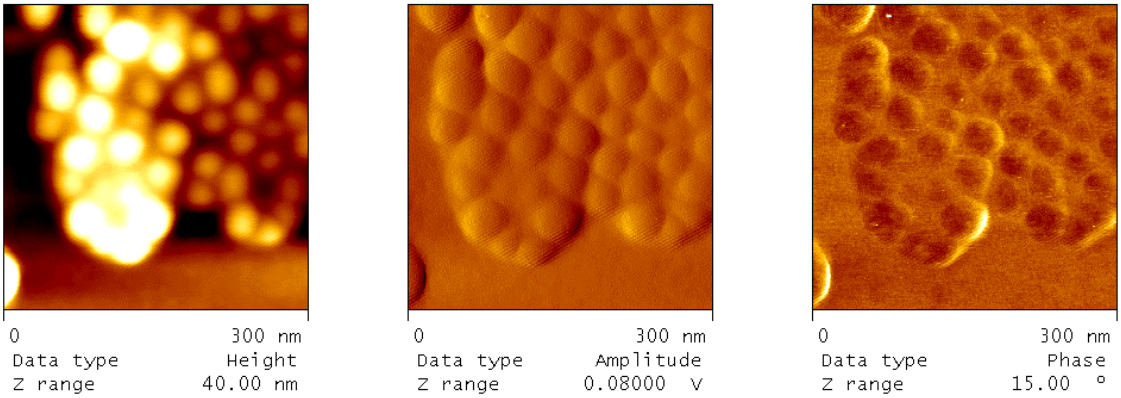

(b)

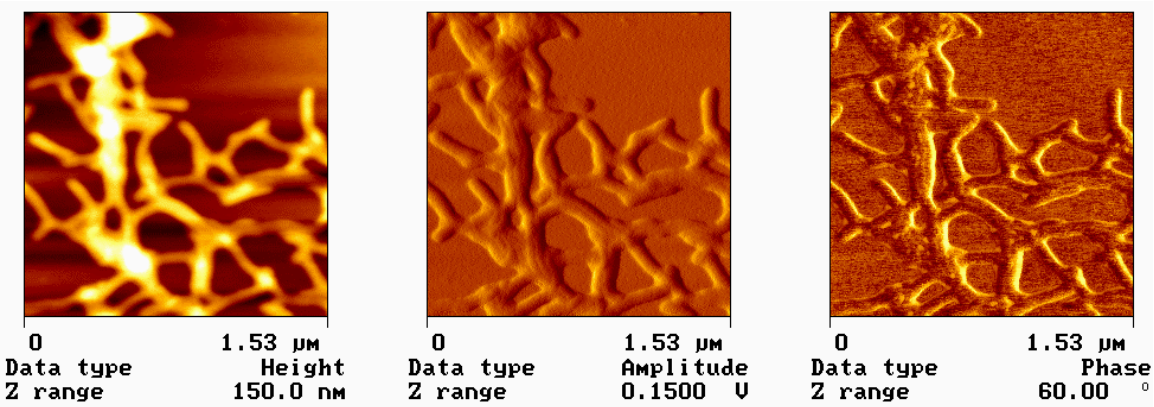

Figure 4.15: *AFM micrographs of: (a) spherical micelles of pBuMA$_{342}$-b-pAEMA$_{39}$ (A-2) and (b) cylindrical micelles of pBuMA$_{74}$-b-pAEMA$_{60}$ (A-3) spin-coated from cyclohexane solution on a mica surface.*

Since all geometrical parameters characterising these micelles were determined, we could proceed and calculate the core radii, the dimensions of the micellar coronas and the interchain distances of the block copolymer chains at the core/corona interface.

The core radius R_c, can be calculated using equation 4.2:

$$R_c = \left(\frac{3}{4\pi} Z N_A \upsilon_o \right)^{1/3} \qquad (4.2)$$

υ_o is the molar monomer volume and is equal to $m_o/\rho_o N_L$, where m_o is the monomer molecular weight, ρ_o the bulk density and N_L Avogadro`s number. With given Z and R_c, the

interchain distance *b* between neighbouring chains in the core/corona interface can be calculated as:

$$b = \left(\frac{4\pi R_c^2}{Z} \right)^{1/2} \tag{4.3}$$

The dimensions of the micellar corona, D_h can be determined using equation 4.4:

$$D_h = R_H - R_c \tag{4.4}$$

In Table 4.5 R_c, D_h and *b* values corresponding to different micellar structures of pBuMA-*b*-pAEMAs formed in cyclohexane are summarised. The shape of the resulting micelles undergoes a phase transition from *spherical* to *elliptical* and finally *cylindrical* by increasing the molar fraction of the pAEMA block within the micelle. This phenomenon was often observed by many groups investigating the effect of different block length ratios on the shape of the resulting aggregates[109,110,111].

Table 4.5: *R_c, D_h and b values corresponding to different micellar structures formed by a series of pBuMA-b-pAEMAs with different block length ratios in cyclohexane.*

Polymer ID	R_c (nm)	b (nm)	D_h (nm)	f_{AEMA}	Shape of micelles
A-2	9.97	1.91	22.03	0.10	Spherical
A-5	8.60	1.7	22.40	0.13	Spherical
A-4	3.97	1.46	7.02	0.15	Spherical
A-1	5.63	1.82	6.37	0.22	Elliptical

Comparing the *b* values calculated for the pBuMA-*b*-pAEMA micelles in cyclohexane with the ones corresponding to the pS-*b*-p4VP amphiphilic micelles (b = 2.73 – 3.03 nm) in toluene we observe a significant decrease in the interchain distance for the first system. Once more, this demonstrates the strong segregation behaviour of pBuMA-*b*-pAEMA block copolymer systems and the increased density of grafted polymer chains along the surface.

As a consequence, a question rises: What is the driving force that brings the individual polymer chains in such proximity within a micelle in this specific system? A possible explanation, besides the high interaction parameter χ existing between BuMA/AEMA which favours strong segregation, might also be the existence of specific interactions between the adjacent β-dicarbonyl groups. As mentioned previously, hydrogen bonding is likely to occur in this case. In the section that follows a more detailed investigation concerning H-bond interactions between the β-dicarbonyl side chains of pAEMA is presented.

4.3 H-bond interactions between adjacent β-dicarbonyl segments in pAEMA

Hydrogen bonding is a directional electrostatic interaction, involving strong dipole-dipole attractions caused by the electron-withdrawing properties of an electronegative atom (for example F, O, N) bound to hydrogen atoms. According to the literature[98,99] such interactions exist in β-dicarbonyl groups. The β-diketo enols provide examples of resonance-assisted intra and intermolecular O-H----O=C hydrogen bonding.

Our target was to investigate whether such interactions existed between adjacent β-dicarbonyl groups in pAEMA, found in the keto form (which is highly favoured (92%) as shown in ^{1}H NMR -see 4.1-). If so, this could be another explanation (apart from χ~0.8) for the very strong segregation behaviour observed for pBuMA-*b*-pAEMA block copolymer systems in selective solvents (see 4.2).

NMR spectroscopy was extensively used throughout this investigation. Two model compounds were chosen: acetyl acetone and ethyl acetoacetate. Our attention was focused on the signals in ^{1}H and ^{13}C NMR, corresponding to the $-CH_2$ group located between the two carbonyl units in the β-dicarbonyl moiety. If H-bonding in pAEMA occurs, we would expect that it takes place between these protons and one carbonyl group of an adjacent β-dicarbonyl unit as depicted in Figure 4.16.

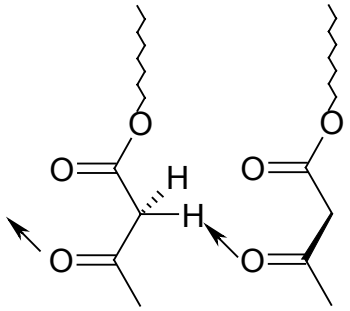

Figure 4.16: *H-bonding occurring between adjacent β-dicarbonyl units in pAEMA.*

Initial investigations were carried out in $CDCl_3$. ^{1}H and ^{13}C NMR spectra were obtained for acetyl acetone, ethyl acetoacetate, AEMA and finally pAEMA. An overview of all NMR results concerning the group of interest is given in Table 4.6.

Table 4.6: *^{1}H and ^{13}C NMR data corresponding to the chemical shifts of the $–CH_2$ group located between the two carbonyls in the β-dicarbonyl moiety in different compounds ($CDCl_3$).*

	^{1}H NMR		^{13}C NMR	
Acetyl acetone	3.6	-	58.5	-
Ethyl acetoacetate	-	3.45	-	50.1
AEMA	-	3.45	-	50.2
pAEMA	3.7	-	-	50.2

Figure 4.19 illustrates the **2-D HSQC (Heteronuclear Single-Quantum Correlation)** and **2-D HMBC (Heteronuclear Multiple Bond Correlation)** NMR experiments. The first one allows obtaining a 2-D heteronuclear chemical shift correlation map between directly bonded ^{1}H and X-heteronuclei (commonly, ^{13}C and ^{15}N) *via* the large $^{1}J_{HX}$ coupling constant as shown in Figure 4.17.

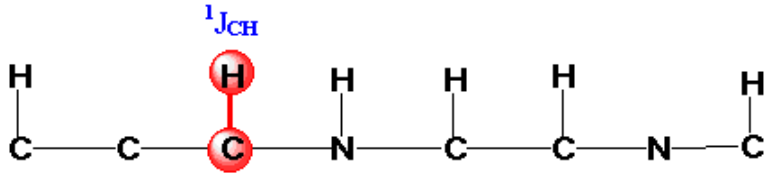

Figure 4.17: 2D *HSQC NMR experiment allowing to trace out directly bonded ^{1}H-X pairs (X = ^{13}C and ^{15}N) via the large $^{1}J_{HX}$ coupling constant.*

The 2-D HMBC experiment allows tracing out long-range (typically two and three bonds away) ^{1}H-X pairs *via* the small $^{n}J_{HX}$ coupling constant (Figure 4.18).

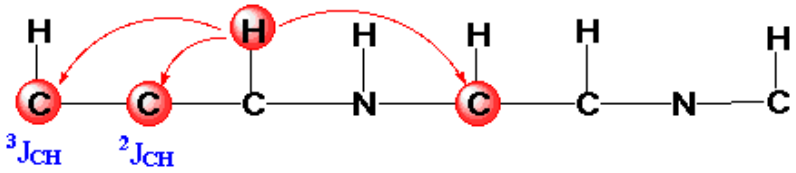

Figure 4.18: 2D *HMBC NMR experiment allowing tracing out long-range (typically two- and three-bonds away) ^{1}H-X pairs via the small $^{n}J_{HX}$ coupling constant.*

From the **2-D HSQC** spectrum it is clearly demonstrated that the -CH_2 protons of the β-dicarbonyl group found between the keto and the ester group appear around 3.7 ppm and they are connected to a carbon with a chemical shift of 50 ppm. The carbons next to them as shown in **2-D HMBC**, correspond to an ester (around 170 ppm) and a keto (200 ppm) group.

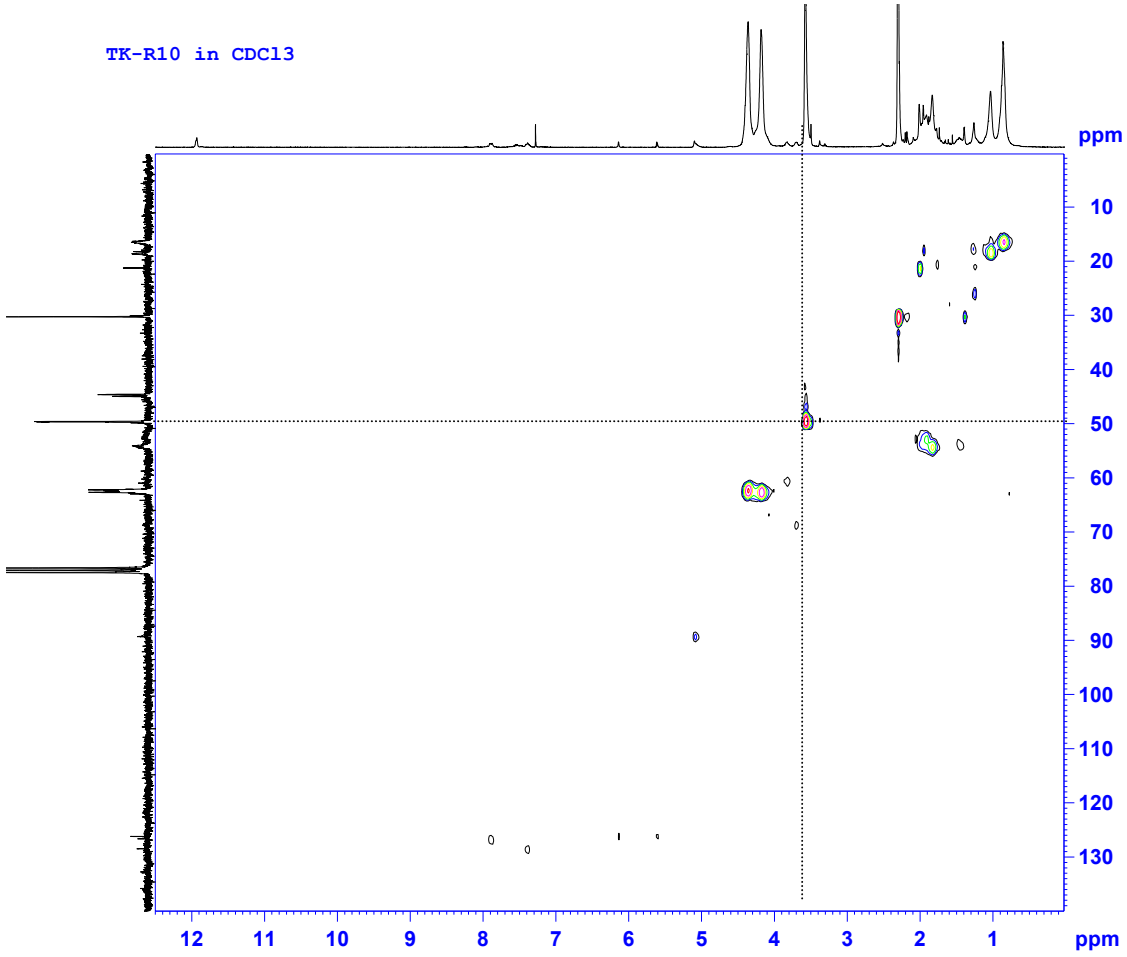

Figure 4.19a: *2-D HSQC (Heteronuclear Single-Quantum Correlation) NMR experiments for pAEMA in $CDCl_3$.*

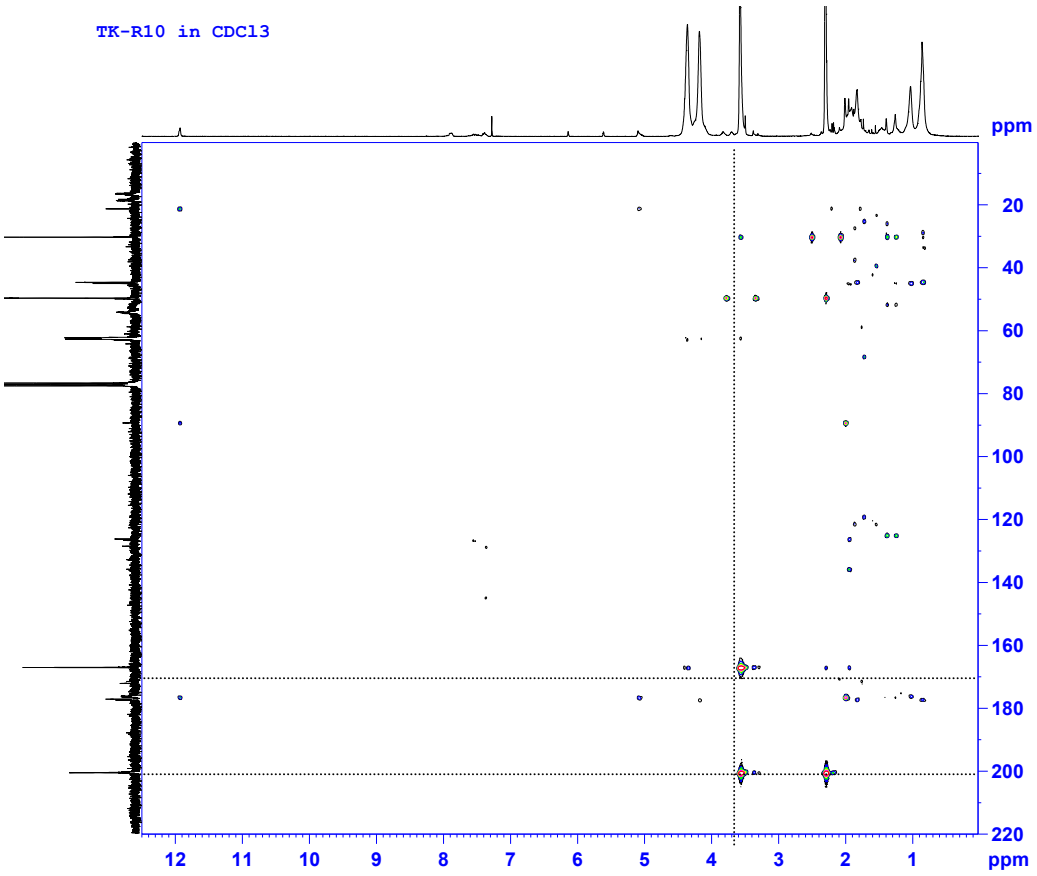

Figure 4.19b: *2-D HMBC (Heteronuclear Multiple Bond Correlation) NMR experiments for pAEMA in $CDCl_3$.*

From the above results interesting observations can be derived:

(a) As expected, the chemical shifts in ^{1}H and ^{13}C NMR of AEMA are very similar to those of ethyl acetoacetate.

(b) Surprisingly, the chemical shift of the $-CH_2$ protons located between the keto and the ester group in the β-ketoester moiety resembles acetyl acetone in ^{1}H NMR, whereas the signal of the corresponding carbon appears at the same chemical shift as in ethyl acetoacetate and AEMA in ^{13}C NMR. In acetyl acetone, due to the presence of two carbonyls which are strong electron-withdrawing groups (stronger than esters), the chemical shifts in ^{1}H and ^{13}C NMR appear more downfield (3.6 and 58.5 ppm), compared to those in ethyl acetoacetate (3.45 and 50 ppm). This indicates that, the protons located between the keto and the ester group in a β-ketoester functionality of pAEMA are affected by an electron-withdrawing group found in their proximity, which makes them more acidic than they should really be. We propose that

this effect results from H-bonding occurring between these protons and a carbonyl group of the adjacent β-ketoester moiety within the polymer chain.

In order to confirm the existence of these specific interactions, we proceeded further, employing TFA in our investigations, a sufficiently strong acid which is able to break H-bond interactions[112]. An upfield shift of the signal appearing at 3.7 ppm to 3.45 ppm in ^{1}H NMR upon TFA addition would have been a good indication for destroying H-bonding. Unfortunately, it was not possible to perform this experiment in $CDCl_3$. As reported in the literature, in order to break H-bonds in polypeptides, approximately a 25% TFA solution is required[112]. The problem is that TFA and $CDCl_3$ are immiscible. Mixing the two solvent results in phase separation with the polymer being preferentially solvated in the TFA phase. By measuring ^{1}H NMR of pAEMA in pure TFA-d_1, we noticed that the signals of the -CH_2 group in the β-ketoester completely disappeared. This experiment has shown that, these acidic protons can be easily exchanged by deuterium, *via* the enolate tautomer, which is present in a small percentage (6-8%) in solution and found in equilibrium with the keto form. The experiment was repeated in DMF-d_7, a solvent which is miscible with TFA. ^{1}H and ^{13}C NMR spectra were obtained for acetyl acetone, ethyl acetoacetate, AEMA and pAEMA. An overview of all NMR results in DMF-d_7 concerning the group of interest is given in Table 4.7.

Table 4.7: *^{1}H and ^{13}C NMR data corresponding to the chemical shifts of –CH_2 group located between the two carbonyls in the β-dicarbonyl moiety in different compounds (DMF-d_7).*

	^{1}H NMR		**^{13}C NMR**	
Acetyl acetone	3.74	-	57.9	-
Ethyl acetoacetate	-	3.65	-	49.6
AEMA	-	3.65	-	49.6
pAEMA	3.71	-	-	49.6
PAEMA + TFA	-	3.63	-	49.4

The addition of TFA (25% v/v) in pAEMA solution in DMF-d_7, caused an upfield shift of the signal corresponding to the -CH_2 (e) protons from 3.71 to 3.63 ppm, as we would have expected upon destruction of H-bond interactions (Figure 4.20). An upfield chemical shift was generally observed for all the signals, however the effect was larger for the protons of the

neighbouring groups (-CH_2, c and d and CH_3 f) of the β-dicarbonyl group and the largest one for the –CH_2 (e).

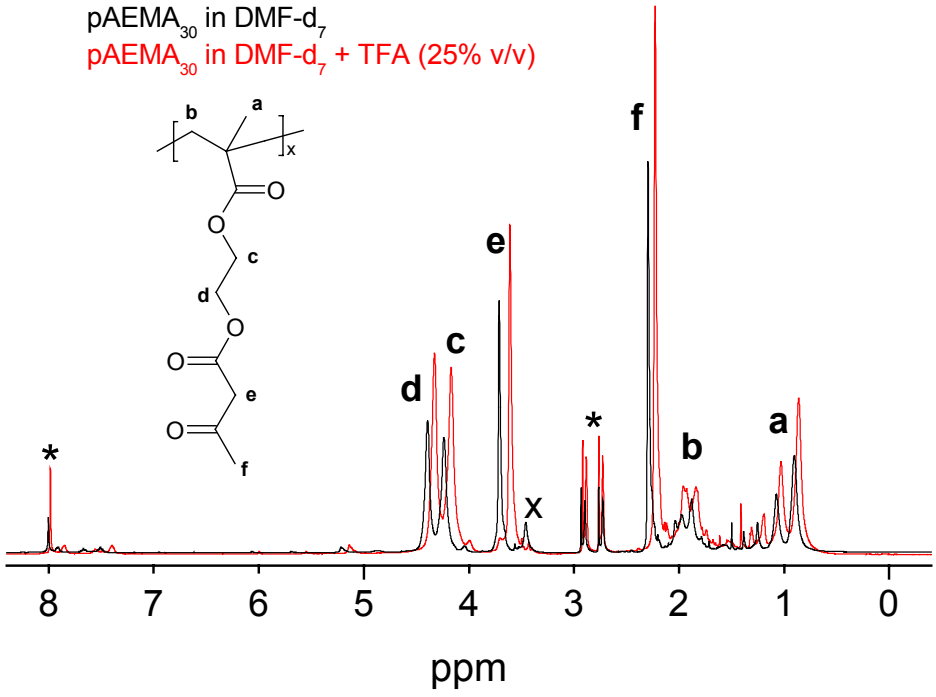

Figure 4.20: *^{1}H NMR spectra of pAEMA$_{30}$ in the absence and presence of TFA (25%. v/v) measured in DMF-d$_7$. * solvent, ^{x}H$_2$O traces in DMF-d$_7$.*

Comparing the IR spectra of pAEMA with that of AEMA we observed no significant differences. The only minor difference is that at 1600 – 1650 cm^{-1} a sharp signal corresponding to the carbonyl group of the β-ketoester appears in AEMA whereas a "shoulder" is present in the spectrum of the polymer (Figure 4.21). This difference might be another indication for the existence of H-bond interactions in pAEMA.

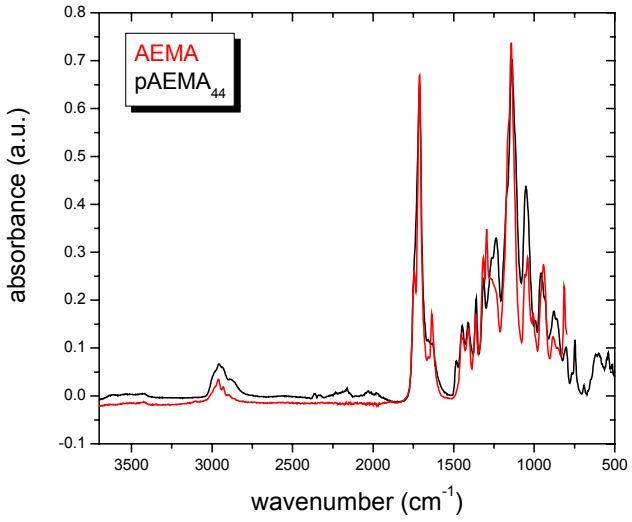

Figure 4.21: *IR spectra of AEMA and pAEMA.*

After placing a drop of a pAEMA solution in THF on graphite followed by solvent evaporation, cylindrical superstructures (fibrils) (~ 10 nm diameter, length: several 100 nm to > 1 µm) were visualised by AFM. A closer look at these structures revealed a helical "sense" (left and right handed) (Figure 4.22 b). However their size was quite large to correspond to a helical structure formed by a single polymer chain. We assume that initially, structures resembling *β*-sheets found in proteins are formed *via* intermolecular H-bonding between *β*-dicarbonyl moieties within different polymer chains. These *β*-sheets may tend to tilt and form "barrel-like" morphologies (left and right handed). Self-assembly of peptides *via* intermolecular H-bonding resulting in the formation of *β*-sheets, which then tilted to produce peptide nanotubes, was also reported in the literature[112a]. A schematic representation of the "barrel-like" morphology is illustrated in Figure 4.22a.

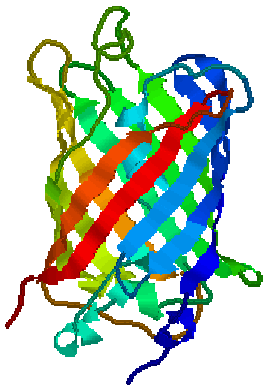

Figure 4.22a: *Schematic representation of "barrel-like" superstructures resulting from tilting of peptides` β-sheets.*

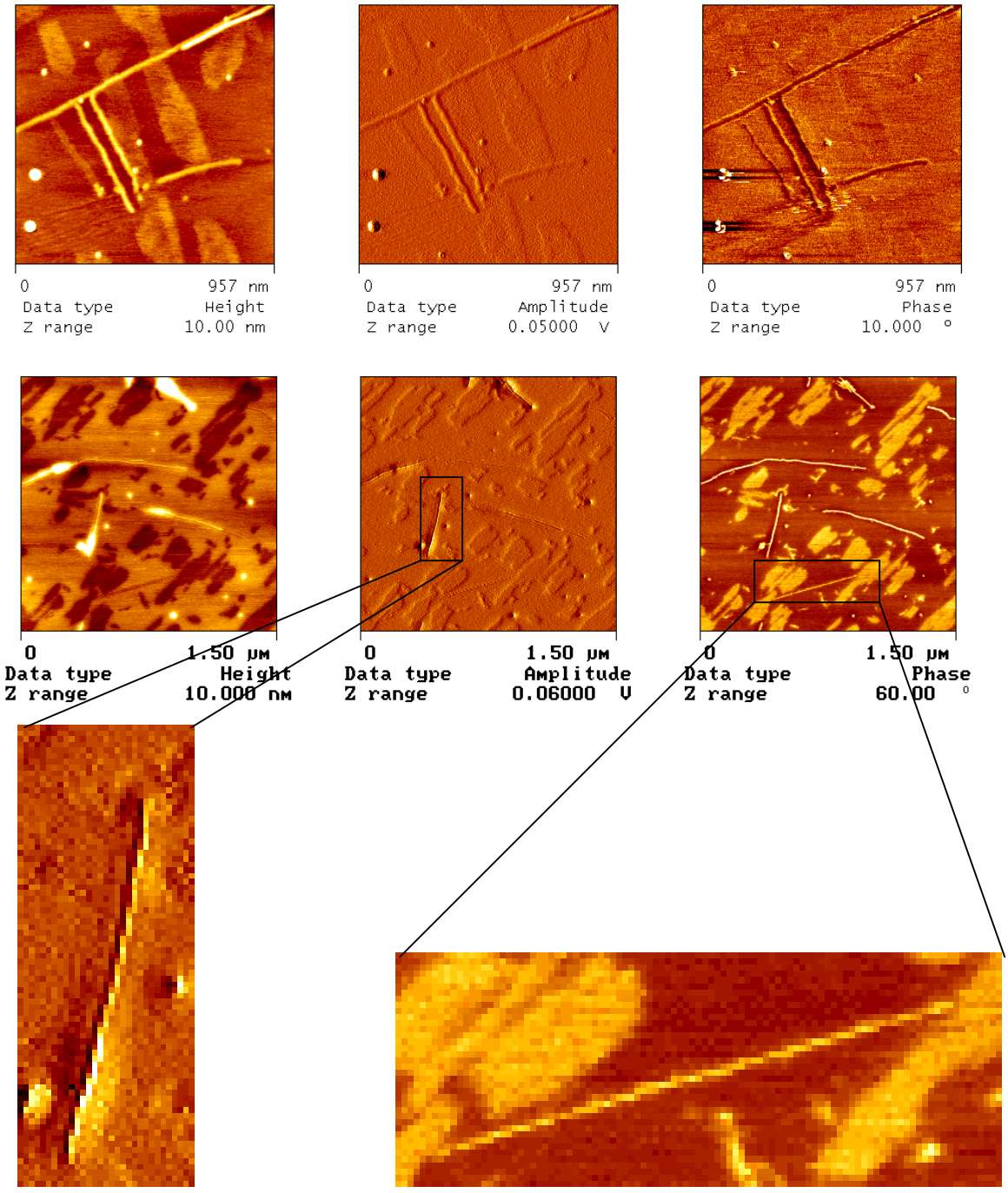

Figure 4.22b: *AFM micrograms of "barrel-like" superstructures of pAEMA observed on graphite.*

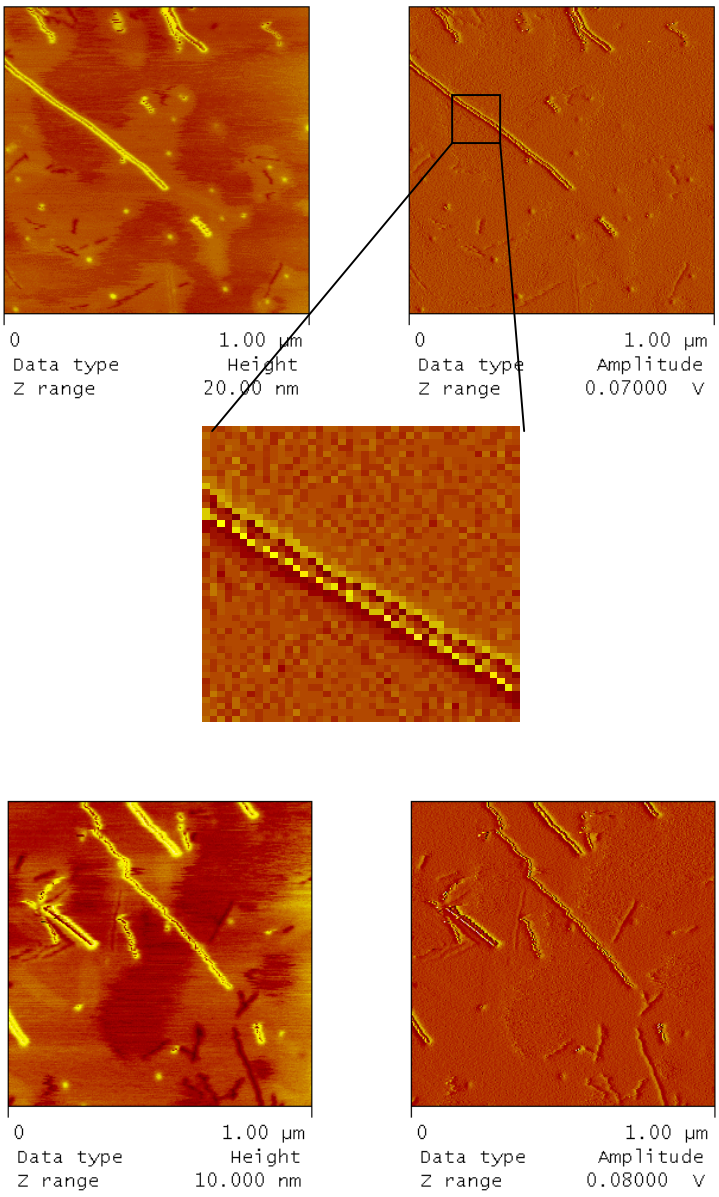

Figure 4.22c: *AFM micrograms of superstructures of pAEMA observed on graphite exhibiting a globular morphology (developed after aging)*

With time (approximately 2 days), the development of globular morphologies was observed as shown in Figure 4.22 c. It might be possible that a phase transition occurred from the "barrel-like" to the more entropically favourable globular morphology. The latter may result from intramolecular H-bonding within the same chain. Theoretical calculations of the dimensions of a single globule that could be formed *via* intramolecular H-bonding in a single polymer chain (approximately 3 nm) were found in agreement with the dimensions observed in AFM micrographs (Figure 4.22 c).

The formation of such superstructures by a non-chiral homopolymer could be only explained by the existence of specific interactions such as hydrogen bonding, which promotes structural organisation.

Furthermore, an effective dipole moment ($\mu_{eff.}$) of the AEMA unit in a pAEMA film was measured and found to be ~ $8.1*10^{-30}$ Cm (2.4 Debye). A detailed description is presented in APPENDIX I. This value lies between those reported for an oligomer of vinyl acetate (0.96 Debye per unit)[113], which basically describes the contribution of ester groups to the dipole moment, and those reported for peptides (3.5 Debye per unit)[113].

4.4 Aggregation Behaviour of Amphiphilic Block Copolymers with a β-Dicarbonyl Segment in the presence of inorganic metal salts in solution

So far, it has been demonstrated that pBuMA-*b*-pAEMA exhibit a micellisation behaviour of strongly segregated block copolymers in selective solvents. H-bond interactions that might occur between adjacent β-dicarbonyl moieties within the polymer chain may enhance the already strong segregation ($\chi \sim 0.8$). Moreover, such polymers bearing metal-ligating functionalities are expected to show interesting behaviour in the presence of transition-metal ions of different geometries and oxidation states.

Standard block copolymers are low surface-energy materials[2]. Therefore, adhesion between metals and polymers is usually poor. The incorporation of inorganic materials into polymeric domains is possible through specific interactions such as dipolar interactions, hydrogen- or covalent bonding and complex formation[2].

The ability of pBuMA-*b*-pAEMAs to complex and solubilise different metal-ion salts in organic media is attributed to the presence of the strong bidentate β-dicarbonyl groups. As already mentioned, two tautomeric forms of the dicarbonyl unit, the keto and the enol, exist in equilibrium. Both are capable of complexing transition metal ions[114]. β-Diketones are mostly considered as potential ligands due to their enolising ability[61].

For the systems investigated in this study, (pAEMA and pBuMA-*b*-pAEMA), ^{1}H NMR spectra in $CDCl_3$ presented in 4.1, show that the keto tautomer is the dominant one (92%). In order to shift the equilibrium towards the enolate form, the addition of a base is necessary. Triethylamine was sufficiently strong to abstract a proton from the β-dicarbonyl moiety resulting in the formation of the enolate anion. As it will be discussed in more detail, the keto tautomer can substitute "L" ligands, for example H_2O molecules (Figure 4.23 a). On the other hand only the enolate anion, a strong bidentate "X" ligand, can easily replace acetate (AcO^-) or chloride (Cl^-) substituents on a metal ion salt (Figure 4.23 b).

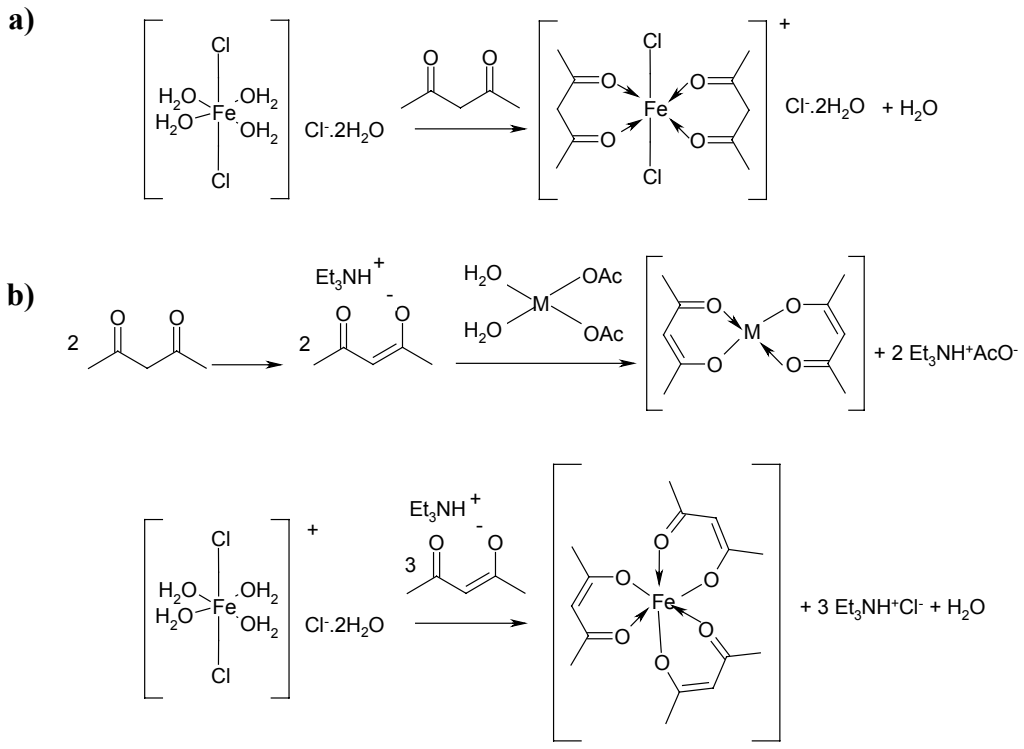

Figure 4.23: *(a) Substitution of "L" type of ligand molecules (H_2O) in $FeCl_3{\cdot}6H_2O$ by the "keto" form of β-dicarbonyl group. (b) Formation of the enolate anion of the β-dicarbonyl moiety in the presence of a strong base (Et_3N); subsequent replacement of the "X" type of acetate or chloride ligands.*

In the present work different metal ion salts bearing H_2O, Cl^- or AcO^- ligands were used in complexation studies with pBuMA-*b*-pAEMA, carried out in cyclohexane, benzene or chloroform. These were $FeCl_3$, $FeCl_3{\cdot}6H_2O$, $Cu(Ac)_2.xH_2O$, $Pd(Ac)_2$ and $Co(Ac)_2.xH_2O$.

Initial studies on the ability of pBuMA-*b*-pAEMAs to complex and solubilise inorganic metal salts in hydrophobic media were carried out by simply mixing a micellar solution of $pBuMA_{342}$-*b*-$pAEMA_{39}$ in cyclohexane (see 4.2) with $FeCl_3{\cdot}6H_2O$ at room temperature. Even though the salt was completely insoluble in this particular solvent, solubilisation assisted by the ligating block copolymer (dissolution in the micellar core) was readily obtained. This was accompanied by a colour change of the solution from colourless to wine red (Figure 4.24), which confirmed the formation of a polymer-metal complex.

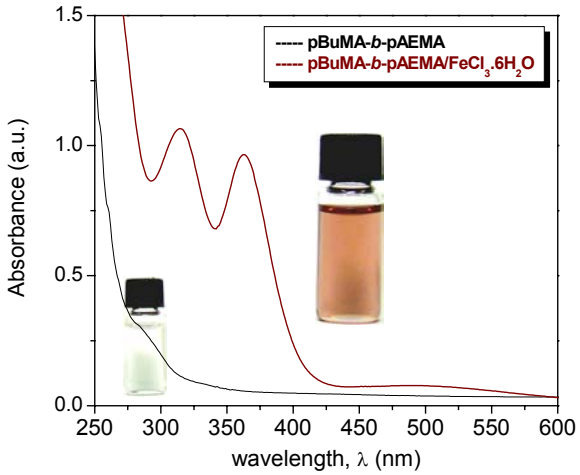

Figure 4.24: *UV-Vis spectra of $pBuMA_{342}$-b-$pAEMA_{39}$ and $pBuMA_{342}$-b-$pAEMA_{39}$ /$FeCl_3.6H_2O$ complex formed by the keto form of β-dicarbonyl ligands in cyclohexane.*

An attempt to complex and solubilise $FeCl_3$ following the same procedure was unsuccessful. No HCl evolution was observed, which would have been the case if the Cl ligands could be substituted by the *β*-dicarbonyl ones. This experiment indicated that in the case of $FeCl_3 \cdot 6H_2O$ complexation occurred only *via* substitution of the H_2O ligands by the keto *β*-dicarbonyl groups (as shown in Figure 4.23 a). Replacement of the Cl substituents is not possible under these conditions. However, addition of a small amount of H_2O/MeOH in a stirred suspension of $FeCl_3$ and the polymer in cyclohexane, resulted in a colour change of the dispersion to red/purple. Presumably, the presence of water in the system causes the transformation of $FeCl_3$ to $FeCl_3 \cdot 6H_2O$. Since substitution of the water ligands is now possible *via* the keto form, complexation occurs.

The addition of Et_3N in a suspension of $FeCl_3 \cdot 6H_2O$ in a cyclohexane solution of $pBuMA_{342}$-*b*-$pAEMA_{39}$ resulted in complexation, this time due to the substitution of not only the water molecules, but also of the Cl^- by the enolate anion. In this case, coordination occurs in a bidentate manner *via* the oxygen atoms and the carbonyl groups of the enolate anion as depicted in Figure 4.23 (b). The coordination geometry is then characterised as a slightly distorted octahedron[115]. Substitution was accompanied by a simultaneous colour change of the solution to deep orange (Figure 4.25) and formation of a white precipitate ($Et_3NH^+Cl^-$).

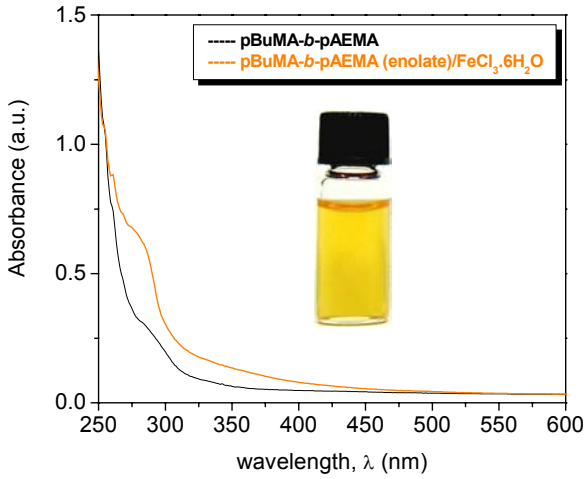

Figure 4.25: *UV-Vis spectra of $pBuMA_{342}$-b-$pAEMA_{39}$ and $pBuMA_{342}$-b-$pAEMA_{39}$ /$FeCl_3 \cdot 6H_2O$ complex formed by the enolate form in cyclohexane.*

Reports of Mastrorilli *et al.*[115] supporting that substitution of the Cl ligands with AEMA in $RuCl_2(PPh_3)_3$ could only be achieved with the deprotonated form of the *β*-dicarbonyl functionality, underline the above results.

Similarly, metal-ion salts with acetate substituents could be complexed and solubilised in cyclohexane only by the enolate anion (Figure 4.23 b), formed by adding Et_3N to the micellar solution of pBuMA-*b*-pAEMA in cyclohexane. In Figure 4.26 UV-*Vis* spectra of the complexes of $pBuMA_{342}$-*b*-$pAEMA_{39}$ with $Cu(Ac)_2.xH_2O$, $Pd(Ac)_2$ and $Co(Ac)_2.xH_2O$ measured in cyclohexane are presented. It is important to emphasise that all changes observed in these spectra compared to that of the "uncomplexed" polymer correspond to the polymer/metal complex, and the presence of any uncomplexed salts is excluded, since the latter are completely insoluble in cyclohexane. Upon metalation of the micelles, transparent coloured solutions were obtained, indicating the formation of polymer-metal complexes. The colour of the solutions varied from green (polymer/Cu (II)) to yellow (polymer/Pd(II)) and pink (polymer/Co(II)) (Figure 4.26). Analogous observations concerning the colours of the resulting metal/acetyl acetone complexes are reported in the literature[62,116,117]. Upon complexation, an insoluble white powder, namely triethylammonium acetate was precipitated.

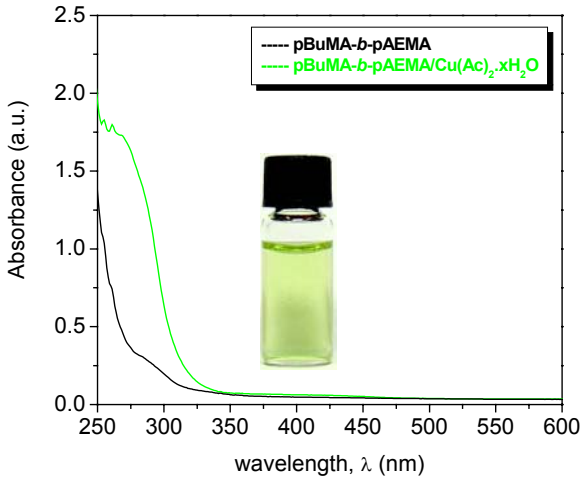

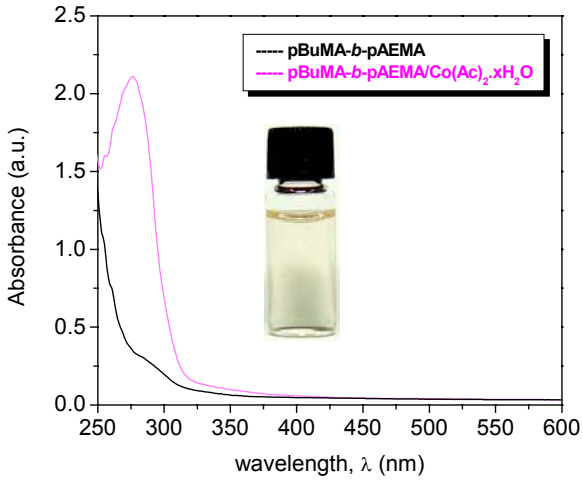

(c)

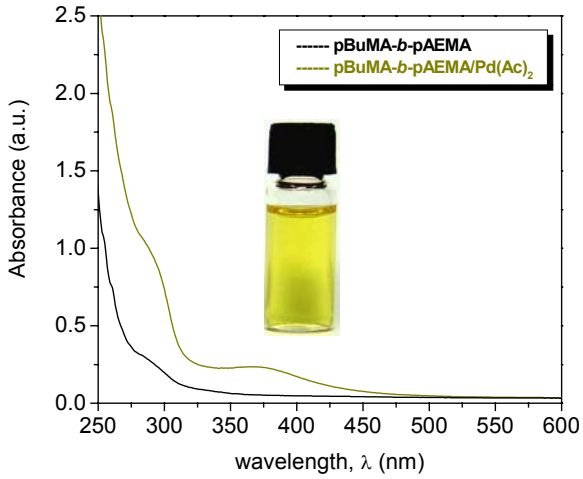

Figure 4.26: *UV-Vis spectra of $pBuMA_{342}$-b-$pAEMA_{39}$ complexes with (a) $Cu(Ac)_2.xH_2O$, (b) $Co(Ac)_2.xH_2O$ and (c) $Pd(Ac)_2$ measured in cyclohexane.*

Considering what is known from the literature, the above polymer-metal complexes are expected to have a four-coordinated square planar geometry. As reported by Hanabusa and co-workers[66] metal-chelating β-diketonate units form square-planar bis(β-diketonate)copper(II) complexes with $CuCl_2.H_2O$ in the presence of NH_3. Furthermore, resemblance of the above spectra with those corresponding to analogous complexes of the same metal ions with acetyl acetone confirms the success of complexation. For example, it is known that the peak at 378 nm appearing in the UV-*Vis* spectrum of polymer/Pd(II) complex (Figure 4.26 c) is typical for Pd(II) complexes[67]. The whole spectrum resembles that of $Pd(ac)_2$ and $Pd(AEMA)_2$, suggesting a square-planar coordination geometry.

As it will be discussed in 4.4.1, the size of the micelles as determined by DLS, remains constant upon loading with a metal salt. Due to the different densities of organic and inorganic components, analytical ultracentrifugation (AUC) could provide information on the chemical composition of the polymer/metal colloids. As exemplarily shown in Figure 4.27, AUC sedimentation velocity runs confirm the successful loading of the polymeric micelles with the metal salt, the sedimentation coefficient distributions (g(S)) being shifted to higher S values. It is also apparent that the distributions of loaded and unloaded micelles exhibit the same shape, indicating that the salt is evenly distributed among the aggregates (even though the metal-ion salt is not soluble in cyclohexane and complexation is a heterogeneous process). Hence, there must exist a dynamic intermolecular exchange of salts between aggregates, indicating that these systems are in thermodynamic equilibrium.

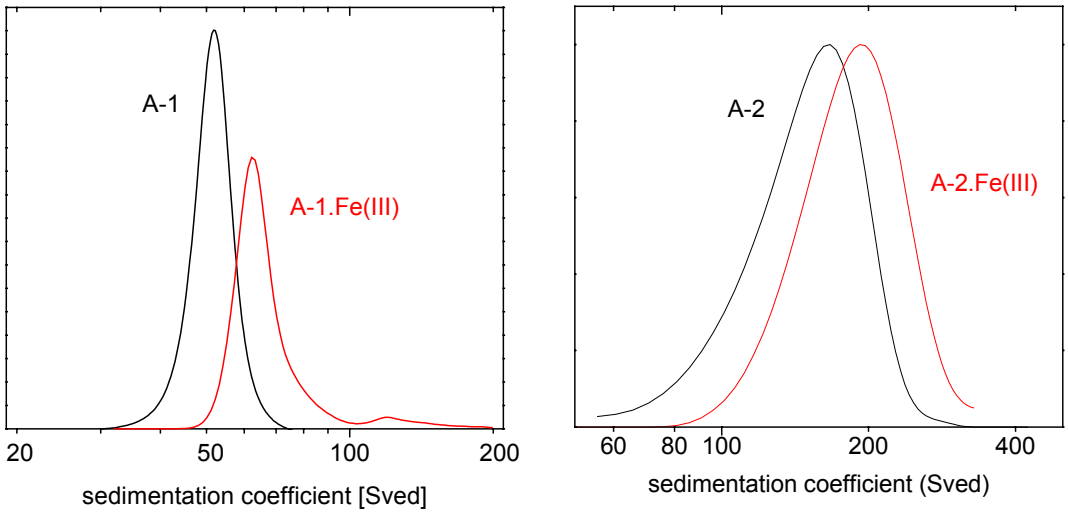

Figure 4.27: *Sedimentation coefficient distribution of A-1, A-2 and A-1.Fe(III), A-2.Fe(III) micellar solutions in cyclohexane ([Fe]/[AEMA] ≈ 0.5 and 0.33 respectively).*

4.4.1 Complexation of $FeCl_3 \cdot 6H_2O$ in hydrophobic media via the keto form of β-dicarbonyl units.

Compared to the number of publications existing on coordination block copolymers with O-, S- and N- containing ligands and polymer-metal complexes, less work has been reported concerning the effect of salt concentration on the aggregation behaviour of these polymers. Therefore, investigation was carried out using LS techniques, aiming to find out if any systematic relation existed between the aggregation behaviour of $pBuMA_{342}$-*b*-$pAEMA_{39}$ in cyclohexane and the amount of $FeCl_3 \cdot 6H_2O$ present in the system.

As discussed in 4.2, these amphiphilic block copolymers can already form micelles in cyclohexane. Addition of an inorganic metal-ion salt in this particular system results in micellar structures consisting of a pBuMA solvating corona and a pAEMA core loaded with the metal salt. However, it is also possible to induce micellisation upon salt addition, when the solubility of the metal binding segment of a block copolymer is reduced by complex formation with an inorganic metal salt. This was shown by Chernyshov and co-workers, who have reported the induced micellisation of *poly*(styrene)-*b*-*poly*(m-vinyltriphenylphosphine) diblock copolymers upon complexation of the triphenylphosphine groups of these polymers with palladium compounds[118].

Chloroform is a common solvent for both blocks in pBuMA-*b*-pAEMA copolymer systems. Therefore, no microphase separation occurs, and only unimers are present in solution as proved by LS and ^{1}H NMR. In LS the measured scattering intensity of polymer solutions in $CHCl_3$ was too low to correspond to any kind of micellar aggregates. (0.2 – 0.3 KHz, 488 nm, 0.3 W). ^{1}H NMR was therefore employed for investigating the induction of micellisation of $pBuMA_{342}$-*b*-$pAEMA_{39}$ (A-2) in $CDCl_3$ upon complexation of $FeCl_3 \cdot 6H_2O$. In Figure 4.28 (a) the ^{1}H NMR spectrum of A-2 in $CDCl_3$ is presented and all signals corresponding to the protons of both blocks can be visualised. Upon salt addition, the solution changes within a few seconds from colourless to deep wine red.

At the same time, the signals corresponding to the ligating pAEMA block disappear and the remaining ones (of the pBuMA block) become broader (Figure 4.28 b). These results clearly indicate that an increase in the selectivity of $CDCl_3$ for the pBuMA block due to complexation is the driving force for the formation of A-2.Fe(III) micelles in chloroform. Such micelles would consist of a pBuMA corona and a pAEMA core loaded with Fe(III). It is necessary to mention that these micellar aggregates are only stable in solution concentrations higher than 2%, due to the fact that $FeCl_3 \cdot 6H_2O$ alone is soluble in chloroform.

Therefore an excess of solvent (e.g concentrations of 0.5%) favours de-complexation. This is indicated by a colour change of the solution upon dilution, from wine red to yellow/orange (colour of $FeCl_3 \cdot 6H_2O$ in $CHCl_3$).

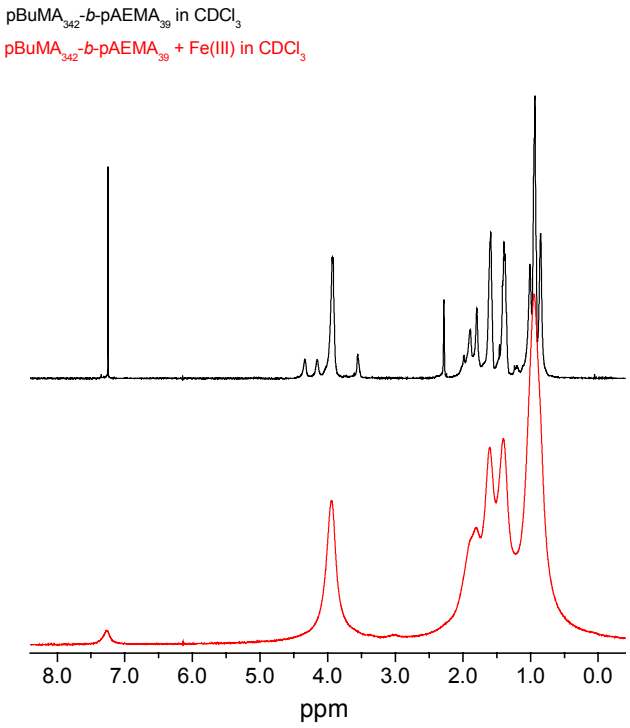

Figure 4.28: *(a) ^1H NMR of $pBuMA_{342}$-b-$pAEMA_{39}$ in $CDCl_3$ indicating the presence of unimers. (b) ^1H NMR of $pBuMA_{342}$-b-$pAEMA_{39}$ complexed with $FeCl_3 \cdot 6H_2O$ ([Fe]/[AEMA] = 0.33) in $CDCl_3$: micellisation is induced via complexation.*

After this small parenthesis, we return to investigate the already pre-existing micellar aggregates of $pBuMA_{342}$-*b*-$pAEMA_{39}$ in cyclohexane and how their structural characteristics are affected by increasing $FeCl_3 \cdot 6H_2O$ in the system. Keeping the polymer amount constant and varying the salt concentration, we would expect to see an effect on the aggregation behaviour of the block copolymer, at least in terms of aggregation numbers and interfacial areas. In Table 4.8 all data obtained by DLS and SLS in cyclohexane at 20 ^oC, for $pBuMA_{342}$-*b*-$pAEMA_{39}$ micelles loaded with different amounts of $FeCl_3 \cdot 6H_2O$ are summarised.

Table 4.8: *Data obtained by LS for spherical micelles of $pBuMA_{342}$-b-$pAEMA_{39}$ (A-2) loaded with different amounts of $FeCl_3 \cdot 6H_2O$ salt in cyclohexane.*

[Fe]/[AEMA]	R_H (nm)	R_g (nm)	$A_2 \times 10^{-8}$ (mol mL/g^2)	Z	D_h (nm)	R_c (nm)	b^2 (nm^2)
0	32	26	0.15	342	22	10	3.4
0.10	40	32	0.14	331	30	10	3.6
0.25	33	29	0.092	274	24	9	4.1
0.33	33	28	0.094	269	23	9	4.3
0.45	31	27	0.13	297	21	10	4.4
0.60	30	27	0.11	266	20	10	4.8
0.85	28	24	-0.061	207	18	10	5.7

[Fe]/[AEMA] represents the molar ratio of salt to β-dicarbonyl ligands. R_H was found to be independent of different measuring angles and solution concentrations, which indicated monodisperse systems. R_g, A_2 and Z were calculated from SLS using a typical Zimm plot (see APPENDIX II). The core radius R_c and the area per molecule at the core/corona interface, b^2 were calculated using equations 4.2 and 4.3. To calculate Z, we considered the molecular weight for each individual chain loaded with the ferric salt as the sum of the molecular weight of the block copolymer and the product $39 * MW_{FeCl_3 \cdot 6H_2O} *ratio([Fe]/[AEMA])$ which corresponds to the mass of the loaded Fe(III) salt. The refractive index increment dn/dc was measured for each individual system and plotted against [Fe]/[AEMA]. The linear fit obtained (see APPENDIX II) was used in the evaluation of aggregation numbers. Usually, by increasing the amount of an inorganic metal salt within a micelle, we would also expect an increase in aggregation numbers. The reason is that complexation of an inorganic material with one of the blocks usually increases incompatibility between the two blocks, thus resulting in stronger segregation. The same effect is expected for the area per molecule at the core/corona interface: more salt "trapped" within the micelle, causes "swelling" of the micellar core and hence enlargement of the interfacial areas, b^2.

Surprisingly, as shown in Figure 4.29 (a) Z follows an opposite behaviour from the expected one: it systematically **decreases**, with increasing amount of $FeCl_3 \cdot 6H_2O$. On the other hand, b^2 is increasing as expected (Figure 4.29 b).

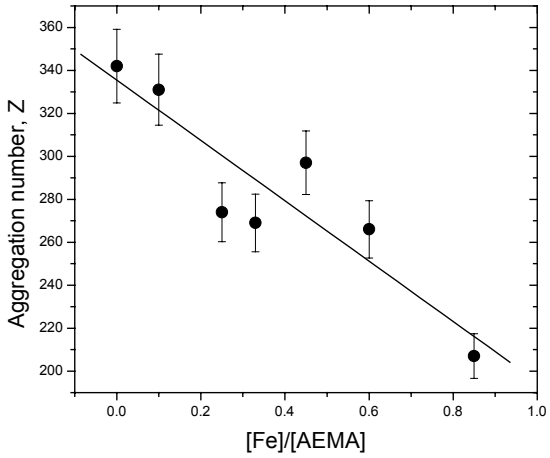

(b)

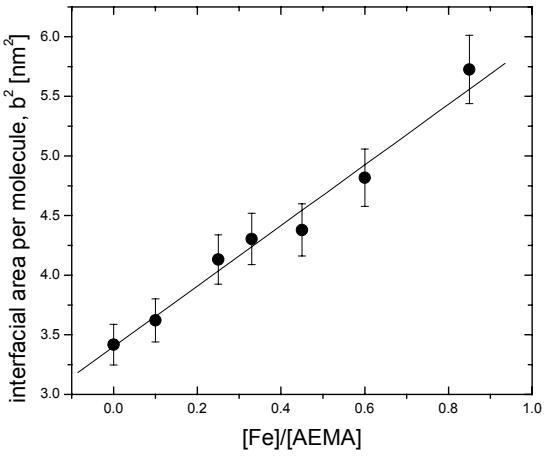

Figure 4.29: *Systematic change in aggregation behaviour of A-2 in the presence of different amounts* of $FeCl_3 \cdot 6H_2O$*: (a) significant decrease in the aggregation number with increasing [Fe]/[AEMA] (Estimated error: Z± 5%). (b) increase of the interfacial area per molecule at the core/corona interface with increasing [Fe]/[AEMA].*

As discussed in 4.3, H-bonding occurring between adjacent *β*-dicarbonyl units in pAEMA, increase incompatibility between the two blocks, resulting in very strong segregation behaviour of pBuMA-*b*-pAEMA block copolymer systems in cyclohexane (see 4.2). We propose that this unusual behaviour is attributed to the fact that the addition of $FeCl_3 \cdot 6H_2O$ destroys these H-bond interactions, due to the higher affinity of the dicarbonyl moiety for metal ions rather than for protons. Complexation of Fe(III) seems to decrease incompatibility between the two blocks compared to the unloaded system, which automatically results in a weaker segregation behaviour. As it will be discussed in 4.4.2, when complexation occurs *via* the enolate anion of the *β*-dicarbonyls, the expected aggregation behaviour is observed, i.e.

Z increases systematically with increasing salt concentration in the system. The difference in this case is that no H-bond interactions exist between β-dicarbonyl moieties found in the enolate anion form. From the data presented in Table 4.8, concerning R_H, R_g as well as the core radius R_c, it can be seen that upon loading, the size and shape of the micellar aggregates remain basically unchanged (the ratio R_g/R_H remains constant, around 0.8, a characteristic value for hard spheres). This is also confirmed by AUC experiments, carried out for micellar solutions of $pBuMA_{342}$-*b*-$pAEMA_{39}$ loaded with $FeCl_3 \cdot 6H_2O$ (Figure 4.30).

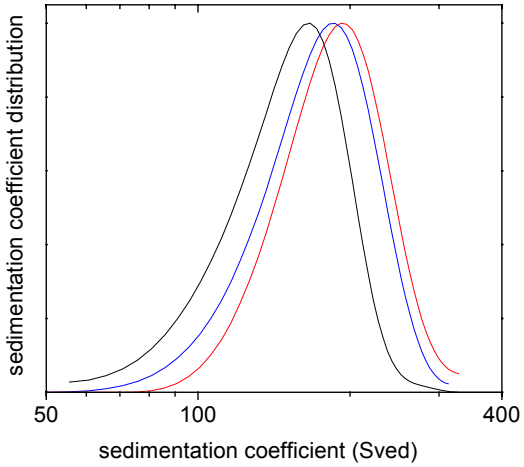

Figure 4.30: *Sedimentation coefficient distribution of A-2 and A-2.Fe(III) micellar solutions in cyclohexane: A-2 (unloaded), black line; A-2.Fe(III) ([Fe]/[AEMA] = 0.33 and 0.5 blue and red lines respectively).*

In Figure 4.31, the AFM micrographs of spherical block copolymers micelles of $pBuMA_{342}$-*b*-$pAEMA_{39}$ loaded with $FeCl_3 \cdot 6H_2O$ in cyclohexane are presented.

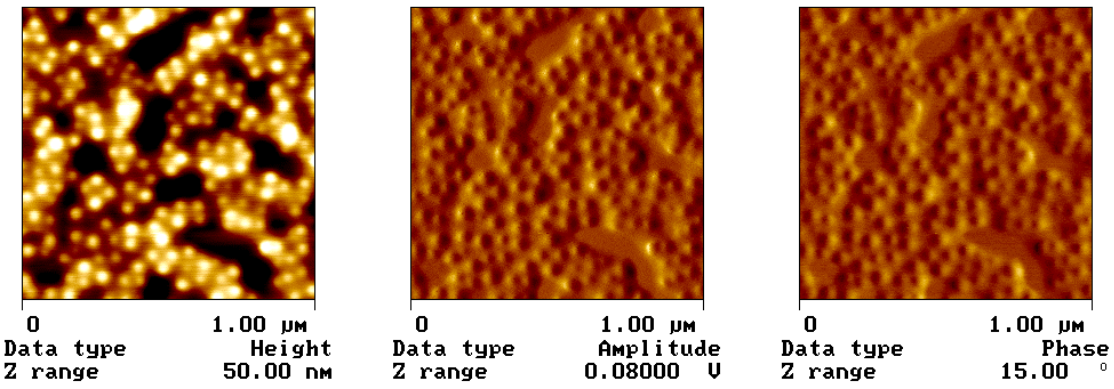

Figure 4.31: *AFM micrographs of $pBuMA_{342}$-b-$pAEMA_{39}$ spherical micelles, loaded with $FeCl_3 \cdot 6H_2O$ in cyclohexane (spin-coating on mica).*

These hybrid organic-inorganic colloidal aggregates are highly stable in cyclohexane solution at various salt concentrations. However, when the [Fe]/[AEMA] molar ratio is around 1, these aggregates tend to coagulate and precipitate. Observing A_2 values in Table 4.8, we can see that this coagulation already starts at [Fe]/[AEMA] = 0.85 (negative A_2 values, indicating the presence of strong attractive forces between the aggregates).

4.4.2 Complexation of $FeCl_3 \cdot 6H_2O$ and $Pd(Ac)_2$ in hydrophobic media via the enolate form of β-dicarbonyl units.

Complexation of $pBuMA_{342}$-*b*-$pAEMA_{39}$ with $FeCl_3 \cdot 6H_2O$, $Pd(Ac)_2$, $Co(Ac)_2.xH_2O$ and $Cu(Ac)_2.xH_2O$ in cyclohexane was accomplished *via* the enolate anion of the *β*-dicarbonyl polymer segments. This was generated by the addition of triethylamine in the polymer solution. Even though the keto tautomer was able to complex and solubilise $FeCl_3 \cdot 6H_2O$ in cyclohexane due to the replacement of water molecules, this was not possible for salts bearing acetate ligands. In this case, the presence of the *β*-dicarbonyl moiety in the form of an enolate anion was necessary. The latter is strong enough to substitute the "X" type chloride and acetate ligands in $FeCl_3 \cdot 6H_2O$ and $M(Ac)_2$ or $M(Ac)_2.xH_2O$ salts. (see Figure 4.23).

Systematic investigations on the aggregation behaviour of $pBuMA_{342}$-*b*-$pAEMA_{39}$ in the presence of various $FeCl_3 \cdot 6H_2O$ concentrations and one of the acetate salts, $Pd(Ac)_2$, analogous to those already described in 4.4.1 were carried out in cyclohexane. Table 4.9 summarises all results obtained by LS (see APPENDIX II) in cyclohexane at 20 ^oC, for $pBuMA_{342}$-*b*-$pAEMA_{39}$ micelles loaded with different amounts of $FeCl_3 \cdot 6H_2O$ and $Pd(Ac)_2$.

Table 4.9a: *Data obtained by LS for spherical micelles of $pBuMA_{342}$-b-$pAEMA_{39}$ (A-2, enolate) loaded with different amounts of $Pd(Ac)_2$ in cyclohexane.*

[Pd]/[AEMA]	R_H (nm)	R_g (nm)	$A_2 \times 10^{-8}$ (mol mL/g^2)	Z
0	35	28	0.15	323
0.12	31	29	0.07	361
0.23	32	28	0.08	398
0.4	32	29	0.06	367
0.55	33	30	0.07	393

Table 4.9b: *Data obtained by LS for spherical micelles of $pBuMA_{342}$-b-$pAEMA_{39}$ (A-2, enolate) loaded with different amounts of $FeCl_3 \cdot 6H_20$ in cyclohexane.*

[Fe]/[AEMA]	R_H (nm)	R_g (nm)	$A_2 \times 10^{-8}$ (mol mL/g^2)	Z
0	35	28	0.15	323
0.35	45	50	0.22	412
0.52	58	69	0.03	784

By plotting Z *versus* [Pd]/[AEMA], we notice virtually no change in Z with increasing salt concentration. Additionally, the added amount of salt seems to have no effect on the micellar size (Figure 4.32).

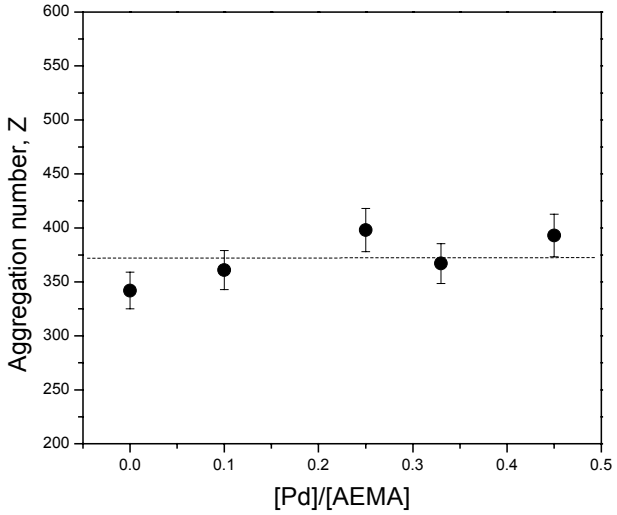

Figure 4.32: *Aggregation behaviour of A-2 (enolate) in the presence of different amounts of Pd(II): (a) virtually no change in aggregation number with increasing $Pd(Ac)_2$. (b) no change of the micellar size (R_g, R_H) upon loading (Estimated error: Z± 5%) .*

In Figure 4.33, AFM micrographs of relatively monodisperse spherical block copolymer micelles of $pBuMA_{342}$-*b*-$pAEMA_{39}$ (enolate) loaded with Pd(II) in cyclohexane is presented.

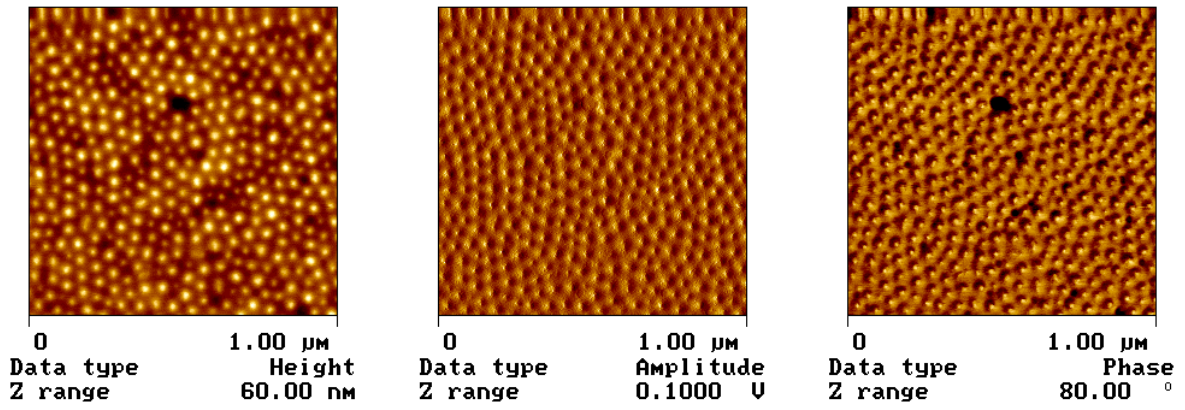

Figure 4.33: *AFM micrographs of $pBuMA_{342}$-b-$pAEMA_{39}$ spherical micelles, loaded with $Pd(Ac)_2$ in cyclohexane (drop of solution on graphite).*

In contrary, as Figure 4.34 (a) illustrates, aggregation number **increases** systematically with increasing salt amount in the case where A-2 found in its enolate form, complexes $FeCl_3 \cdot 6H_2O$. A reason for this different behaviour when complexation occurs either with Pd(II) or Fe(III) salts might be that the first, being a "group VIII soft" metal ion and having free *f* orbitals, can form bonds which are covalent in character. On the other hand, Fe(III), a more "hard" metal ion, favours the formation of electrostatic bonds. Loading the micellar core with larger amounts of the ferric salt, causes not only an increase in Z, but also a significant enlargement of the micelles (Figure 4.34 b).

(a)

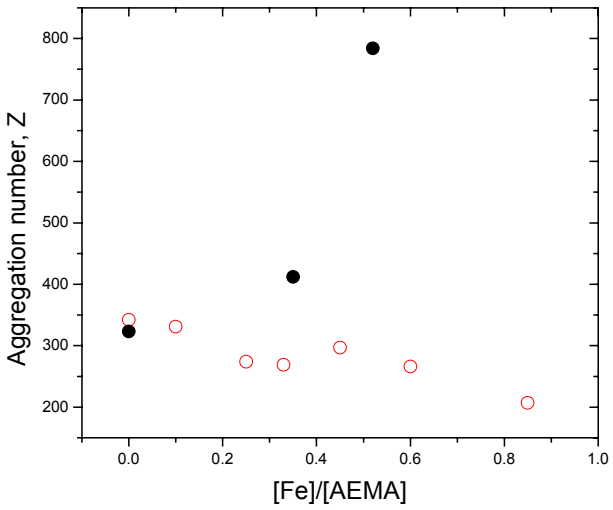

(b)

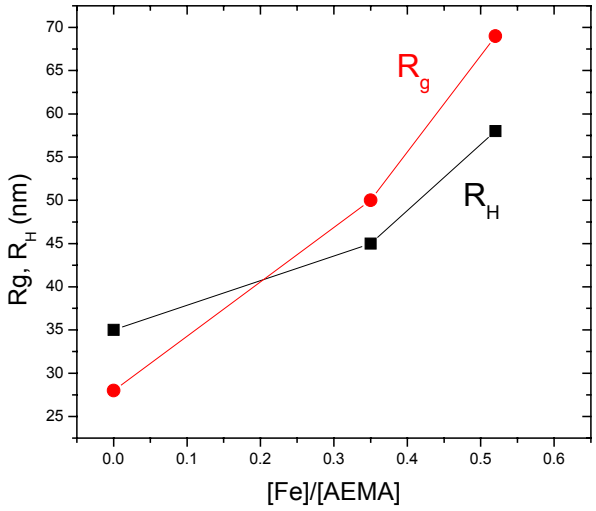

Figure 4.34: *Systematic change in aggregation behaviour of A-2(enolate) in the presence of different amounts of $FeCl_3 \cdot 6H_2O$: (a) significant increase in Z with increasing $FeCl_3 \cdot 6H_2O$. For comparison, Z is plotted against [Fe]/[AEMA] for A-2(keto)/Fe(III) (red circles). (b) increase of the micellar size (R_g, R_H) by increasing [Fe]/[AEMA].*

The most interesting observation was the differences in the aggregation behaviour of pBuMA-*b*-pAEMA found in either the keto or enolate form, in the presence of $FeCl_3 \cdot 6H_2O$. In Figure 4.34 (a), it is clearly demonstrated that the two systems behave differently. When complexation occurs *via* the enolate anion, Z increases systematically with increasing salt concentration. This is what is normally expected, since complexation of an inorganic material with one of the blocks usually increases incompatibility between the two blocks, resulting in stronger segregating systems. A decrease in Z could be explained if the formation of a polymer-metal complex was the reason for destroying some other specific interactions already pre-existing between the *β*-dicarbonyl units in the micellar core. Indeed, as presented in 4.2 and 4.3, H-bonding occurring between adjacent *β*-dicarbonyl units in pAEMA, increase incompatibility between the two blocks, resulting in very strong segregation behaviour of pBuMA-*b*-pAEMA (keto) block copolymer systems in cyclohexane.

Addition of $FeCl_3 \cdot 6H_2O$ causes destruction of these H-bonds, due to the higher affinity of the *β*-dicarbonyl moiety for metal ions rather than for protons. Complexation of $FeCl_3 \cdot 6H_2O$ decreases incompatibility between the two blocks compared to the unloaded system, which automatically results in weaker segregation behaviour. When the polymer is found in the

enolate anion form, this unusual behaviour is not observed upon loading, simply because there is no H-bonding existing in the first place.

4.4.3 Shape transition upon complexation in different solvent systems

It was demonstrated that $pBuMA_{342}$-*b*-$pAEMA_{39}$ forms spherical micelles in cyclohexane, which retain their spherical shape upon complexation of different metal salts. These micelles are highly stable in solution, regardless of the nature or amount of salt incorporated (up to approximately 1.1 molar ratio). In 4.2.1. it has been illustrated that the more symmetrical $pBuMA_{74}$-*b*-$pAEMA_{60}$ (A-3) block copolymer forms cylindrical micelles in cyclohexane. Since these micelles tend to coagulate, LS measurements were performed at very low concentrations (0.025%), at which the micelles were stable in solution. Loading this system with Fe(III) generated hybrid colloidal aggregates unable to remain in solution even at very low concentrations (Figure 4.35). The pBuMA block is not long enough to stabilise these aggregates in cyclohexane at room temperature.

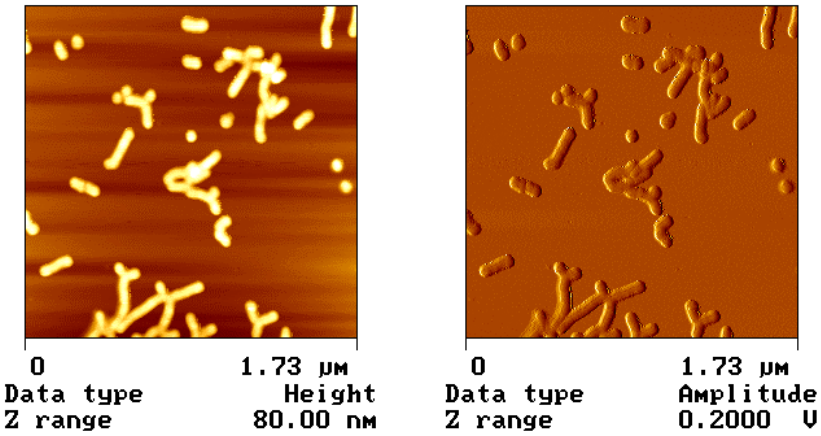

Figure 4.35: *AFM micrographs of coagulating A-3.Fe(III) micelles in cyclohexane (spin-coating on graphite).*

At higher temperatures, A-3.Fe(III) ([Fe]/[AEMA] = 0.33) micelles become more stable in solution. Time-dependence right-angle DLS measurements (107 in total, each of 600 seconds duration) performed at 50 – 60 ^{o}C, revealed that initially very large aggregates are present in solution. With time, the intensity of this signal decreased whereas a simultaneous appearance and increase of a signal corresponding to smaller particles was observed as shown in Figure 4.36. After a certain time, no further change in the relative ratio between the two signals occurred.

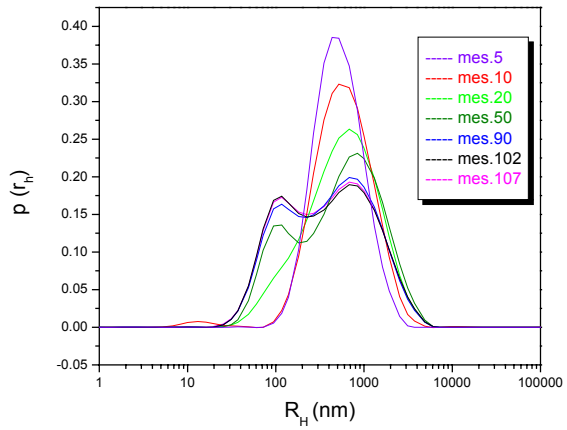

Figure 4.36: Time-dependence right-angle DLS measurements for A-3.Fe(III) micelles in cyclohexane at 50 °C.

Observing the light scattering cuvette at this point, we could see a deep wine-red precipitate at the bottom, whereas the remaining solution had a light red/purple colour, indicating that some particles were still present in solution. When an equilibrium state was established, a sample was taken from the solution and placed on graphite to be visualised by AFM. As shown in Figure 4.37, cylindrical micelles loaded with the ferric salt were present in solution. Presumably their high tendency to coagulate eventually results in their precipitation.

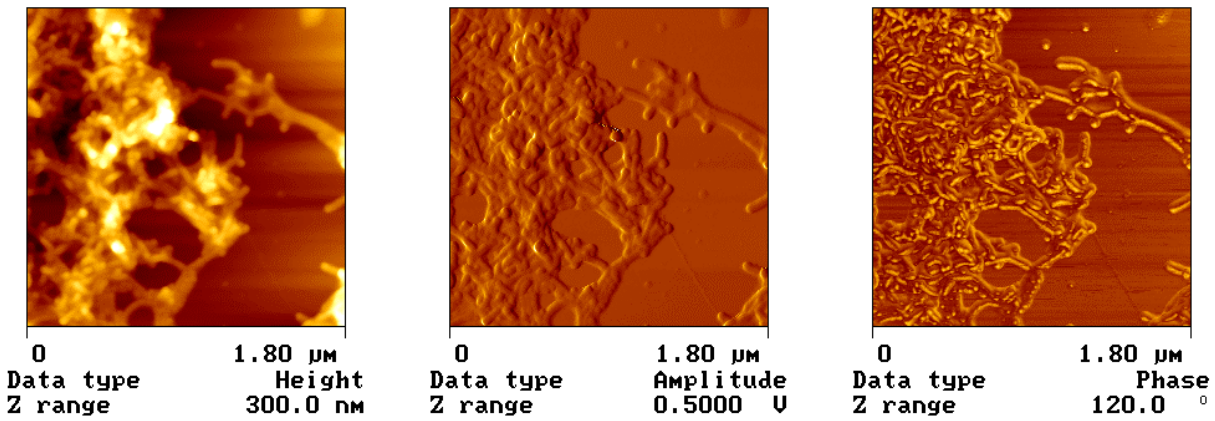

Figure 4.37: *AFM phase micrographs of A-3.Fe(III) cylindrical micelles in cyclohexane, (drop on graphite).*

By using a more polar solvent such as benzene, stable micellar aggregates of A-3.Fe(III) could be obtained. In the absence of any inorganic salt, it is expected that A-3 forms colloidal aggregates in benzene, since the latter is a good solvent for the pBuMA block whereas pAEMA is completely insoluble. Even though the polymeric aggregates of A-3 were

completely stable in benzene, (unlike in cyclohexane), LS measurements were unfortunately not possible, due to the similar refractive index of the polymer and the solvent (around 1.5). We hoped that complexation of the Fe(III) with the polymer would induce a change in the refractive index of the hybrid particles, which in turn could make them "visible" in LS. Indeed, the introduction of the iron salt induced a contrast between the solvent and the polymer making DLS measurements accessible. A hydrodynamic radius of approximately 14 nm was measured for A-3.Fe(III) micellar systems in which the salt amount varied ([Fe]/[AEMA] = 0.33, 0.5 and 1). The colour of the solution was deep purple, indicating once more polymer-metal complex formation. The A-3.Fe(III) micelles are spherical in shape and highly monodisperse as depicted in Figure 4.38. AFM analysis was carried out using two different substrates: mica (spin-coating) and graphite (drop of solution). On the latter the micelles are organised in well-ordered domains upon solvent evaporation.

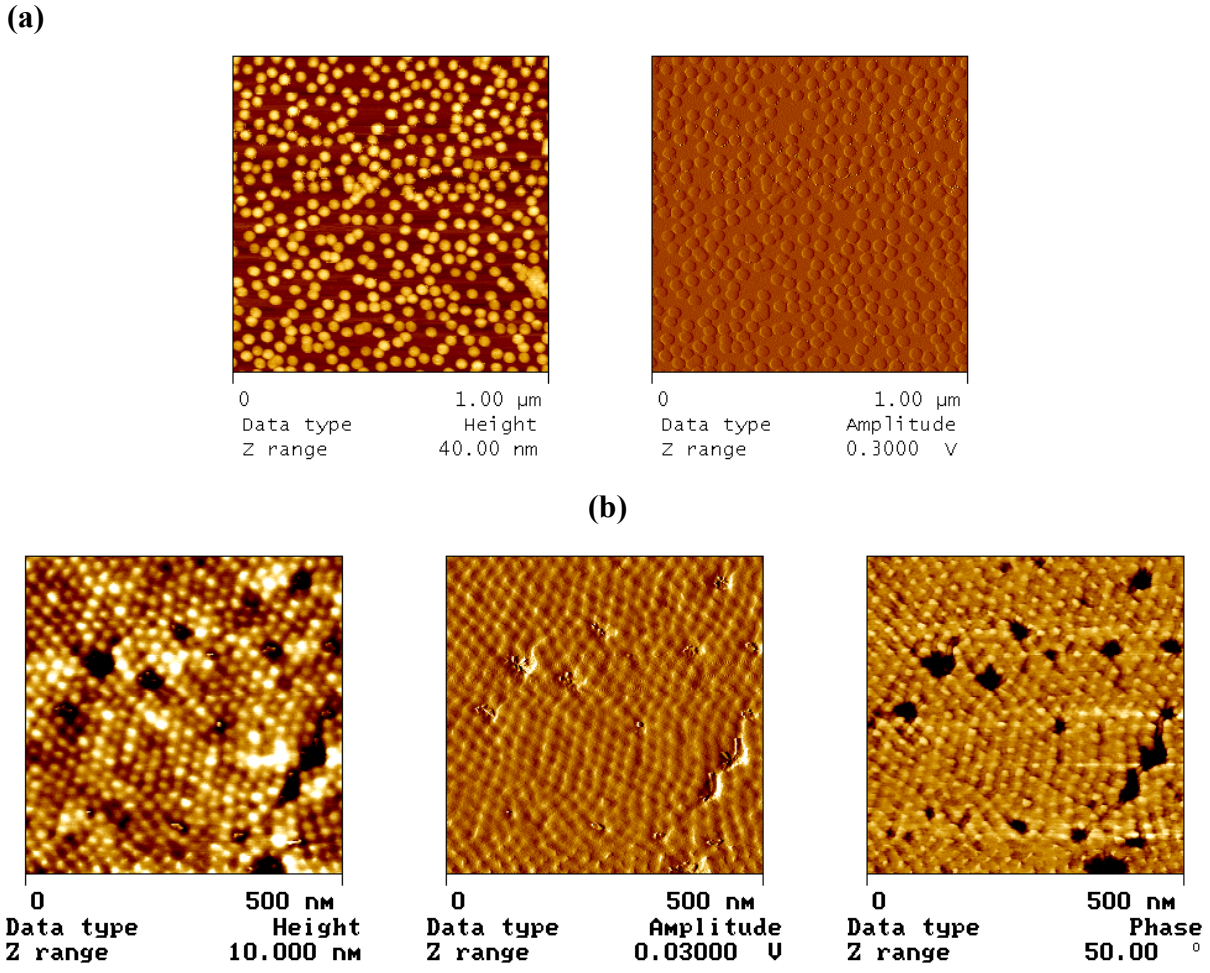

Figure 4.38: *AFM micrographs of A-3.Fe(III) monodisperse micelles formed in benzene: (a) micellar solution spin coated on mica (individual particles); (b) drop from a micellar solution placed on graphite followed by solvent evaporation (formation of ordered micellar domains).*

Similarly, Antonietti and Förster[2] reported that micelles of poly(styrene)-*b*-poly(4-vinylpyridine) in toluene, observed using electron microscopy, tend to form ordered domains upon evaporation of the solvent during sample preparation due to their narrow size distribution.

4.5 Formation of sheet-like superstructures from micellar solutions of pBuMA-*b*-pAEMA loaded with $FeCl_3.6H_2O$.

After leaving a vial containing a micellar solution of $pBuMA_{80}$-*b*-$pAEMA_{22}$ (A-1) loaded with $FeCl_3 \cdot 6H_2O$ in cyclohexane open for several days, the solvent was slowly evaporated. Surprisingly, when THF was added to dissolve the remaining solid substance, insoluble purple-colour needles were observed.

Optical as well as scanning electron microscopy were used to visualise these structures. A folded sheet-like morphology was observed by both methods, as illustrated in Figure 4.39. Elemental analysis in SEM revealed that among other components such as C, H, O (found in the highest percentage since they correspond to the polymeric material) and some Al, probably coming from the substrate, Fe and Cl were also incorporated within these structures.

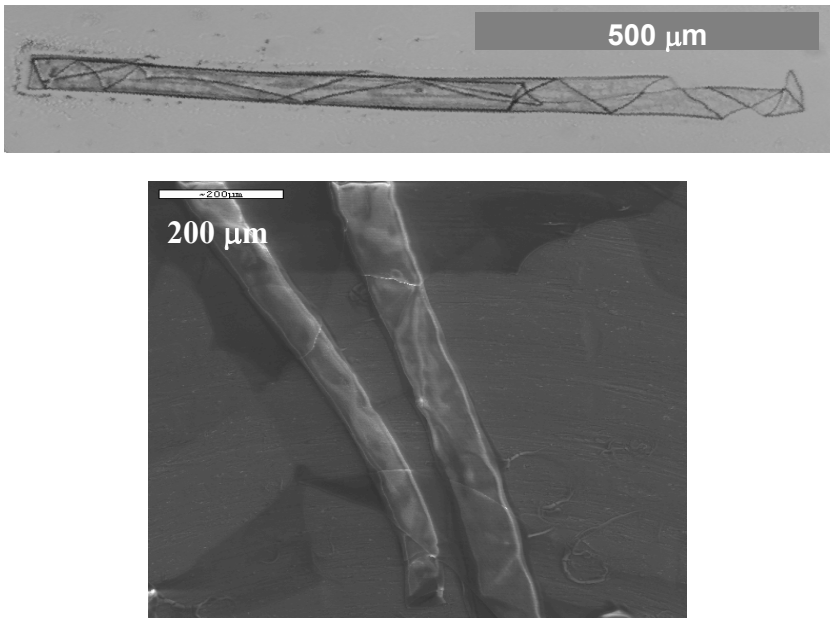

Figure 4.39: *2-D sheet-like superstructures (size in the μm scale), obtained after slow evaporation of cyclohexane from a solution of A-1.Fe(III) at r.t.: (a) Optical Microscopy (b) SEM micrograph.*

The next step was to examine if those structures could be obtained, starting from polymer/Fe(III) complexes in cyclohexane of block copolymers with different block length ratios i.e. $pBuMA_{342}$-*b*-$pAEMA_{39}$(A-2) and $pBuMA_{74}$-*b*-$pAEMA_{60}$ (A-3).

Indeed, slow evaporation of cyclohexane and aging at room temperature resulted in the formation of these sheets. Aging seems to play an important role in the formation mechanism involved. It has been observed that, in the case of A-2.Fe(III), an immediate addition of THF as soon as cyclohexane was evaporated off, resulted in complete re-solvation of the material without any insoluble sheets being formed. However heating cyclohexane solutions of A-2.Fe(III) and A-3.Fe(III) to high temperatures using a heat-gun till complete solvent evaporation these insoluble sheets were directly formed. Furthermore, in the case where a solution of A-3.Fe(III) was prepared in $CDCl_3$, evaporation of the latter resulted once more in insoluble purple sheet-like structures.

SEM and AFM were employed for visualising the "inner" structure of these sheets. This was of interest since it could provide information on the mechanism involved in their formation. With SEM we could visualise lamellae bilayers, aggregated together in bundles, which in turn segregated further to form a 2-D sheet-like structure as illustrated in Figure 4.40.

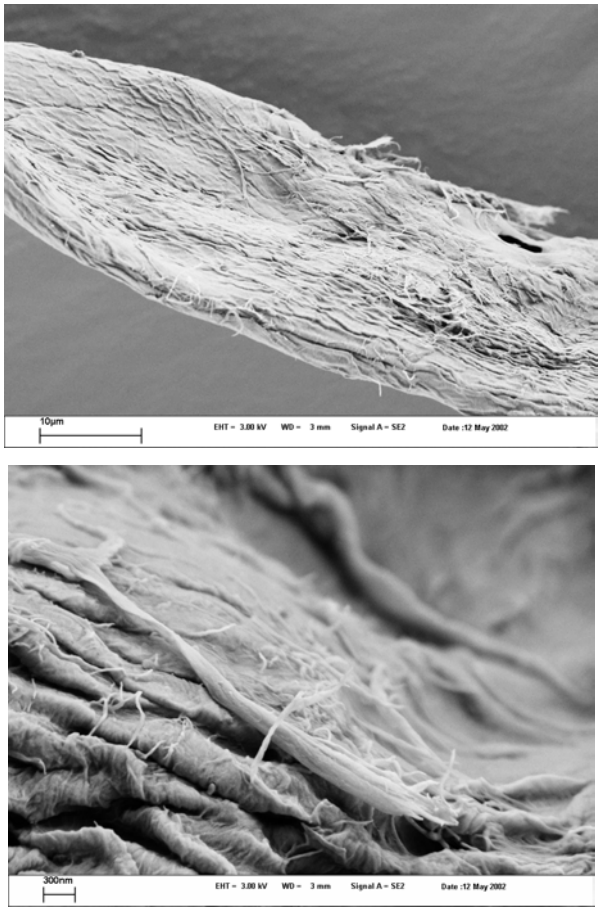

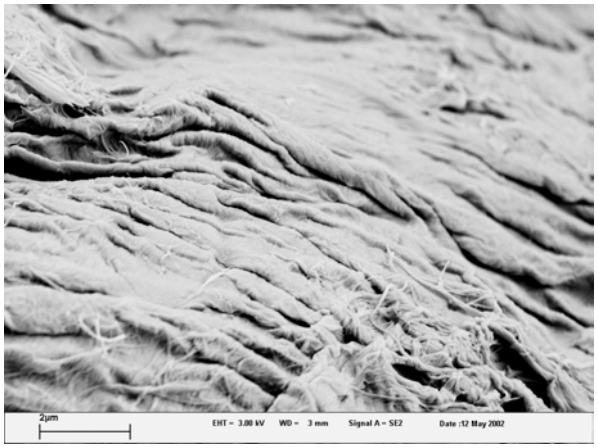

Figure 4.40: *Surface morphology of the insoluble A-2.Fe(III) sheet-like structures visualised in SEM. Lamellae bilayers organised in bundles, which in turn segregate further to form these 2-D sheets.*

In addition, the material was embedded in epoxy resin and microtomed. Thin sections were placed on a copper grid to be visualised in AFM. The lamellae microdomains, presumably the primary building nanodomains of these insoluble sheets, could be visualised in high resolution as shown in Figure 4.41.

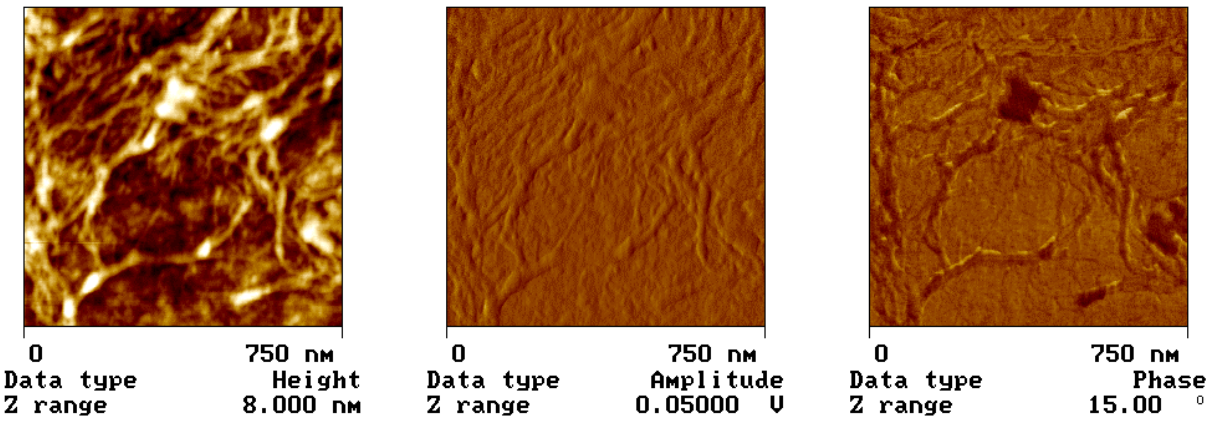

Figure 4.41: *AFM micrographs of the microtoms performed on the embedded in epoxy resin A-2.Fe(III) insoluble sheets.*

From all the above, a question rises: What is the mechanism involved in the formation of these structures? How can we end-up from a micellar solution of a polymer/metal complex with these insoluble sheets? A possible explanation could be an aldol condensation reaction occurring between adjacent β-dicarbonyl moieties, due to the presence of the ferric salt, a Lewis acid catalyst[119]. This reaction causes the crosslinking of the already preorganised micellar nanodomains resulting in a well-ordered hybridal network. In order to confirm this

mechanism, we performed an aldol condensation reaction of the β-dicarbonyl ligating groups of pAEMA using another Lewis acid, namely *para*-toluene sulfonic acid in THF at 60-70 ^{o}C. After the reaction was completed, THF was evaporated off and the resulting film obtained was visualised by SEM, revealing the presence of a crosslinked material (Figure 4.42).

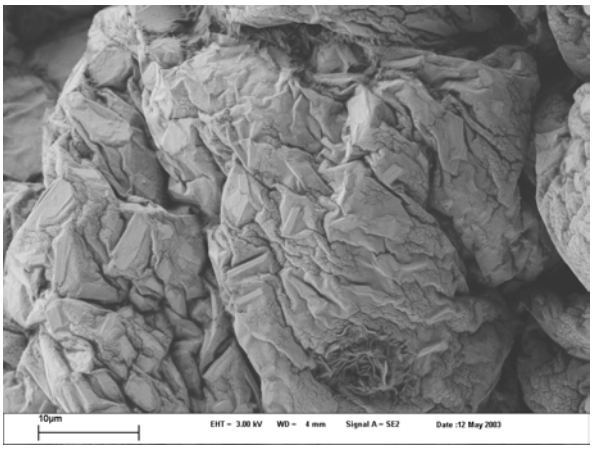

Figure 4.42: *SEM of a film obtained after aldol condensation reaction performed on pAEMA catalysed by a Lewis acid*.

The above figure indicates that this morphology does not result *via* crosslinking in a statistical manner. Since this is only a homopolymer, it is unlikely that these are colloidal micellar aggregates. Presumably the existence of specific H-bond interactions between β-carbonyl moieties of pAEMA lead to an organised pseudo-lamellar morphology, which is further crosslinked. Reports on crosslinking of lyotropic pB-*b*-pEO block copolymer micellar, hexagonal, lamellae and cubic phases resulting in generation of mesostructured hydrogels in which the original mesoscopic structure is retained, appeared in the literature[120].

In conclusion, sheet-like "superstructures" were obtained from micellar solutions of pBuMA-*b*-pAEMA complexed with $FeCl_3 \cdot 6H_2O$, after slow evaporation and aging, or quick removal of the solvent by heating. The mechanism involved in the formation of these structures might be an aldol condensation of the β-dicarbonyl side chains due to the presence of the iron salt, which can catalyse this reaction. An aldol condensation performed on a pAEMA using another Lewis acid as a catalyst, resulted in the formation of a crosslinked material, a result that enforces the above assumption.

4.6 Water soluble Block Copolymers with β-Dicarbonyl ligating Segments: Biomineralisation Applications

4.6.1 Preface

The remarkable synthetic capability of biological organisms to produce intricate materials such as seashells, pearls and corals *by* "sculpturing" simple minerals (e.g $CaCO_3$, $Ca_3(PO_4)_2$) is certainly very impressive for every observer[121]. The process of growing crystals of a compound is an order of magnitude more simple than controlling their size, shape orientation and assembly[121]. The latter could be achieved by using supramolecular assemblies of organic molecules such as surfactant micelles, synthetic phospholipid vesicles[122], block copolymer aggregates[123] or microemulsion droplets[124]. The existence of specific molecular interactions at the organic-inorganic interface may define the crystallographic orientation of inorganic particles. Such processes are characterised as "organic matrix-mediated" and the unusual nucleation of an inorganic mineral on the surface of an organic material involves surface and bulk processes[125]. For ion binding and nucleus growth at the interface, not only stereochemical requirements need to be fulfilled, but also other parameters must be considered, for example the lattice geometry, the spatial charge distribution, hydration and surface relaxation[121].

The question rising from all the above, is how an organic surface in contact with an inorganic mineral is involved in its crystallisation process? The answer lies on lowering of the activation energy of nucleation[121]. This requires structural and stereochemical compatibility between the inorganic and organic surface.

Coordination environments in the mineral phase can be simulated by metal-ion binding to appropriate ligands found on the organic surface[121]. It has been reported in the literature that, synthetic polymers with functional groups on their surfaces can be very efficient as active substrates for crystal nucleation[126]. Block copolymers bearing -$COCH_3$, COOH, or SO_3H functionalities have been proved capable of nucleating salts such as hydroxyapatite, calcite or CdS[127]. In the present work, the effect of water-soluble amphiphilic block copolymers with β-dicarbonyl ligating segments on the nucleation behaviour of calcium carbonate is investigated in aqueous solution.

4.6.2 Effect of pAEE-b-pEO block copolymers on the nucleation behaviour of $CaCO_3$ in water.

As already described in 3.5, double-jet method is commonly employed in biomineralisation processes since it can provide fast crystallisation and narrow size distributions of the desired

nanocrystals. We therefore decided to introduce this technique aiming to investigate the effect of pAEE-b-pEO on the crystallisation of $CaCO_3$. The polymer was dissolved in water and subsequently aqueous solutions of $CaCl_2$ and Na_2CO_3 was added into the solution during stirring. The experiment was carried out at constant flow rate. After some time, the solution turned turbid. The solid powder obtained was analysed by Wide-Angle X-Ray Scattering (WAXS) and Transmission Electron Microscopy (TEM).

In the absence of any additives, $CaCO_3$ crystallises in a well-defined rhombohedral morphology characteristic of calcite, one of the three possible crystallisation morphologies of this mineral (calcite, aragonite, vaterite) (Figure 4.43).

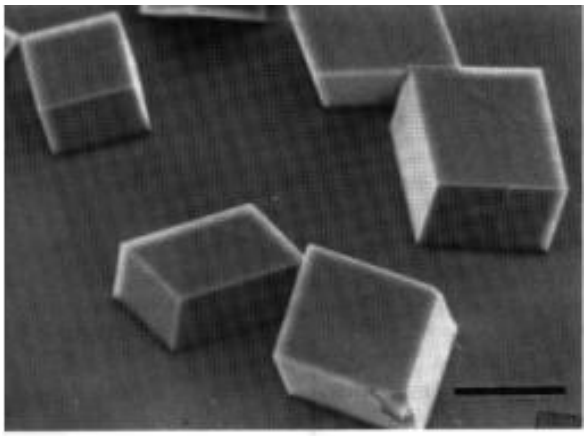

Figure 4.43: *$CaCO_3$ crystals in a well-defined rhombohedral morphology*[128].

In biomineralisation processes functionalised molecules act as templates for the growth of nanocrystals. Specific interactions occurring between these molecules with some crystallographic surfaces of the initial nuclei, are responsible for controlling the size and shape of the final crystal structure of the inorganic product[129]. Control over nucleation of an inorganic material can also be achieved by using supramolecular or colloidal preorganisation that can build-up a structural "cage" for the construction of an inorganic nanostructure (exo-template)[129].

Antonietti *et al.* have reported the formation of "nanonugget" morphologies of gold colloids, resulting from the reduction of gold salts incorporated in poly(styrene sulfonate) microgels.

As proven in WAXS, the presence of the non-ionic pAEE-b-pEO additive promoted the precipitation of pure calcite nanocrystals (Figure 4.44). However, TEM revealed an unusual structure, which resembled "nanonugget" morphologies (Figure 4.45). Hence, it might be possible that nucleation of $CaCO_3$ in the presence of pAEE-*b*-pEO involves an

"exo-template" route: Micelles of pAEE-*b*-pEO formed in aqueous solution may play the role of spherical polymer gel particles (microgels) which act as exo-template for the nucleation of $CaCO_3$, resulting in this unusual "nugget-like" morphology. In addition, the fact that the size of these structures (approximately 300 nm) is too small for biominerals (normally crystallising in the μm scale), underlines the above statements.

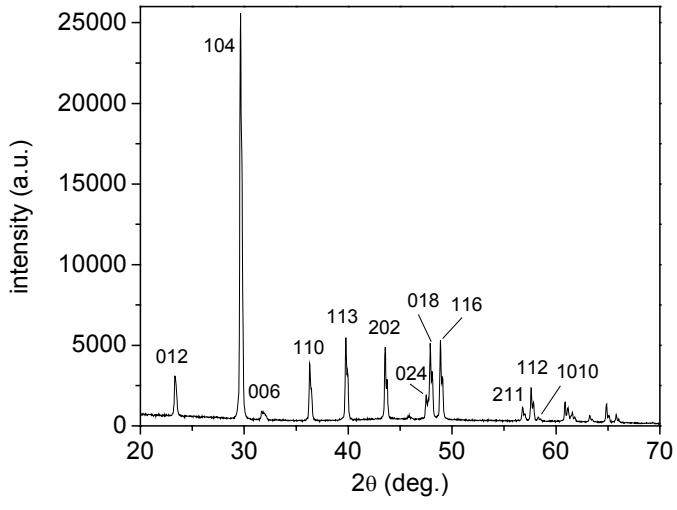

Figure 4.44: *WAXS spectrum of $CaCO_3$ nanocrystals (pure calcite) obtained in the presence of 0.1 w% pAEE-b-pEO.*

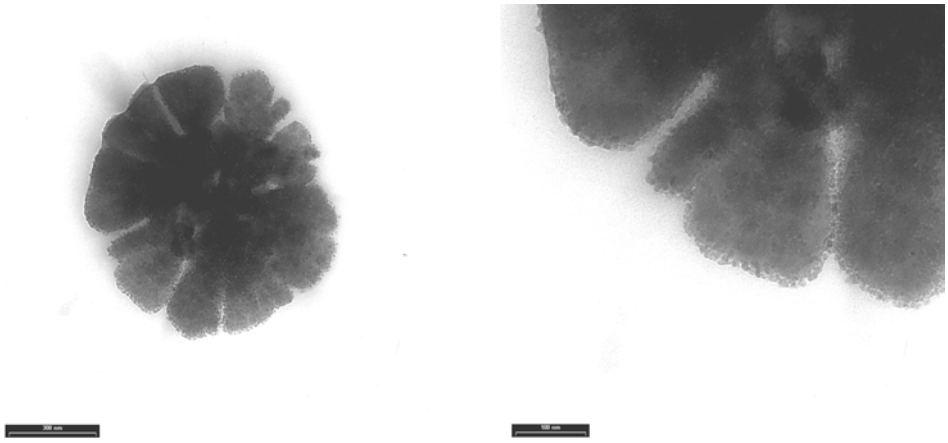

Figure 4.45: *TEM micrograph of the resulting hybridal $CaCO_3$/pAEE-b-pEO colloid material with an unusual "nugget-like" morphology, presumably formed via nucleation of $CaCO_3$ following an " exo-template" mechanism.*

Furthermore, it is important to mention that, this unique nucleation behaviour of $CaCO_3$ in the presence of pAEE-*b*-pEO, is not attributed to the pEO block. The latter has no effect on the crystallisaiton behaviour of $CaCO_3$ and the calcite crystals obtained have the usual rhombohedral morphology[130]. Thus the presence of the *β*-dicarbonyl moieties, seem to play

an important role in the nucleation mechanism resulting to this particular morphology. However, further experiments are required for confirming the mechanism involved in the formation of such morphologies.

CHAPTER 5

Summary and Outlook

In the present work the first synthesis of well-defined block copolymers with a *β*-dicarbonyl segment was introduced *via* two alternative routes. The first one involved preparation of well-defined block copolymers employing "living"/controlled polymerisation techniques (Anionic and Group Transfer Polymerisation) and subsequent modification reactions. With the second method, direct synthesis of homopolymers and block copolymers based on AEMA was accomplished using a controlled Reversible Addition-Fragmentation Chain-Transfer radical polymerisation. It has been demonstrated that polymerisation of AEMA *via* RAFT proceeds in a controlled manner, following a first-order kinetics. This procedure seems to be the most appropriate method for the controlled synthesis of pAEMAs. ATRP failed to give monodisperse polymers, since the *β*-dicarbonyl moiety of AEMA interfered with the metal-ion complex catalyst involved in the ATRP process.

The amphiphilic character of this novel type of block copolymer systems allows microphase separation in selective organic media. The aggregation behaviour of a series of pBuMA-*b*-pAEMA was investigated in cyclohexane and dimethyl sulfoxide. In cyclohexane, a selective solvent for the pBuMA block, micelles are formed with pBuMA chains being located at the exterior of the micelle and pAEMA constructing the micellar core. In DMSO, "reverse" micellar structures are obtained with pAEMA being the solvating block. Differences in block length ratios induce a phase transition in the micellar shape varying from spherical to elliptical and cylindrical. Geometrical parameters characterising pBuMA-*b*-pAEMA micelles formed in cyclohexane, for example hydrodynamic radii, core radii, radii of gyration, dimensions of micellar coronas and interchain distances were determined by light scattering. Furthermore, it has been illustrated that these block copolymer systems exhibit aggregation behaviour like strongly segregated diblock and triblock copolymer systems.

The incorporation of strong bidentate *β*-dicarbonyl ligands in pBuMA-*b*-pAEMA fascilated coordination and solubilisation of $FeCl_3 \cdot 6H_2O$, $Pd(Ac)_2$, $Cu(Ac)_2 \cdot xH_2O$, and $Co(Ac)_2 \cdot xH_2O$ in organic media. Complexation occurred *via* the keto tautomer or the enolate anion of the *β*-dicarbonyl moiety. Upon salt addition, the micellar core was loaded with the inorganic material *via* coordination with the pAEMA ligating block segment. Complexation was accompanied by a simultaneous colour change of the solution.

The aggregation behaviour of pBuMA-*b*-pAEMA was extensively studied in the presence of different amounts of $FeCl_3 \cdot 6H_2O$ and $Pd(Ac)_2$ in cyclohexane using light scattering techniques. Most commonly, complexation of an inorganic material with one of the blocks increases incompatibility between the two block segments, thus resulting in stronger segregation. However, by increasing the amount of $FeCl_3 \cdot 6H_2O$ in a micellar solution of pBuMA-*b*-pAEMA (keto tautomer), a decrease in aggregation numbers was observed. We suppose that this unusual behaviour derives from the destruction of the already pre-existing H-bond interactions between the β-dicarbonyl moieties in the micellar core. When complexation of $FeCl_3 \cdot 6H_2O$ occurs *via* the enolate anion of the β-dicarbonyl groups, aggregation follows the expected behaviour, i.e. aggregation numbers as well as micellar size increase systematically with increasing salt concentration. This result supported our initial statements concerning H-bonding, since in this case no such interactions existed in the first place, to be destroyed upon loading. Complexation of $Pd(Ac)_2$ in cyclohexane *via* the enolate anion had virtually no effect on the aggregation number and micellar size (unlike in the case of complexation of $FeCl_3 \cdot 6H_2O$). The reason for this difference might be that Pd(II), a group VIII "soft" metal ion with unoccupied *f* orbitals, forms bonds which are covalent in character. On the other hand, Fe(III), a more "hard" metal ion favours the formation of electrostatic bonds.

2-D insoluble sheet-like structures were obtained from micellar solutions of pBuMA-*b*-pAEMA/Fe(III) in cyclohexane after solvent evaporation and aging. As illustrated by SEM, these structures consist of lamellae bilayers organised in bundles, which in turn aggregate together to form these hybridal "superstructures". Presumably, the ferric salt incorporated, as a Lewis acid can catalyse an aldol condensation between neighbouring β-dicarbonyl moieties. This reaction causes crosslinking of the already preorganised lamellae leading to a well-ordered hybridal network. Performing an aldol reaction on pAEMA using a different Lewis acid catalyst leaded to the formation of a crosslinked material. SEM images indicated that crosslinking occurred on already preorganised domains. Since this was only a homopolymer, it was unlikely that those were colloidal micellar aggregates. "Preorganisation" in this case could only derive from the existence of H-bond interactions.

Investigation carried out employing NMR, IR and AFM indicated the existence of H-bond interactions between adjacent β-dicarbonyl units in pAEMA. "Barrel-like" or globular morphologies of pAEMA, (resulting from inter or intramolecular H-bonding respectively), similar to those found in polypeptides or proteins were observed on graphite by AFM. Thus,

the presence of H-bond interactions between β-dicarbonyl side chains in pAEMA -a non-chiral synthetic homopolymer- may be the driving force that promoted structural organisation leading to generation of superstructures resembling those appearing in nature.
The effect of the water-soluble pAEE-*b*-pEO block copolymer bearing β-dicarbonyl segments on crystallisation of $CaCO_3$ was investigated in aqueous solution. WAXS has shown the presence of pure calcite nanocrystals and TEM revealed the presence of an unusual "nugget-like" morphology. This suggested that nucleation of $CaCO_3$ in the presence of pAEE-*b*-pEO involved an "exo-template" route: Micelles of pAEE-*b*-pEO formed in aqueous solution may build-up a structural "cage" for the construction of an inorganic nanostructure, hence acting as exo-template for the nucleation of $CaCO_3$.

There is no doubt that these novel well-defined block copolymer systems bearing β-dicarbonyl segments have great potential to be used in very diverse areas of chemistry. In this work only a small part of what could be done with such systems was presented. The fact that inter- and intramolecular hydrogen bonding may take place between the β-dicarbonyl groups within the polymer chains generating superstructures similar to those appearing in nature, makes these polymers highly interesting in the area of supramolecular chemistry. An interest aspect could be the synthesis of chiral polymers with β-dicarbonyl segments: The presence of chiral centres combined with hydrogen bonding could lead in the formation of fascinating superstructures which may resemble secondary, tertiary or even quartenary structures found in proteins.
As illustrated in the present work, hybrid organic/inorganic monodisperse micelles can form well-organised monolayers. These metal salt-containing micelles can be transformed into metal colloids *via* reduction. The resulting particles are expected to retain their colloidal characteristics thus providing a good stabilisation of the metal colloids by the block copolymer shells. The ability of the β-dicarbonyl moiety to form complexes with a wide range of metal-ions enhances the number of applications these hybrid materials may have, depending on the nature of the inorganic compound incorporated. Catalytic nanoreactors, colloidal semiconductors, colloids with optical and magnetic properties are some of them.
In addition, water-soluble block copolymers with β-dicarbonyl segments may be potential candidates in biomineralisation applications and waste-water treatment.

CHAPTER 6

Experimental Part

6.1 Experimental techniques

Nuclear Magnetic Resonance (NMR) spectra were recorded at room temperature on a Bruker DPX-400 Spectrometer operating at 400.1 MHz. For classifying the signals on the NMR spectra, abbreviations such as s (singlet), d (doublet), t (triplet), m (multiplet) and br (broad) were used. The solvents for ^{1}H and ^{13}C NMR used were $CDCl_3$ (δ = 7.26 ppm), DMSO-d_6 (δ = 2.62 ppm) DMF-d_7 (δ = 8 ppm) and cyclohexane-d_6 (δ = 1.44 ppm). Win-NMR (Bruker) program was used for further spectra analysis.

Infra-red (IR) spectra were recorded on a BioRad 6000 FT-IR. All samples were measured in the solid state using a Single Reflection Diamond ATR. For classifying the intensities of the signals on the IR spectra, abbreviations such as vs (very strong), s (strong) and w (weak) were used.

Ultra-Violet/Visible (UV-Vis) spectra were recorded at room temperature using a UVIKON 940/941 dual-beam grating spectrophotometer (Kontron Instruments) with a 1-cm quartz cell. Measurements were carried out in cyclohexane (concentrations: 1-2 g/L).

Gel Permeation Chromatography (GPC) analysis was performed in THF (at 25 ^{o}C) or 0.5 wt % LiBr in DMA (70 ^{o}C). The column set for analysis in THF consisted of three 300 x 8 mm columns, MZ-SD*plus* (spherical polystyrene particles with an average diameter of 5 μm) with pore sizes of 10^3, 10^5, 10^6 Å. In DMA, a 4 x 30 cm column was used (spherical polyester particles of 10 μm diameter), with pore sizes 30, 30, 100 and 3000 Å. A UV-(TS PUV 1000) and an RI (Shodex RI-71) detector systems were employed. All samples were filtered prior use. For all measurements 100 μl of approximately 0.2% w/v of polymer solution was injected in the GPC column and the flow-rate was maintained at 1.0 ml/min.

Standard calibration curves of pBuMA, or pMMA were used and the MW as well as MWD were calculated by using the Program-Packet NTeqGPC V5.1.5 (GmbH).

For Light Microscopy (LM) an Olympus Microscope (Model BX50) directly connected with a digital camera was used.

Transmission Electron Microscopy (TEM) micrograms were obtained with a Zeiss EM 912 OMEGA instrument operating at an acceleration voltage of 120 kV. The diluted colloidal solutions were placed on a 400-mesh carbon-coated copper grid and left to dry; no further contrasting was applied.

Scanning Electron Microscopy (SEM) micrograms were obtained with a Zeiss instrument, Model DSM 940A.

Atomic Force Microscopy (AFM) was performed on a Nano-Scope IIIa Microscope (Digital Instruments, *USA*) using a 10x10 μm cantilever (Model TESP; resonant frequency: 300 KHz; force constant: 42 N/m). All measurements were carried out with Tapping Mode. Dilute sample solutions (0.05 – 2g/l) were spin-coated or droped on mica or graphite surface to be visualised by AFM.

Dynamic Light Scattering (DLS) measurements were carried out using a standard, laboratory-built scattering spectrometer operating at 633 nm or 488 nm (Argon-Ions-Laser, Firma Coherent, Model Innova 300) (power: 30-600 mW). DLS experiments were performed at scattering angles 30^o, 50^o, 70^o and 90^o. High quality of the scattering curves was ensured by repeating measurements several times. The radius-distribution of the particles in solution was calculated from the experimental correlation functions using the program FASTORT.EXE[131].

For **Static Light Scattering (SLS)**, a commercial spectrometer from ALV consisting of an ALV goniometer with temperature controller (± 0.05K) and an ALV 5000 multi-tau correlator was used. The refractive index increment dn/dc was measured using an NFT-Scanref differential refractometer. SLS experiments, were performed at scattering angles from 15^o to 150^o at 3^o intervals. However, due to the large fluctuations in the scattered intensities at the

lower angle-range, the data from 15^o - 30^o were often excluded from the calculations. Data were evaluated by a standard Zimm analysis.

All solutions were filtered through 0.45 μm millipore filters prior measurement. The cylindrical quarz cuvettes (1 cm diameter) were extensively cleaned first with THF and ethanol followed by cleaning with ultrasound using a Tensid solution (Hellmanex, Hellma). They were subsequently washed several times with distilled water to completely remove any Tensid remained. Finally, they were washed with acetone in a dust-free fountain for 20 minutes and placed in a desiccator.

Wide Angle X-ray Scattering (WAXS) measurements were performed using a Nonius PDS120 powder diffractometer in transmission geometry. A FR590 generator was used as the source of Cu K_α radiation (λ = 0.154 nm). Monochromatisation of the primary beam was achieved by means of a curved Ge crystal. Scattered radiation was measured using a Nonius CPS120 position-sensitive detector. The resolution of this detector in 2θ is 0.018°.

Differential Scanning Calorimetry (DSC) was measured on a Netzsch DSC 200 at a heating/cooling rate of 10K min^{-1}. The Glass Transition Temperature (T_g) was determined from the inclination point of the second heating curve.

Thermogravimetric Analysis (TGA) was performed on a Netzsch TG 209 at a scanning rate of 20 K min^{-1}.

Density measurements were carried out on a density meter DMA 5000 (Anton Paar) at 25 ^oC. The specific density of the bulk polymer was extrapolated from the density data measured for a particular solvent and a 0.9 wt % solution of the polymer in the same solvent.

For the **Double-Jet method**, 10 mg of polymer were dissolved in 10 ml of water. The flow-rate of Na_2CO_3 and $CaCl_2$ addition was 333 µl/hr, i.e. 0.28 10^{-2} mmol/min of $CaCO_3$ formation. The whole system was thermostated at the 25°C. Addition time was approximately 15 min., when the solution became turbid. The whole process was terminated after 53 min. The precipitate was then left to stand in its mother solution for at least 24 hr to ensure equilibration.

6.2 Solvents and Reagents

All solvents used in NMR experiments were commercially obtained and used as received: $CDCl_3$, DMF-d_7, DMSO-d_6, cyclohexane-d_6, CF_3COOH-d_1 (deutero GmbH).

Where dry solvents were used, these were distilled and dried over suitable drying agents: THF (KOH, Na/K alloy, $LiAlH_4$), cyclohexane (sodium), toluene (CaH_2), pyridine (Na_2SO_4, CaH_2), acetone, *n*-hexane, ethyl acetate and dioxane (CaH_2). Methanol, ethanol, DMSO, diethyl ether, etc. were used as received.

The following reagents were obtained commercially in the highest purity available from Aldrich and Fluka and were used as received unless otherwise stated: 1,1,1,3,3,3-hexamethyldisilazane, benzene, hydroxyethyl methacrylate (HEMA), *n*-butyl methacrylate (BuMA), 2-(acetoacetoxy) ethyl methacrylate (AEMA), *n*-butyl acrylate (BuA), *N*-isopropyl acrylamide (NiPAM), ethylene oxide (EO), 1,3-butadiene (B), 1-methoxy-1-trimethylsiloxy-2-methylprop-1-ene (MTS), trimethylchlorosilane, etc. Tetrabutylammonium bibenzoate (TBABB) was synthesised by following a published procedure[132].

All inorganic materials used ($CaCO_3$, NaOH, KOH, $FeCl_3$, $FeCl_3.6H_2O$, $Pd(CH_3COO)_2$, $Cu(CH_3COO)_2.xH_2O$, $Co(CH_3COO)_2.xH_2O$, etc.) were of standard quality.

6.3 Synthesis

6.3.1 Monomer synthesis

2-(Trimethylsilyloxy)ethyl methacrylate (TMSHEMA), **1**[133]

2-hydroxyethyl methacrylate (23 ml, 0.192 mol) was dissolved in a mixture of dried pyridine (52 ml, 0.64 mol, - dried over Na_2SO_4, filtered and dried over CaH_2 for 2 hr at 50 ^oC and for 20 hr at room temperature and distilled -) and 1,1,1,3,3,3-hexamethyldisilazane (59 ml, 0.280 mol) under inert atmosphere. Trimethylchlorosilane (34 ml, 0.269 mol) was added slowly during stirring. A white precipitate was formed during addition (pyridinium chloride salt). The mixture was subsequently stirred for 48 hr at room temperature. It was then filtered under argon by using a glass frit filter. Distillation was followed to remove the excess of trimethylchlorosilane and hexamethyldisilazane.

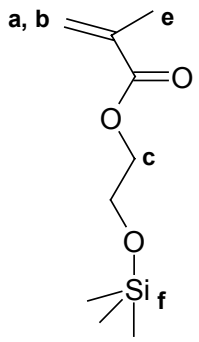

1.

bp : 27 ^oC, $3.1*10^{-2}$ mbar.

^1H NMR (400 MHz, $CDCl_3$) δ [ppm]: 6.19 (s, 1H, $=CH_2$ (**b**)), 5.58 (s, 1H, $=CH_2$ (**a**)), 4.32-4.18 (t, $-CH_2$ (**c**)), 3.88-3.78 (t, $-CH_2$ (**d**)), 1.96 (s, $-CH_3$ (**e**)), 0.14 (s, $-Si(CH_3)_3$ (**f**)).

6.3.2 Polymer Synthesis

6.3.2.1 Synthesis by Group Transfer Polymerisation, GTP

6.3.2.1.1 Poly(*n*-butyl methacrylate)-*block*-poly[(2-trimethylsilyloxy)ethyl methacrylate], **2**

A series of pBuMA-*b*-pTMSHEMA diblock copolymers was synthesised by GTP[34,132]. Polymerisations were carried out at ambient temperature (20 ^{o}C). The polymerisation exotherm, which was monitored by a digital thermometer, was used to follow the reaction process. A general GTP procedure is detailed as below.

The initiator used was MTS and TBABB served as the polymerisation catalyst. Initially, the reactor was evacuated and heated so as to exclude all moisture. When cooled down to room temperature, TBABB (~ 20 mg) was transferred into the flask under argon. After that, THF (dried over $LiAlH_4$ overnight) was condensed into the reactor. The amount of THF used was such, that the final concentration of polymer solution not to exceed 35-40%. Continuously, MTS (distilled prior use and kept under argon) was fast added at room temperature and under inert atmosphere in the reaction flask. Approximately 15-30 minutes later, freshly distilled BuMA was added dropwise *via* a plastic syringe at ambient temperature. During the addition an exotherm (ΔT = 8-12 ^{o}C) was observed. After the exotherm had ceased, an aliquot was extracted from the reactor and quenched with methanol to be analysed by GPC. Then TMSHEMA was added dropwise. A second exotherm was observed and the reaction mixture was left to stir until temperature dropped down to room temperature and finally quenched with methanol. After polymerisation was completed, THF was removed under reduced pressure and the resulting polymer was precipitated from *n*-hexane, petroleum ether or methanol and dried *in vacuo* for one day at 40 ^{o}C.

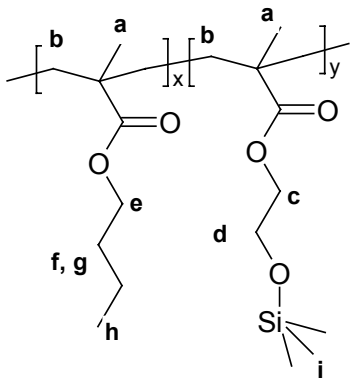

2.

^{1}H NMR (400 MHz, $CDCl_3$) δ [ppm]: 3.88 (m, -CH_2 (**c, e**)), 3.68 (t, -CH_2 (**d**)), 1.95-1.20 (m, br, -CH_2 (**b**, **f, g**)), 0.96-0.80 (m, br, -CH_3 (**a**, **h**)), 0.10 (s, -Si(CH_3)$_3$ (**i**)).

6.3.2.1.2 Poly(*n*-butyl methacrylate)-*block*-poly(2-hydroxyethyl methacrylate), **3.**

pBuMA-*b*-pHEMA diblock copolymers were obtained by HCl-catalysed hydrolysis of trimethylsilyl-protecting groups in **2**. The silyl-protected block copolymers were dissolved in THF and to the solution HCl (6M) was added (9:1 v/v, THF/HCl). The mixture was left to stir overnight at room temperature. The next day the solution was concentrated under reduced pressure and the resulting polymer was precipitated from methanol and left to dry *in vacuo* for two days at 40 ^{o}C.

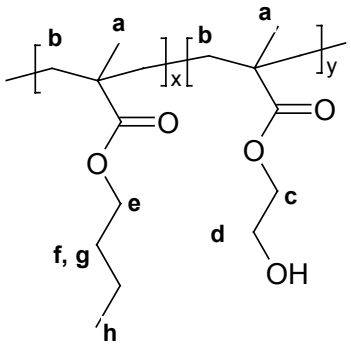

3.

^{1}H NMR (400 MHz, $CDCl_3$) δ [ppm]: 4.20-3.90 (br, -CH_2 (**c, d, e**)), 2.10-1.30 (m, br, -CH_2 (**b**, **f, g**)), 1.20-0.70 (m, br, -CH_3 (**a, h**)).

6.3.2.1.3 Poly(*n*-butyl methacrylate)-*block*-poly[2-(acetoacetoxy)ethyl methacrylate], **4.**

The hydroxylated block copolymers **3**, were reacted with *tert*-butyl acetoacetate in toluene or benzene/water to yield the functionalised pBuMA-*b*-pAEMA, **4.** The two procedures are reported in detail as follows. The second one was preferentially used.

Procedure 1: Reaction in toluene [92]

In a pre-heated solution (70 ^{o}C) of **3** in toluene (10 ml), *tert*-butyl acetoacetate (2-fold molar excess in respect to –OH groups) was added dropwise during stirring. The reaction flask was connected to a distillation bridge for the removal of *tert*-butyl alcohol, the side-product of the reaction (b.p. 82 ^{o}C). The solution was then heated up slowly to 130 ^{o}C. During this time, a product was distilled out and the solution turned from white transparent to yellow transparent. Approximately 4 hours later, no more product was further distilled. The reaction was stopped and the solvent was removed under dynamic vacuum. The resulting polymer was precipitated from methanol, to yield a yellow-colour substance, **4**.

Procedure 2: Reaction in benzene/water[53]

3 was dissolved in benzene (30 ml) and the solution was pre-heated to 70 ^{o}C. *tert*-butyl acetoacetate (2-fold molar excess in respect to –OH groups) was then added dropwise at this temperature and the solution was left to stir for 15-20 minutes before the addition of water (10 ml). Consequently, the suspension turned from white to pink and subsequently to orange colour. The reaction mixture was then heated to 100 ^{o}C overnight. *Tert*-butyl alcohol was distilled off in the aqueous phase by using a Dean-Stark apparatus due to the formation of an azeotrope with benzene and water (composition 8.1, 21.4 and 70.5 wt % respectively). The b.p. of the azeotrope of this ternary system is 67.3 ^{o}C. Therefore, by following this procedure, what remained at the end in the reaction flask was the solution of the functionalised block copolymer in benzene, whereas t-BuOH/H_2O were distilled off and separated. Finally, benzene was removed under reduced pressure and the resulting polymer was precipitated from methanol or from *n*-hexane resulting to a light-creamy colour substance, **4**.

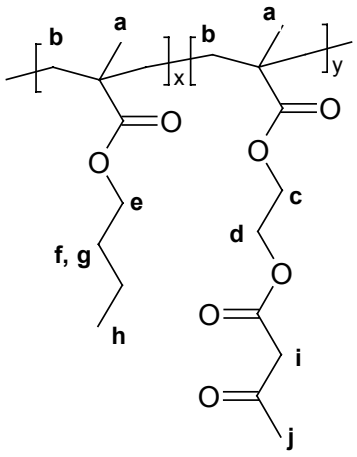

4.

^{1}H NMR (400 MHz, $CDCl_3$) δ [ppm]: 4.33 (br, -CH_2 (**d**)), 4.15 (br, -CH_2 (**c**)), 3.92 (m, br, -CH_2 (**e**)), 3.54 (s, br, -CH_2 (**i**)), 2.27 (s, -CH_3 (**j**)), 2.0-1.30 (m, br, -CH_2 (**b**), -CH_2 (**f, g**)), 1.0-0.75 (m, br, -CH_3 (**a**), -CH_3 (**h**)).

FT-IR, $\bar{\nu}$ (cm^{-1}): 3100-2800 (s; C-H), 1720 (vs), 1650 (w; C=O), 1140 (vs; C-O).

6.3.2.2 Synthesis by Anionic Polymerisation

6.3.2.2.1 Poly(1,2 - butadiene)-*block*-poly(ethylene oxide), **5**[134].

A general synthetic procedure for obtaining pB-*b*-pEO block copolymers is described as follows. Initially, the reactor was evacuated and heated so as to exclude all moisture. *t*-BuP_4-base (1M solution in hexane) was then added *via* a septum. Dynamic vacuum was applied for the removal of hexane and the remaining powder was further dried for 10 minutes. Continuously, THF was directly condensed into the reactor. 1,3-butadiene was stirred over dibutylmagnesium and BuLi at –60 ^oC for purification. The reactor was cooled down to –78 ^oC and the monomer was directly condensed in it. 1,3-butadiene was left to polymerise overnight at –78 ^oC (using an Ethanol/dry ice mixture). The next day an aliquot was extracted and quenched with methanol to be analysed by GPC. EO was purified over CaH_2, Na mirror and *n*-BuLi before condensed into the reactor. After the solution was stirred for a while at –76 ^oC, it was left to warm up to room temperature and subsequently heated at 50 ^oC for three days. During polymerisation the colour of the solution turned deep violet.

Finally, heating was removed, and the resulting polymer was quenched with acetic acid. Precipitation was achieved in cold acetone to yield a white powder, **5,** which was left to dry under *vacuo* at 40 ^{o}C.

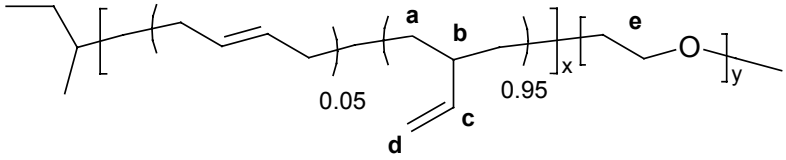

5.

^{1}H NMR (400 MHz, $CDCl_3$) δ [ppm]: 5.60-5.32 (m, br, =CH (**c**)), 4.92-4.80 (m, br, $=CH_2$ (**d**)), 3.80-3.60 (br, $-CH_2$ (**e**)), 1.80-0.80 (br, $-CH_2$ (**a**), -CH (**b**)).

6.3.2.2.2 Poly[2-(hydroxyethyl) ethylene]-*block*-poly(ethylene oxide), **6.**

pHEE-b-pEO was obtained from hydroboration/oxidation reaction of **5**. The quantities mentioned refer to the case of hydroboration/oxidation of pB_{13}-*b*-pEO_{84} [93].

5, was dissolved in benzene and freeze-dried. The reactor was evacuated and heated under dynamic vacuum so as to exclude any moisture. The reaction took place under inert atmosphere. To the dried polymer (2 g, 4.95 mmol pB), THF (50 ml) was added under inert atmosphere and the polymer solution was transferred in the reactor *via* a septum. 9-BBN (12.9 ml, 6.44 mmol, 0.5M solution in THF) was added slowly and the solution was subsequently heated up to 60 ^{o}C for 24 hrs. The following day it was left to reach room temperature and cooled down to 0 ^{o}C. At this temperature NaOH (1.07 ml, 6.44 mmol, 6M) was added dropwise. Approximately 10 minutes later, H_2O_2 (0.66 ml, 30% w/v solution in H_2O, 6.44 mmol) was slowly added. Continuously, the ice bath was removed and the white dispersion was left to reach room temperature and subsequently heated further to 60 ^{o}C for 24 hrs. After the completion of the reaction, heating was removed, the solvent was evaporated off and the resulting polymer was precipitated in diethyl ether. Further purification was achieved by dialysis in water and freeze-drying to yield a white powder, **6**.

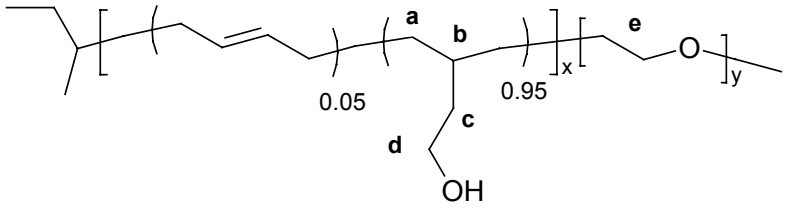

6.

^{1}H NMR (400 MHz, $CDCl_3$) δ [ppm]: 3.80-3.60 (br, -CH_2 (**e**), -CH_2 (**d**)), 1.80-0.80 (m, br, -CH_2 (**a**), -CH (**b**), -CH_2 (**c**)).

6.3.2.2.3 Poly[2-(acetoacetoxy)ethyl ethylene]-*block*-poly(ethylene oxide), **7.**

6 was dissolved in benzene (30 ml) and the solution was pre-heated to 70 ^{o}C. To the solution *tert*-butyl acetoacetate (2-fold molar excess in respect to –OH groups) was added at this temperature, and the reaction mixture was left to stir for 15-20 minutes. Continuously, water (10 ml) was added and the two-phase suspension was heated to reflux overnight. The H_2O/*t*-BuOH fraction was separated from the organic phase by distillation using a Dean-Stark apparatus. The remaining organic phase was concentrated and the resulting polymer was precipitated in diethyl ether to yield a light-orange colour substance, which was left to dry in *vacuo* at 30 ^{o}C for 2 days.

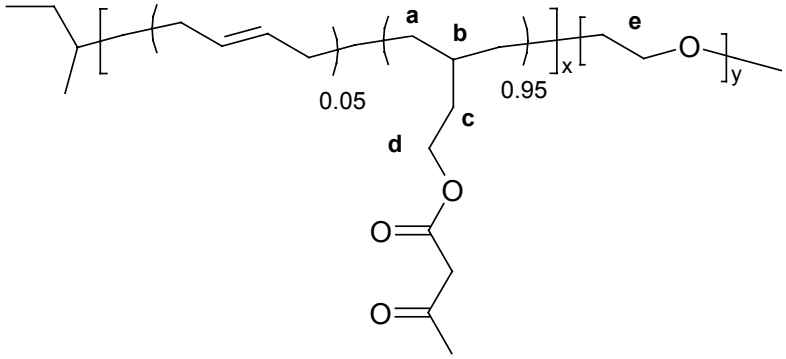

7.

^{1}H NMR (400 MHz, $CDCl_3$) δ [ppm]: 4.12 (br, -CH_2 (**d**)), 3.80-3.60 (br, -CH_2 (**e**)), 3.45 (br, -CH_2 (**f**)), 2.23 (s, -CH_3 (**g**)), 1.40-0.80 (m, br, -CH_2 (**a**), -CH (**b**), -CH_2 (**c**)).

FT-IR, $\bar{\nu}$ (cm^{-1}): 3000-2700 (s; C-H), 1737 (s), 1711 (s), 1642 (w; C=O), 1103 (vs; C-O).

6.3.2.3 Synthesis by Radical Polymerization Methods

(i) HOMOPOLYMERS

A. Free Radical Polymerisation

6.3.2.3.1 Poly[2-(acetoacetoxy)ethyl methacrylate], **8.**

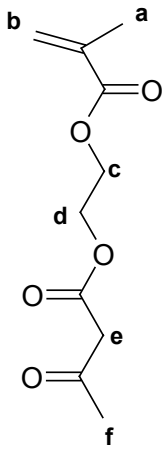

AEMA

^{1}H NMR (400 MHz, $CDCl_3$) δ [ppm]: 11.92 (s, -OH (enol)), 6.12 (s, $=CH_2$, (**b)**), 5.59 (s, $=CH_2$ (**b**)), 5.01 (s, =CH (**e,** enol)), 4.40 (t, $-CH_2$, (**d**)), 4.35 (t, $-CH_2$, (**c**)), 3.48 (s, $-CH_2$, (**e**)), 2.26 (s, $-CH_3$ (**f**)), 2.15 (s, $-CH_3$ (**f,** enol)), 1.93 (s, $-CH_3$ (**a**)).

Polymerisation in Bulk

AEMA (5 ml, 26.2 mmol) and AIBN (0.086 g, 0.52 mmol) were placed together in a flask and left to stir for half hour at room temperature. The mixture was then freeze-dried under dynamic vacuum so as to remove oxygen from the system. Polymerisation was carried out at 60 ^oC. After a short time, the formation of a gel-like residue was observed.

Polymerisation in Solution

By performing a free radical polymerisation of AEMA in ethyl acetate, ($[AEMA]_0$ = 2.1 M; $[AIBN]_0$ = 10.0 mM, 60 ^oC, 20 hr), a linear polydisperse homopolymer **8**, (PDI = 2.75) was obtained.

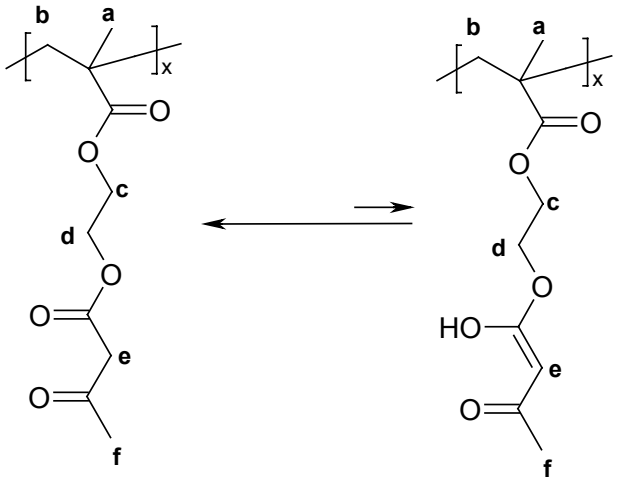

8.

^{1}H NMR (400 MHz, $CDCl_3$) δ [ppm]: 11.90 (s, -OH (enol)), 5.10 (br, s, =CH (**e,** enol)), 4.37 (br, -CH_2 (**d**)), 4.18 (br, -CH_2 (**c**)), 3.57 (br, -CH_2 (**e**)), 2.30 (s, br, -CH_3 (**f**)), 2.15 (s, br, -CH_3 (**f,** enol)), 2.0 – 0.70 (m, br, -CH_3 (**a**), -CH_2 (**b**)).

B. Reversible Addition-Fragmentation Chain-Transfer Polymerization (RAFT)

RAFT was utilised for the synthesis of well-defined homo and block copolymers based on AEMA. As second monomers MMA, BuMA, BuA or NiPAM were used. Polymerisations were carried out at 60 °C under argon. AIBN was the initiator. As RAFT Chain Transfer Agents (CTAs) different dithionyl compounds synthesised in our laboratory following reported synthetic methodologies[135] were used.

6.3.2.3.2 Poly[2-(acetoacetoxy)ethyl methacrylate]s, **8**[69]

A series of pAEMA homopolymers with different polymerisation degrees varying from 30 to 145 was prepared by RAFT. A typical polymerisation procedure is detailed below. The theoretical polymerisation degree was determined from the monomer/CTA molar ratio.

The reaction flask was initially flamed out under dynamic vacuum to eliminate surface moisture. AIBN (30 mg, 0.1827 mmol) and 2-cyanoprop-2-yl dithiobenzoate (300 mg, 1.3553 mmol) dissolved in freshly distilled ethyl acetate (5 ml) were placed in the flask together with AEMA (5 ml, 26 mmol). The monomer concentration was 5.2 M. The reaction mixture was twice de-gased and subsequently heated to 60 °C for 20 hours. After this time,

an aliquot was extracted to be analysed by GPC. The resulting polymer **8** (pink colour) was precipitated in petroleum ether, washed several times and dried *in vacuo* at 30 ^{o}C for one day (quantitative).

^{1}H NMR (400 MHz, $CDCl_3$) δ [ppm]: 11.89 (s, -OH (enol)), 7.86 (d, 2H (Ph of CTA), 7.52 (m, 1H (Ph of CTA), 7.36 (dd, 2H (Ph of CTA), 5.07 (br, s, =CH (**e**, enol)), 4.33 (br, -CH_2 (**d**)), 4.15 (br, -CH_2 (**c**)), 3.55 (s, -CH_2 (**e**)), 2.27 (s, br, -CH_3 (**f**)), 2.15 (s, br, -CH_3 (**f,** enol)), 2.0 – 0.70 (m, br, -CH_3 (**a**), -CH_2 (**b**)).

(ii) BLOCK COPOLYMERS

6.3.2.3.3 Poly(methyl methacrylate)-*block*-poly[2-(acetoacetoxy) ethyl methacrylate], **9.**

PMMA synthesised by RAFT was used as a macroinitiator for the synthesis of pMMA-*b*-pAEMA. AIBN (8 mg, 0.0487 mmol) and pMMA-CTA (2000 mg (MW = 8000), 0.3614 mmol) dissolved in freshly distilled ethyl acetate (6.5 ml) were placed in the polymerisation flask together with AEMA (1 ml, 5 mmol). The monomer concentration was 0.8 M and the molar ratio initiator/CTA 0.195. The reaction mixture was de-gased twice and subsequently heated to 60 ^{o}C for 20 hours. The resulting polymer **9** was precipitated in methanol, washed and left to dry *in vacuo* at 30 ^{o}C for 2 days (conversion: 95%).

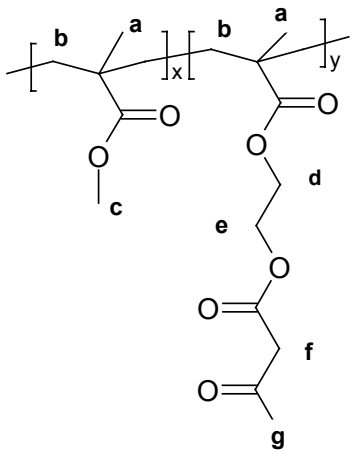

9.

^{1}H NMR (400 MHz, $CDCl_3$) δ [ppm]: 11.89 (s, -OH (enol)), 7.85 (d, 2H (Ph of CTA), 7.51 (m, 1H (Ph of CTA), 7.36 (dd, 2H (Ph of CTA), 5.07 (br, s, =CH (enol)), 4.33 (br, -CH_2 (**e**)), 4.15 (br, -CH_2 (**d**)), 3.57-3.55 (s, -CH_2 (**f**), s, -CH_3 (**c**)), 2.27 (s, br, -CH_3 (**g**)), 2.15 (s, br, -CH_3 (**g,** enol)), 2.0 – 0.70 (m, br, -CH_3 (**a**), -CH_2 (**b**)).

6.3.2.3.4 Poly[2-(acetoacetoxy) ethyl methacrylate]-*block*-poly(*n*-butyl methacrylate), **10**.

pAEMA synthesised by RAFT was used as a macroinitiator for the synthesis of pAEMA-*b*-pBuMA block copolymers.

AIBN (5 mg, 0.0305 mmol) and pAEMA-CTA (1000 mg; MW = 6426, 0.156 mmol) dissolved in freshly distilled ethyl acetate (5 ml) were placed in the polymerisation flask together with freshly distilled BuMA (5 ml, 31 mmol). The monomer concentration was 6.3 M and the molar ratio initiator/CTA 0.195. The reaction mixture was de-gased twice and subsequently heated to 60 ^{o}C for 20 hours. The resulting polymer **10** was precipitated in methanol and left to dry *in vacuo* at 30 ^{o}C overnight (conversion: 90%).

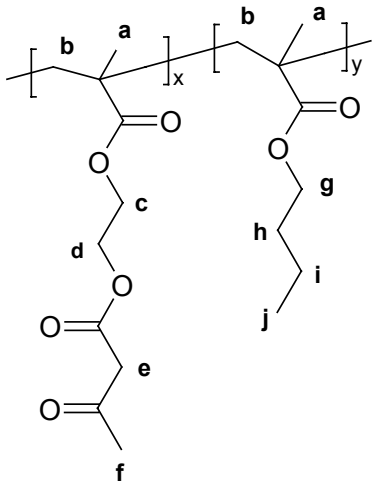

10.

^{1}H NMR (400 MHz, $CDCl_3$) δ [ppm]: 11.89 (s, -OH (enol)), 7.82 (d, 2H (Ph of CTA)), 7.49 (m, 1H (Ph of CTA), 7.33 (dd, 2H (Ph of CTA)), 5.07 (br, s, =CH (**e**, enol)), 4.33 (br, -CH_2 (**d**)), 4.14 (br, -CH_2 (**c**)), 3.91 (br, -CH_2 (**g**)), 3.55 (s, -CH_2 (**e**)), 2.27 (s, br, -CH_3 (**f**)), 2.15 (s, br, -CH_3 (**f,** enol)), 2.0 – 0.70 (m, br, -CH_2 (**b, h, i**), -CH_3 (**a, j**)).

6.3.2.3.5 Poly[2-(acetoacetoxy) ethyl methacrylate)]-*block*-p(*n*-butyl acrylate), **11**.

pAEMA synthesised by RAFT was used as a macroinitiator for the synthesis of pAEMA-*b*-pBuA block copolymers.

AIBN (2 mg, 0.0244 mmol) and pAEMA-CTA (1000 mg; MW = 8760, 0.1142 mmol) dissolved in freshly distilled ethyl acetate (5 ml) were placed in the polymerisation flask together with freshly distilled BuA (2 ml, 14 mmol). The monomer concentration was 2.8M and the molar ratio initiator/CTA 0.213. The reaction mixture was de-gased twice and

subsequently heated to 60 ^{o}C for approximately 15 hours. The resulting polymer **11** was precipitated in ethanol/water 50:50 v/v and left to dry *in vacuo* at 30 ^{o}C for 2 days (conversion: 49%).

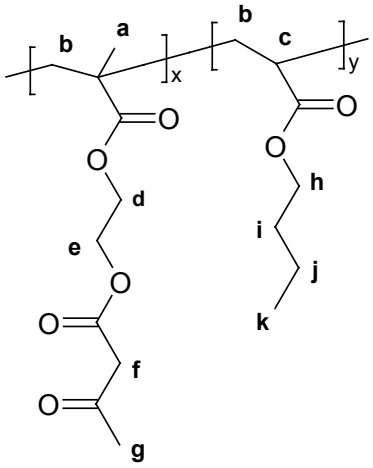

11.

^{1}H NMR (400 MHz, $CDCl_3$) δ [ppm]: 11.90 (s, -OH (enol)), 7.93 (d, 2H (Ph of CTA)), 7.51 (m, 1H (Ph of CTA), 7.35 (dd, 2H (Ph of CTA)), 5.07 (br, s, =CH (enol)), 4.34 (br, -CH_2 (**e**)), 4.16 (br, -CH_2 (**d**)), 4.01 (br, -CH_2 (**h**)), 3.55 (s, -CH_2 (**f**)), 2.28 (s, br, -CH_3 (**g**)), 2.15 (s, br, -CH_3 (**g,** enol)), 2.0 – 0.70 (m, br, -CH (**c**), -CH_2 (**b, i, j**), -CH_3 (**a, k**)).

6.3.2.3.6 Poly[2-(acetoacetoxy)ethyl methacrylate]-*block*-poly(*N*-isopropyl acrylamide), **12**.

pAEMA synthesised by RAFT was used as a macroinitiator for the synthesis of pAEMA-*b*-pNiPAM block copolymers.

AIBN (5 mg, 0.0305 mmol) and pAEMA-CTA (1000 mg; MW = 6426, 0.156 mmol) dissolved in freshly distilled dioxane (9 ml) were placed in the polymerisation flask together with *N*-isopropylamide (1.75 g, 15.5 mmol). The monomer concentration was 1.72M and the molar ratio initiator/CTA 0.196. The reaction mixture was twice de-gased and subsequently heated to 60 ^{o}C for approximately 18 hours. The resulting polymer **12** was precipitated in petroleum ether and left to dry *in vacuo* at 30 ^{o}C for 1 day (conversion: 56%).

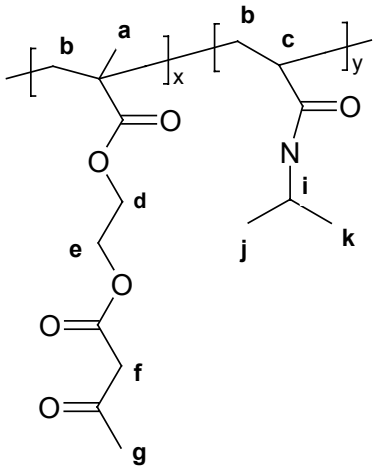

12.

^{1}H NMR (400 MHz, $CDCl_3$) δ [ppm]: 11.90 (s, -OH (enol)), 8.03 (d, 2H (Ph of CTA)), 7.64 (m, 1H (Ph of CTA), 7.47 (dd, 2H (Ph of CTA)), 5.84 (br, -NH (**h**)), 5.15 (br, s, =CH (**f**, enol)), 4.43 (br, -CH_2 (**e**)), 4.24 (br, -CH_2 (**d**)), 4.08 (br, -CH (**i**)), 3.65 (s, -CH_2 (**f**)), 2.28 (s, br, -CH_3 (**g**)), 2.15 (s, br, -CH_3 (**g,** enol)), 2.0 – 0.70 (m, br, -CH (**c**), -CH_2 (**b**), -CH_3 (**a, j**)).

APPENDIX I

1. **Dielectric relaxation on a pAEMA film (determination of T_g).**

2. **Effective dipole moment of the AEMA unit in a pAEMA film.**

20th February 2003

Dielectric relaxation on a poly(2-(acetoacetoxy)ethyl methacrylate) (poly(AEMA)) film

Doerte Blischke and Peter Frübing
Applied Condensed-Matter Physics, University of Potsdam,
Am Neuen Palais 10, 14469 Potsdam
E-mail: fruebing@rz.uni-potsdam.de

Summary: The dielectric spectrum of poly(AEMA) shows a relaxation caused by the onset of micro-brownian chain motions at the glass-transition. A glass-transition temperature of about 274 K and a relaxation strength $\Delta\epsilon \approx 8$ are determined.

The film was prepared by dropping the polymer solution on a gold-coated glass substrate. A circular gold electrode with a diameter of 8.0 mm was evaporated onto the film and a polished stainless-steel plate with the same diameter was laid on the electrode in order to obtain the electric contact. Blistering outside the electrode was observed after the evaporation, but it vanished after two days. The film thickness was determined with a profilometer to about 80 μm. The film is very soft, such that a groove was observed on the surface by scanning it with a force of 1 mg.
Dielectric relaxation spectroscopy (DRS) was performed in dry nitrogen between −140 and +60 °C and from 0.1 Hz to 10 MHz. The Novocontrol ALPHA frequency-response analyser was used together with the QUATRO cryosystem. The data was acquired as a function of frequency under nearly isothermal conditions ($\Delta T_{\max} = 0.25$ K) in steps of 10 K and 5 K below and above −10 °C, respectively.

Below 0 °C no dielectric loss peaks with an unambiguous temperature dependence of the permittivity could be observed. In general, there are only weak dielectric losses in this region.
Above 0 °C a relaxation region was observed which was supposed to be related to the onset of micro-brownian chain motions at the glass transition. The temperature dependences of the relaxation frequency $f = 1/(2\pi\tau)$ with τ being the relaxation time and the relaxation strength $\Delta\epsilon$ were determined. For this purpose, an empirical relaxation function (Havriliak-Negami function) was fitted to the data (Fig. 1 and 2). The Arrhenius plots of the relaxation frequency or the loss-peak frequency $f_{\max}$ are significantly bent, which indicates co-operative behaviour. By fitting the Vogel-Fulcher-Tammann-Hesse (VFTH) equation

$$f(T) = f_\infty \exp\left(-\frac{T_0}{T - T_V}\right)$$

with f_∞, T_0 and T_V being parameters to the relaxation frequencies or loss peak frequencies, the glass-transition temperature T_g can be determined. T_g is usually defined as the temperature where the relaxation time is $\tau = 100$ s [1]. Thus, T_g is obtained by extrapolating the VFTH fit to $1/(2\pi \times 100\text{s}) =$

1.59×10^{-3} Hz. The fits are indicated in Fig. 3 and 4 (relaxation frequency $f = 1/(2\pi\tau)$), and Fig. 5 and 6 (loss peak frequency $f_{\max}$). In Fig. 4 and 6 each data point is weighted, but the results do not differ much from those of the unweighted fits. The VFTH fit parameters and the glass-transition temperatures are presented in Tab. 1. The fits of $f_{\max}$ can be regarded as more reliable

Fig.	f_∞ [GHz]	T_0 [K]	T_V [K]	T_g [K]
3	0.95 ± 1.70	1506 ± 397	217.7 ± 14.5	273.2
4	13.9 ± 49.5	2161 ± 961	195.9 ± 29.9	268.5
5	0.34 ± 1.55	900.0 ± 794.5	240.0 ± 38.7	274.5
6	1.00 ± 23.6	1053 ± 4539	235.0 ± 206.6	273.8

Table 1: The Parameters f_∞, T_0, and T_V of the VFTH fits and the glass-transition temperatures T_g

because τ depends on the shape of the peak. This cannot be considered here because low-frequency (conductivity) and high-frequency contributions cannot be separated unambiguously.

The determination of loss-peak frequencies is not very accurate because of the exponential increase of the conductivity above the glass-transition temperature. Therefore, the temperature range in which the VFTH equation can be used to determine the temperature dependence of the relaxation frequency is rather small, which makes the determination of the glass-transition temperature uncertain. In spite of these difficulties the obtained values for T_g agree well with the value of 3 °C measured with DSC.

The temperature dependence of the relaxation strength $\Delta\epsilon$ is presented in Fig. 7. Due to the above mentioned difficulties in determining the shape of the loss peaks, the values at lower and higher temperatures are rather uncertain. For an orientation, a value of $\Delta\epsilon \approx 8$ can be considered. This value can be used for an estimation of the effective dipole moment of the relaxing species.

More accurate measurements require homogeneous layers with high purity and a well defined thickness. Above the glass-transition temperature, the film should be prepared with spacers between metal plates or metallised glass plates because of its low viscosity.

[1] E. Donth, *Relaxation and thermodynamics in Polymers*, Berlin: Akademie-Verlag, 1992, p.181

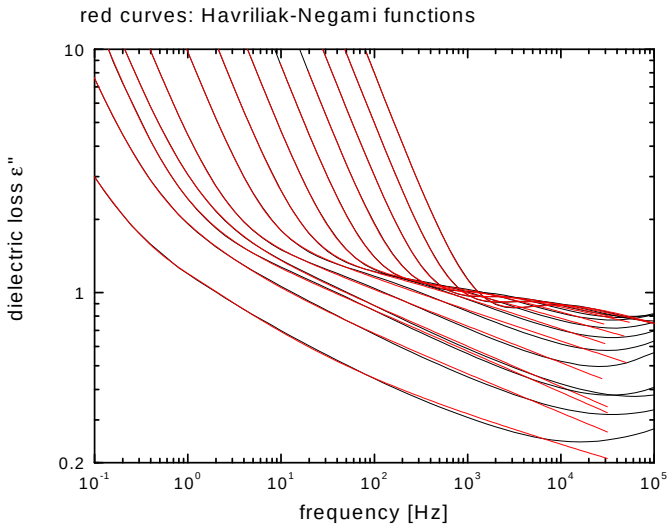

Figure 1: Havriliak-Negami fits at all temperatures (5 to 60 °C)

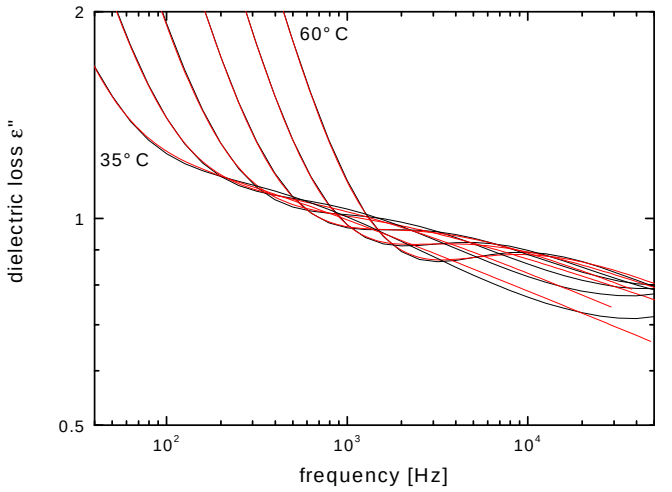

Figure 2: Havriliak-Negami fits at higher temperatures (35 to 60 °C)

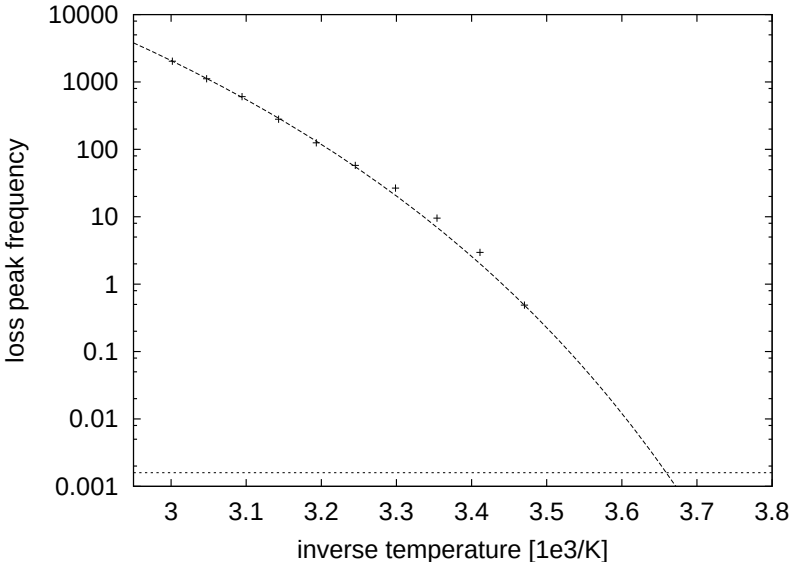

Figure 3: VFTH fit of the relaxation frequency $f = 1/(2\pi\tau)$

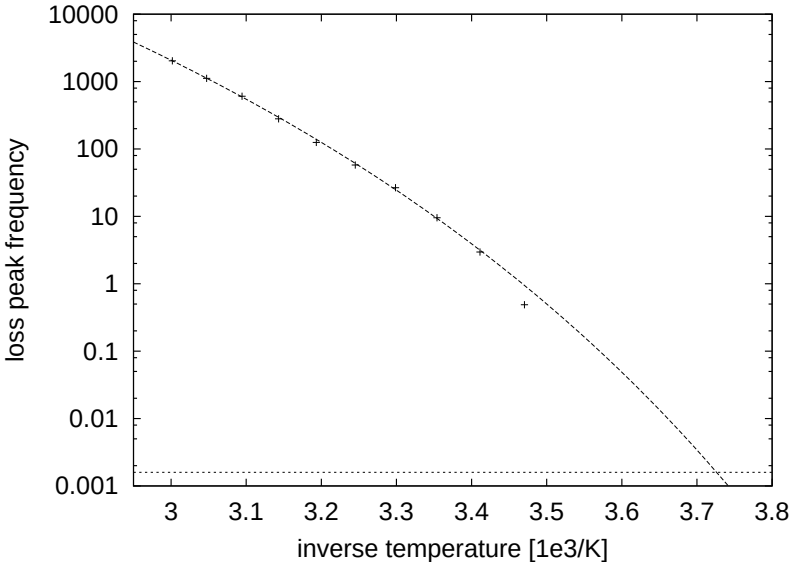

Figure 4: Weighted VFTH fit of the relaxation frequency $f = 1/(2\pi\tau)$

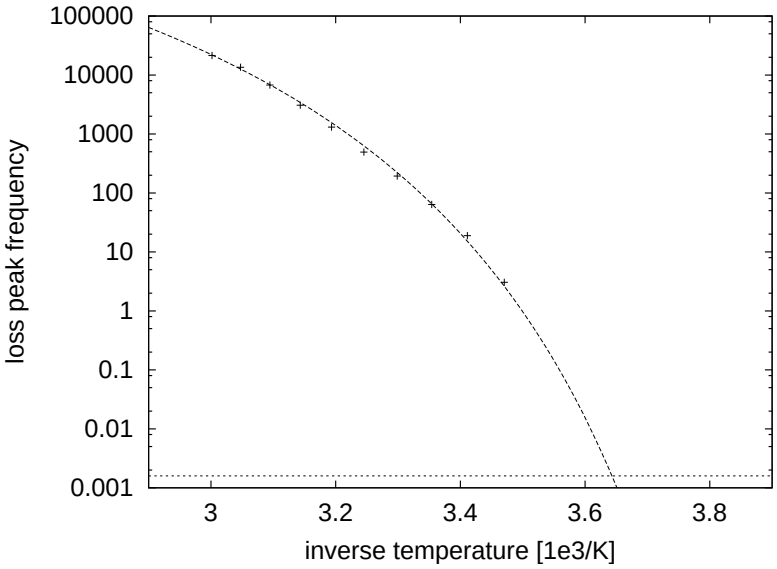

Figure 5: VFTH fit of the loss-peak frequency $f_{\max}$

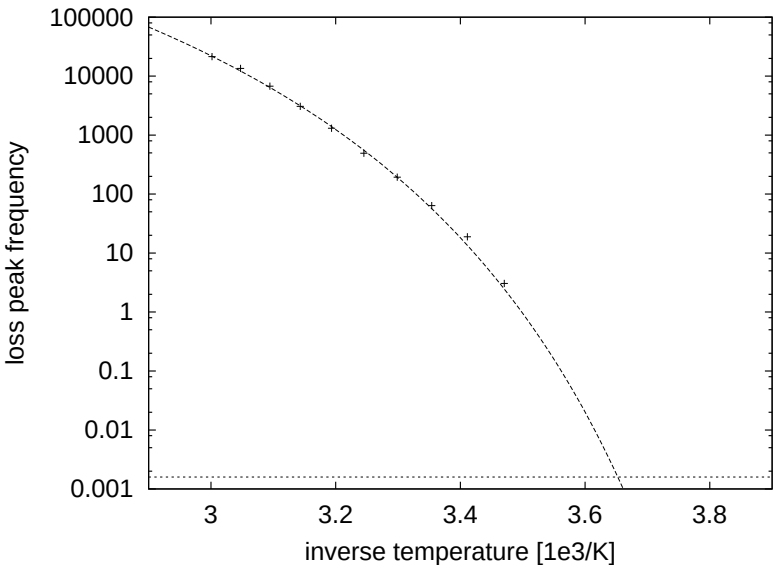

Figure 6: Weighted VFTH fit of the loss-peak frequency $f_{\max}$

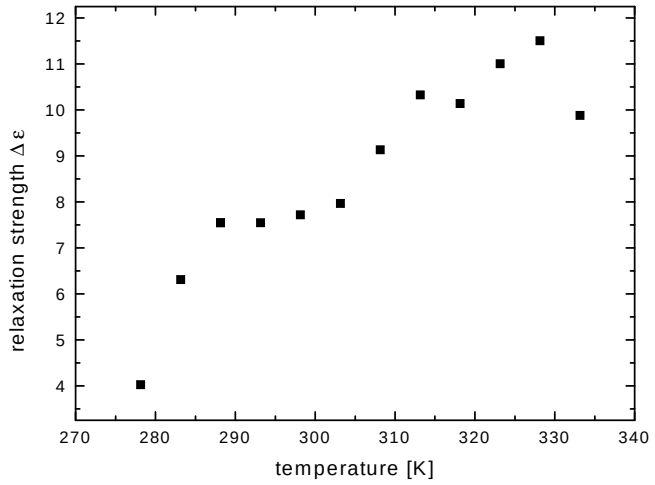

Figure 7: Relaxation strength $\Delta\epsilon$ versus temperature

February 27, 2003

Effective dipole moment of the AEMA unit in the poly(AEMA) film

P. Frübing
Applied condensed-matter physics
University of Potsdam

The dielectric strength $\Delta\epsilon$ which was determined by integration of the loss peak associated to the glass transition can be used to estimate the effective dipole moment of the AEMA unit in the poly(AEMA) film. Because the molecular dipoles in the polymer chain are chemically bonded, always an effective dipole moment in the polymer chain is determined which can differ considerably from the dipole moment of the corresponding free dipolar molecule.

The estimation is based on Curie's law, which describes the dependence of the orientational part of the electric susceptibility χ_o on temperature T above the glass transition where the dipoles are free to move. In the limit of small fields ($\mu_{eff}E_{loc} \ll kT$) the orientational polarisation P_o is given by

$$P_o = \frac{n_D \mu_{eff}^2 E_{loc}}{3kT}\,,$$

where n_D is the dipole concentration, μ_{eff} the effective dipole moment, E_{loc} the local electric field acting on the dipole and k Boltzmann's constant. On the other hand, the orientational polarisation is always given by

$$P_o = \epsilon_0 \chi_o E\,,$$

where ϵ_0 the permittivity of free space and E is the macroscopic field. Considering the Lorentz approximation for the local field

$$E_{loc} = \frac{\chi_o + 3}{3} E\,,$$

and combining these equations, the orientational part of the susceptibility χ_o is given by

$$\chi_o = \frac{n_D \mu_{eff}^2}{3\epsilon_0 kT} \left(\frac{\chi_o + 3}{3}\right)\,.$$

Furthermore, assuming that only one kind of molecular dipoles contributes to $\Delta\epsilon$, it is $\chi_o = \Delta\epsilon$. Rearranging Curie's law gives

$$\mu_{eff} = \sqrt{\frac{9\epsilon_0 kT}{n_D} \frac{\Delta\epsilon}{\Delta\epsilon + 3}}\,.$$

The dipole concentration n_D is calculated from molar mass and density.

Here, the application of Curie's law seems to be justified, if the repeating unit (the AEMA unit) can rotate freely around the polymer backbone. With the electrode diameter $d = 8.0$ mm, film thickness $h = 80$ µm, density $\rho = 1.263$ g/cm^3, molar mass of 1 repeating

unit $m_{mol} = 214.21$ g/mol, a dipole density of $n_D = 3.55 \times 10^{27}$ m^{-3} is calculated. With $\Delta\epsilon = 8$ and $T = 293$ K, this leads to the effective dipole moment $\mu_{eff} = 8.1 \times 10^{-30}$ Cm (2.4 D). It must be emphasised that this is only a rough estimation. At first, the local field cannot be calculated exactly. At second, the film thickness and the measured $\Delta\epsilon$ are affected by relatively large uncertainties (20 % are realistic). However, this could be improved by use of well prepared films with defined thickness and high purity.

APPENDIX II

1. **Experimental plot of refractive index increments dn/dc for the A-2.Fe(III) systems in cyclohexane *versus* [Fe]/[AEMA].**

2. **Zimm Plots for complexes of $pBuMA_{342}$-*b*-$pAEMA_{39}$ (A-2) with $FeCl_3 \cdot 6H_2O$ (i)in the absence and (ii) presence of Et_3N in cyclohexane.**

3. **Zimm Plots for complexes of $pBuMA_{342}$-*b*-$pAEMA_{39}$ (A-2) with $Pd(Ac)_2$ in the presence of Et_3N in cyclohexane.**

1. Refractive index increments dn/dc measured individually for A-2.Fe(III) system (with Fe(III) concentrations) in cyclohexane plotted against [Fe]/[AEMA] (Experimental linear fit).

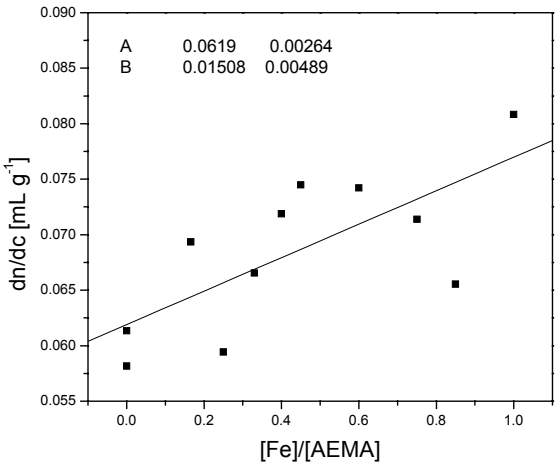

2. Zimm Plots for complexes of $pBuMA_{342}$-*b*-$pAEMA_{39}$ (A-2) with $FeCl_3 \cdot 6H_2O$ in the absence and presence of Et_3N in cyclohexane

(i) Absence of Et_3N

M/L = 0.1

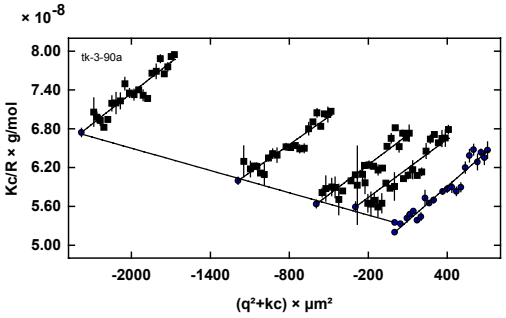

Mw(c): 1.869e7 g/mol Mw(q²): 1.923e7 g/mol
A2: 1.44e-9 mol dm³/g² Rg: 32.02 nm
D:\Theodora\static LS\tk-3-93b\393B1.STA; D:\Theodora\static LS\tk-3-93b\393B2.STA; D:\Theodora\static LS\tk-3-93b\393B3.STA; D:\Theodora\static LS\tk-3-93b\393B4.STA

M/L =0.25

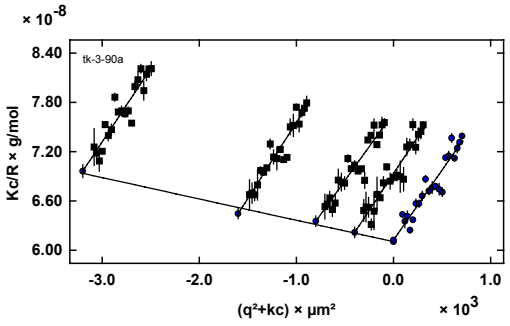

Mw(c): 1.638e7 g/mol Mw(q²): 1.633e7 g/mol
A2: 1.04e-9 mol dm³/g² Rg: 28.89 nm
D:\Theodora\static LS\tk-3-93a\393A4.STA; D:\Theodora\static LS\tk-3-93a\393A1.STA; D:\Theodora\static LS\tk-3-93a\393A2.STA; D:\Theodora\static LS\tk-3-93a\393A3.STA

M/L = 0.33

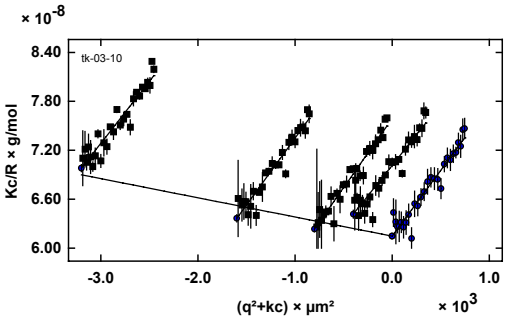

Mw(c): 1.627e7 g/mol Mw(q²): 1.627e7 g/mol
A2: 9.41e-10 mol dm³/g² Rg: 28.08 nm
D:\Theodora\static LS\tk-03-11\311A.STA; D:\Theodora\static LS\tk-03-11\311B.STA; D:\Theodora\static LS\tk-03-11\311C.STA; D:\Theodora\static LS\tk-03-11\311D.STA

M/L = 0.45

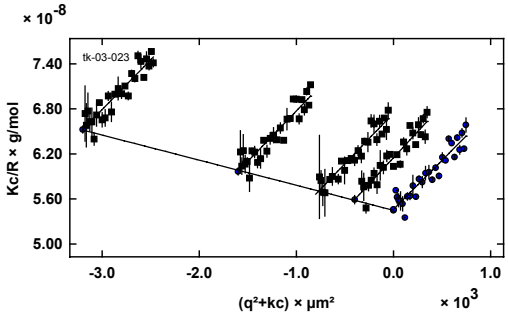

Mw(c): 1.835e7 g/mol Mw(q²): 1.831e7 g/mol
A2: 1.34e-9 mol dm³/g² Rg: 26.78 nm
D:\Theodora\static LS\tk323\323A.STA; D:\Theodora\static LS\tk323\323B.STA; D:\Theodora\static LS\tk323\323C.STA; D:\Theodora\static LS\tk323\323D.STA

M/L = 0.6

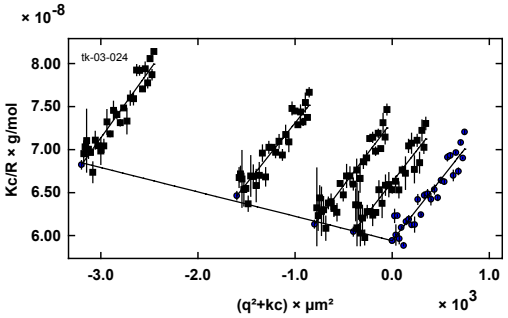

Mw(c): 1.683e7 g/mol Mw(q²): 1.683e7 g/mol
A2: 1.13e-9 mol dm³/g² Rg: 26.83 nm
D:\Theodora\static LS\tk324\324A.STA; D:\Theodora\static LS\tk324\324B.STA; D:\Theodora\static LS\tk324\324C.STA; D:\Theodora\static LS\tk324\324D.STA

M/L = 0.85

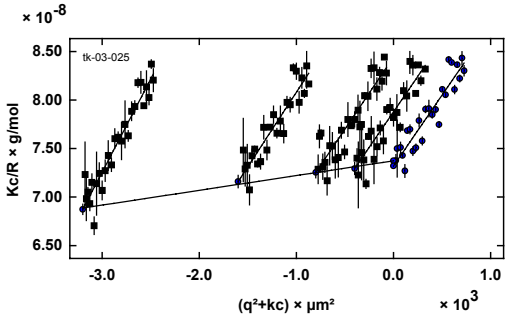

Mw(c): 1.356e7 g/mol Mw(q²): 1.366e7 g/mol
A2: -6.09e-10 mol dm³/g² Rg: 24.44 nm
D:\Theodora\static LS\tk325\325A.STA; D:\Theodora\static LS\tk325\325B.STA; D:\Theodora\static LS\tk325\325C.STA; D:\Theodora\static LS\tk325\325D.STA

(ii) Presence of Et_3N

M/L = 0.35

M/L = 0.52

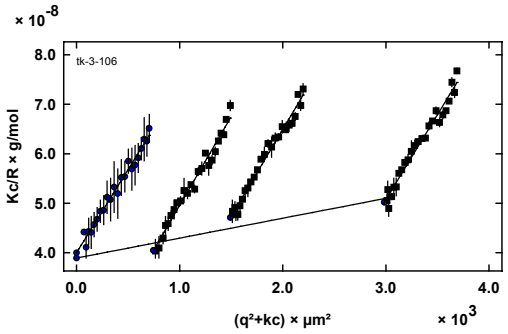

Mw(c): 2.568e7 g/mol Mw(q²): 2.499e7 g/mol
A2: 2.18e-9 mol dm³/g² Rg: 50.22 nm
D:\Theodora\static LS\3106b\3106B2.STA; D:\Theodora\static LS\3106b\
3106B3.STA; D:\Theodora\static LS\3106b\3106B4.STA

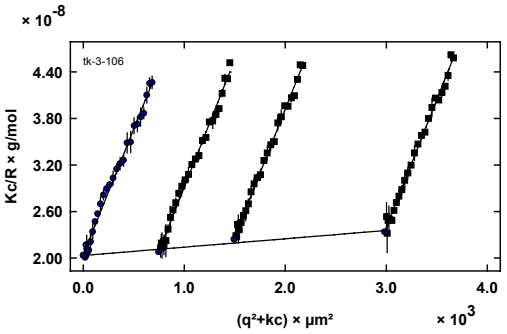

Mw(c): 4.92e7 g/mol Mw(q²): 4.903e7 g/mol
A2: 2.84e-10 mol dm³/g² Rg: 69.13 nm
D:\Theodora\static LS\3106a\3106A1.STA; D:\Theodora\static LS\3106a\
3106A2.STA; D:\Theodora\static LS\3106a\3106A3.STA

3. Zimm Plots for complexes of $pBuMA_{342}$-b-$pAEMA_{39}$ (A-2) with $Pd(Ac)_2$ in the presence of Et_3N in cyclohexane

M/L = 0.12

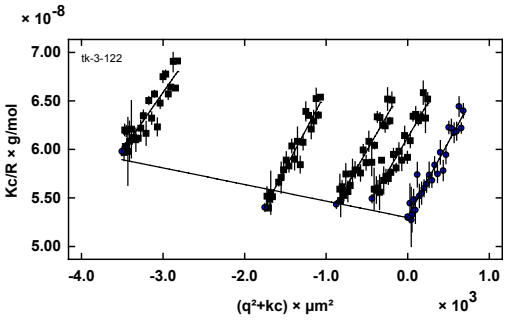

Mw(c): 1.888e7 g/mol Mw(q²): 1.884e7 g/mol
A2: 6.83e-10 mol dm³/g² Rg: 29.53 nm
D:\Theodora\static LS\3122a\3122A1.STA; D:\Theodora\static LS\3122a\
3122A2R.STA; D:\Theodora\static LS\3122a\3122A3.STA; D:\Theodora\static LS\
3122a\3122A4.STA

M/L = 0.23

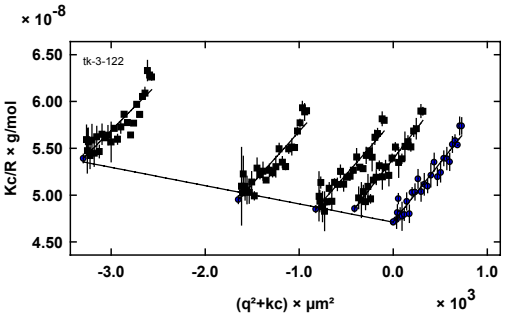

Mw(c): 2.123e7 g/mol Mw(q²): 2.121e7 g/mol
A2: 7.81e-10 mol dm³/g² Rg: 28.35 nm
D:\Theodora\static LS\3122b\3122B1.STA; D:\Theodora\static LS\3122b\
3122B2.STA; D:\Theodora\static LS\3122b\3122B3.STA; D:\Theodora\static LS\
3122b\3122B4.STA

M/L = 0.4

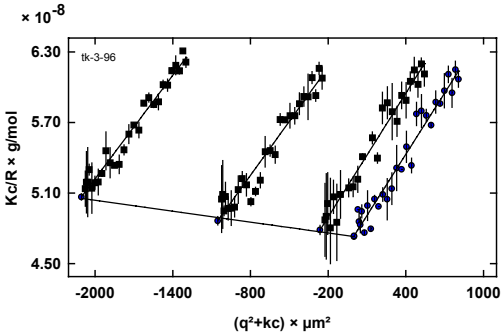

Mw(c): 2.114e7 g/mol Mw(q²): 2.112e7 g/mol
A2: 6.19e-10 mol dm³/g² Rg: 33.17 nm
D:\Theodora\static LS\tk-3-96\396A.STA; D:\Theodora\static LS\tk-3-96\
396B.STA; D:\Theodora\static LS\tk-3-96\396D.STA

M/L = 0.55

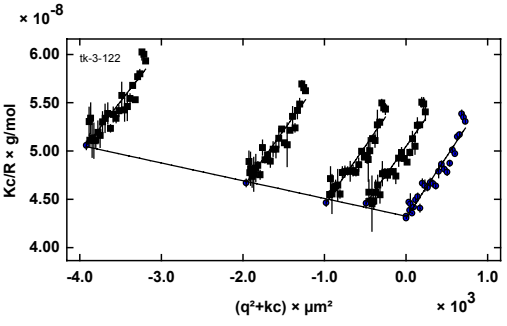

Mw(c): 2.312e7 g/mol Mw(q²): 2.323e7 g/mol
A2: 7.35e-10 mol dm³/g² Rg: 29.87 nm
D:\Theodora\static LS\3122c\3122C1.STA; D:\Theodora\static LS\3122c\
3122C2.STA; D:\Theodora\static LS\3122c\3122C3.STA; D:\Theodora\static LS\
3122c\3122C4.STA

APPENDIX III

1. Calculation of the interaction parameter χ between BuMA/AEMA

Calculation of the interaction parameter χ between BuMA/AEMA

The polymer/polymer interaction parameter is a sum of entropic and enthalpic contributions:

$$\chi = \chi_s + \chi_H \tag{III.1}$$

where χ_s in the entropic and χ_H the enthalpic term of the interaction parameter. χ_s is usually taken as a constant ($\chi_s = 0.34$) for non-polar systems. The enthalpic component is related to the Hildebrand parameters δ of each block in a block copolymer system as:

$$\chi_H = \frac{V_1}{RT}(\delta_1 - \delta_2)^2 \tag{III.2}$$

thus,

$$\chi = 0.34 + \frac{V_1}{RT}(\delta_1 - \delta_2)^2 \tag{III.3}$$

The molar attraction constant F_j defined in equation III.4, can be used to calculate the solubility parameter using III.5.

$$F_j = \left(\Delta E^v_{i,j} V_{i,j}\right)^{1/2} \tag{III.4}$$

$$\delta_i = \left(\frac{\Delta E^v_i V_i}{V_i^2}\right)^{1/2} = \frac{\sum_j F_j}{V_i} = \frac{\rho_{ij}\sum_j F_j}{M_i} \tag{III.5}$$

ΔE_i^v is the energy of vaporisation and V_i the molar volume of species i. ρ_i is the polymer density and M_i its molecular weight. For polymers, δ_i can be evaluated for the repeating group by using group contribution calculations for the molar volume and the molar attraction constant. In Table III.1, the calculated values of molar attraction constants and Hildebrand parameters corresponding to the two blocks in pBuMA-*b*-pAEMA block copolymers are presented. Using equation III.3, the BuMA/AEMA interaction parameter was found to be 1.14. This is an extremely high value, which indicates that the two blocks are highly immiscible, thus exhibiting high tendency for phase separation.

Table III.1: *Calculated values of molar attraction constants F and Hildebrand parameters δ, corresponding to pBuMA and pAEMA blocks in pBuMA-b-pAEMA.*

	F $(MPa^{0.5}cm^3mol^{-1})$	**δ** $(MPa)^{0.5}$	**V** $(cm^3\ mol^{-1})$
PBuMA	2406	15.1	161
pAEMA	3602	18.9	

8 Abbreviations

A_2	Second virial coefficient
αBiB	*Tert*-butyl α-bromoisobutyrate
ac	Acetyl acetone
AEMA	(2-acetoacetoxy)ethyl methacrylate
AFM	Atomic force microscopy
AIBN	2,2'-azobis(isobutyronitrile)
ATRP	Atom transfer radical polymerisation
AUC	Analytical ultracentrifugation
b.p.	Boiling point
b^2	Area per molecule at the core/corona interface of micelles
BuLi	*n*-Butyl lithium
9-BBN	9-borabicyclo[3.3.1]nonane
BuMA	*n*-butyl methacrylate
CH	Cyclohexane
cod	Cyclooctadiene
CPDB	2-cyano-prop-2-yl dithiobenzoate
CTA	Chain transfer agent
D_h	Dimensions of micellar corona
DJ	Double-jet method
DLS	Dynamic light scattering
DMA	Dimethyl amide
DMF	Dimethyl formamide
DMSO	Dimethyl sulfoxide
dNbipy	4,4'-dinonyl-2,2'-bipyridine
DP, N	Degree of polymerisation
DRI	Differential refractometer
DRS	Dielectric relaxation spectroscopy
DSC	Differential scanning calorimetry

EA	Ethyl acetate
FT-IR	Fourier transform infrared
GPC	Gel permeation chromatography
GTP	Group Transfer Polymerisation
ID	Identity
LS	Light scattering
Me6TREN	Tris[2-(dimethylamino)ethyl]amine
MEK	Methyl ethyl ketone
MeOH	Methanol
MMA	Methyl methacrylate
MTS	1-methoxy-1-trimethylsiloxy-2-methylprop-1-ene
MW,M	Molecular weight
MWD	Molecular weight distribution
NMR	Nuclear magnetic resonance
p4VP	Poly(4-vinylpyridine)
pAEE	Poly[2-(acetoacetoxy)ethyl ethylene]
pAEMA	Poly[(2-acetoacetoxy)ethyl methacrylate]
pB	Poly(1,2-butadiene)
pBuA	Poly(*n*-butyl acrylate)
pBuMA	Poly(*n*-butyl methacrylate)
pEO	Poly(ethylene oxide)
pHEE	Poly[2-(hydroxyethyl) ethylene]
pHEMA	Poly(2-hydroxyethyl methacrylate)
pLA	Poly(lactic acid)
pMAc	Poly(methacrylic acid)
pMMA	Poly(methyl methacrylate)
pNiPAM	Poly(N-isopropyl acrylamide)
PPDB	2-phenyl-prop-2-yl dithiobenzoate
ppm	Parts per million

pS	Poly(styrene)
pTMSHEMA	Poly[(2-trimethylsilyloxy)ethyl methacrylate]
RAFT	Reversible addition-fragmentation chain-transfer polymerisation
R_c	Core radius
R_g	Radius of gyration
R_H	Hydrodynamic radius
RI	Refractive index
SEC	Size exclusion chromatography
SEM	Scanning electron microscopy
SFRP	Stable free radical polymerisation
SLS	Static light scattering
SSL	Strong segregation limit
SSSL	Super strong segregation limit
TBABB	Tetrabutylammonium bibenzoate
t-BuOH	Tert-butyl alcohol
t-BuP_4	Phosphazene base P4
TFA	Trifluoroacetic acid
T_g	Glass transition temperature
THF	Tetrahydrofuran
UV-Vis	Ultraviolet/visible
v/v	Volume ratio
WSL	Weak segregation limit
Z	Aggregation number

9 Acknowledgements

One or two more pages left to write...Reaching this last part of the Thesis, many students may already feel that they have reached the end. The "Acknowledgements" part, may seem much easier to write comparing to all the others. For me, thanking all the people the way I would have liked to, for everything they offered me these last years, another Thesis, dealing more with friendship, support, care, concern, trust and love should be submitted together with this one. Unfortunately, since the number of pages is limited, I will have to be short...

Firstly, I would like to thank all the people whose contribution in this work was valuable:

Prof. Dr. Dr. Markus Antonietti, for the nice opportunity he offered me to work on this fascinating project and all the fruitful discussions with him, which helped to find answers in many questions concerning this work.

My supervisor, Dr. Helmut Schlaad, for his continuous help and concern: For the numerous discussions, the useful suggestions, as well as all the "teaching hours" he kindly offered me.

Dr. Reinhard Sigel and Andreas Erbe for all the time they spent to teach me all about Light Scattering techniques.

Dr. Peter Frübing and Dr. Doerte Blischke (Physics Department, University of Potsdam) for the dielectric measurements.

Dr. Rémi Soula for carrying out the 2-D HSQC and HMBC NMR experiments and teaching me RAFT polymerisation techniques among others.

My former supervisor in Cyprus, Dr. Costas Patrickios for providing the catalyst for GTP and Dr. Jan Rudloff for the synthesis of poly(ethyl ethylene)-*b*-poly(ethylene oxide) block copolymer.

Dr. Jürgen Hartmann and Rona Pitschke for the SEM and TEM images, as well as Anne Heilig and Roy Knocke for numerous AFM measurements.

Dr. habil. Helmut Cölfen for the discussions concerning biomineralisation processes and Dr. Pavla Kasparova for showing me the use of the Double-Jet method.

Dr. Charl Faul for all the corrections/suggestions he made on this Thesis, and the "chocolate-break rescues" during writing-up.

Dr. habil. Klaus Tauer for all the help concerning FTIR experiments.

Olaf Niemeyer for carrying out numerous NMR experiments and Marlies Gräwert for the GPC measurements.

Finally, I would like to thank Birgit Schonert for the determination of refractive index increments, Ingrid Zenke for X-ray scattering, Antje Völkel for AUC experiments and Carmen Remde for TGA and DSC measurements on pAEMA samples.

For the financial support I would like to thank the Deutscher Akademischer Ausstauschdienst (DAAD) and the Max-Planck-Gesellschaft.

A special "Thank you" goes to all the people in my group: Ivo, Hilde and Stefan for the time they spent helping and teaching me many things. Rémi for his friendship, the nice sense of humour which always created a nice atmosphere in the office and in the lab, and his continuous efforts (sometimes successful sometimes not) to keep me motivated. Ines, for teaching me all the lab "secrets", but mostly for her love, trust and friendship, help and support in many personal situations. Magda and Justyna for being great office-mates, all the office material they "borrowed" me and for teaching me the beauty of the polish language!

A big "Thank you" also to Alexandra, Sascha, Charl and Jacqueline for their love, help and friendship throughout these years. So many people still to thank...Each one of them for different reasons, impossible to enumerate here… Bernd and Jennifer, Ilka, Franck and Sandrine, Céline, Rumi, Irina, Jeremy, Chris, Hans, Andreas, Arne, Matthijs, Markus, Julien, Hartmut, Byram, Danielle, Oychai, Christian, Arkadi, Jan and Nena, Atul, Victor, Jessica, Sebastian, Gordon, Rivelino, Doreen, Patrycia, Sophie, Liliana, Matthieu, Ufuk, Shu-Hong, Cony, Hannes, Samira, Karin, Quan, Klaus, and many others...I enjoyed a lot working with

them, but mostly I thank all of them for the great time we had in the Institute during the day, the nice afternoons spent in Chez Briel (even tolerating my Greek singing!), the funny "basketball" afternoons, the numerous dinners, barbecues, picnics, concerts, birthday parties at the familiar coffee corners, for all these special and enjoyable moments that made my time here in Germany **really** unforgettable!

Last but not least, I would like to say a big "Thank you" to all my friends and family in Cyprus. Especially my parents, Christos and Froso and my brother and sister Giorgos and Ioanna, for always being by my side, supporting me every day with their continuous love and believe in me.

A special "more than Thank you" goes to Tryfonas, for all his love, support and patience throughout all these years.

Well, I think I managed...OK a bit more than the usual two pages... But I guess the rest of this Second Thesis is quite familiar to all of you and you even wrote most of the pages inside... It has been already submitted in our hearts and guess what? It has been already given a mark: EXCELLENT!!

THANK YOU!

ΣΑΣ ΕΥΧΑΡΙΣΤΩ!

10 Literature

[1] Elias, H-G. *An Introduction to Plastics*,1st Ed.; VCH Verlagsgesellschaft mbH, Weinheim (Germany) and VCH Publishers, Inc., New York, NY (USA), **1993.**

[2] Förster S.; Antonietti, M. *Adv. Mater*., **1998**, 10, (3), 195.

[3] Yamashita, Y. Ed., *Chemistry and Industry of Macromonomers*, Hüthig and Wepf, Basel, Heidelberg, New York, **1993**.

[4] Kukula, H. *PhD Thesis*, University of Potsdam, **2001**.

[5] Faust, R.; Schlaad, H. *Applied Polymer Science: 21st Century, Elsevier Science:* Amsterdam, The Netherlands, **2000**, 999.

[6] Faust, R.; Schlaad, H.; *Applied Polymer Science : 21st Century, Craver, C. D.; Carraher Jr., Ch. E. (Eds); Elsevier,* Oxford, **2000.**

[7] Faust, R.; Kennedy, J. P. *Polym. Bull.*, **1986**, 15, 317.

[8] Faust, R.; Kennedy, J. P. *Polym. Sci., Polym. Chem. Ed.,* **1987**, 25, 1847.

[9] Miyamoto, M.; Sawamoto, M.; Higashimu, T. *Macromolecules,* **1984**, 17, 265.

[10] Hawker, C.; *J. Trends in Polym. Sci.,* **1996**, 4, 183

[11] Matyjaszewski, K. *Curr. Opin. Solid State Interface Sci.,* **1996**, 1, 769.

[12] Scollard, H. D.; McConville, D. H. *J. Am. Chem. Soc.*, **1996**, 118, 10008.

[13] Baumann, R.; Davis, W. M.; Schrock, R. R. *J. Am. Chem. Soc*., **1997**, 119, 3830.

[14] Sperling, L.H. *Introduction to Physical Polymer Science,* 3rd Ed. **2001.**

[15] Meredith, C. R.; VanDusen, J. G.; Williams, D. J. *Macromolecules*, **1982**, 15, 1385.

[16] Bates, F. S.; Fredrickson, G. H.; *Annu. Rev. Phys. Chem*., **1990**, 41, 525.

[17] Förster, S.; Zisenis, M.; Wenz, E.; Antonietti, M. *J. Chem. Phys*., **1996**, 104, 24, 9956.

[18] Nyrkova, I. A.; Khokhlov, A. R.; Doi, M. *Macromolecules*, **1993**, 26, 26.

[19] Matsen, M. W.; Bates, F. S. *Macromolecules***, 1996**, 29, 1091.

[20] Matsen, M. W.; Bates, F. S. *Macromolecules***, 1996**, 29, 7641.

[21] Tuzar, Z.; Kratochvíl, P. *Adv. Colloid Interface Sci.,* **1976**, 6, 201 and references therein.

[22] Riess, G.; Hurtrez, G.; Bahadur, P. *Encyclopedia of Polymer Science and Engineering*, 2nd ed.; Wiley-Inter-science: New York, **1985**; Vol. 2, p.324. and references therein.

[23] Tuzar, Z.; Kratochvil, P. *Surface and Colloid Science* (Ed: E. Matijevic), Plenum, New York, **1993**.

[24] Chu, B. *Langmuir*, **1995**, 11, 414.

[25] Alexandridis, P. *Curr. Opin. Colloid Interface Sci.,* **1996**, 1, 490.

[26] Selb, J.; Gallot, Y. *Developments in Block Copolymers* (Ed: Goodman, I.) Elsevier, Amsterdam **1985**, Vol. 2, p.27.

[27] Moffitt, M.; Khougaz, K.; Eisenberg, A. *Acc. Chem. Res*., **1996**, 29, 95.

[28] (a) Astafieva, I.; Zhong, X. F.; Eisenberg, A. *Macromolecules,* **1993**, 26, 7339. (b) Astafieva, I.; Khougaz, K.; Zhong, X. F.; Eisenberg, A. *Macromolecules,* **1995**, 28, 7127.

[29] Qin, A.; Tian, M.; Ramireddy, C.; Webber, S. E.; Munk, P.; Tuzar, Z. *Macromolecules*, **1994**, 27, 120.

[30] Van Os, M. N.; Haak, J. R.; Rupert, L. A. M. *Physico-chemical properties of selected anionic, cationic and nonionic surfactants,* Elservier, Amsterdam, **1993**.

[31] (a) Chiefari, J.; Chong, Y. K.; Ercole, F.; Krstina, J.; Jeffery, J.; Le, T. P. T.; Mayadunne, R. T. A.; Meijs, G. F.; Moad, C. L.; Moad, G.; Rizzardo, E.; Thang, S. H. *Macromolecules,* **1998**, 31, 5559-5562. (b) Chong, Y. K. B.; Le, T. P. T.; Moad, G.; Rizzardo, E.; Thang, S. H. *Macromolecules*, **1999**, 32, 2071.

[32] Szwarc, M.; Levy, M.; Milkovich, R. *J. Am. Chem. Soc.,* **1957**, 78, 2656.

[33] Allcock, H. R.; Lampe, F. W. *Contemporary Polymer Chemistry*, 2nd Ed., **1990**.

[34] Webster, O. W.; Hertler, W. R.; Sogah, D. Y.; Farnham, W. B.; RajanBabu, T. V. *J. Am. Chem. Soc*., **1983**, 105, 5706.

[35] Masar, B.; Vlcek, P.; Kríz, J.; Kovárová, J. *Macromol. Chem. Phys*., **1994**, 195, 289.

[36] Narasaka, K.; Soai, K.; Aikawa, Y.; Mukaiyama, T. *Bull Chem Soc Jpn,* **1976**, 49, 779.

[37] Webster, O. W. *J. Polym. Sci., Part A: Pol. Chem*., **2000**, 38, 2855.

[38] Baskaran, D. *Prog. Polym. Sci*., **2003**, in press.

[39] Mai, P.M.; Müller, A. H. E. *Makromol. Chem. Rapid Commun.,* **1987**, 29 (2), 73.

[40] Müller, A. H. E. *Makromol. Chem, Makromol. Symp.*, **1990**, 32, 87.

[41] (a) Quirk, R. P.; Ren, J. *Macromolecules*, **1992**, 25, 6612. (b) Quirk, R. P.; Ren J.; Kim, J. S. *Makromol. Chem, Makromol. Symp.*, **1993**, 67, 351.

[42] Krasia, T., *Diploma Thesis*, University of Cyprus, **1999**.

[43] Mayadunne, R. T.A.; Rizzardo, E.; Chiefari, J.; Chong, Y. K.; Moad, G.; Thang, S. H. *Macromolecules,* **1999**, 32, 6977.

[44] Hawthorne, D. G.; Moad, G.; Rizzardo, E.; Thang, S. H. *Macromolecules,* **1999**, 32, 5457.

[45] Mayadunne, R. T.A.; Rizzardo, E.; Chiefari, J.; Krstina, J.; Moad, G.; Postma, A.; Thang, S. H. *Macromolecules,* **2000**, 33, 243.

[46] Kanagasabapathy, S.; Sudalai, A.; Benicewicz, B. C. *Macromol. Rapid Commun*., **2001**, 22, 1076.

[47] Stenzel-Rosenbaum, M.; Chen, V.; Fane, A. G.; Davis, T. P. *J. Polym. Sci., Part A: Pol. Chem*., **2001**, 39, 2777.

[48] Shinoda, H.; Matyjaszewski, K. *Macromol. Rapid Commun*., **2001**, 22, 1176.

[49] Quinn, J. F.; Barner, L.; Kowollik, C. B.; Rizzardo, E.; Davis, T. P. *Macromolecules,* **2002**, 35, 7620-7627.

[50] Dörr, N. *Diploma Thesis*, Laboratoire de Chimie et Procédés de Polymérisation (LCPP) von CPE Lyon/CNRS, Institüt für Chemische Technologie organischer Stoffe der Technischen Universität Wien, **2000**.

[51] Kaliyappan, T.; Kannan, P. *Prog. Polym. Sci.,* **2000**, 25, 343.

[52] Cölfen, H. *Macromol. Rapid Commun*., **2001**, 22, 219.

[53] Schlaad, H.; Krasia, T.; Patrickios, C. S. *Macromolecules*, **2002**, 34, 7585.

[54] Antonietti, M.; Förster, S.; Hartmann, J.; Oestreich, S. *Macromolecules,* **1996**, 29, 3800.

[55] Chernyshov, D.; Bronstein, L. M.; Börner, H.; Berton, B.; Antonietti, M. *Chem. Mater.,* **2000,** 12, 114.

[56] Fendler, J. H. N*anoparticles and Nanostructured Films*; Ed.; Wiley – VCH: Weinheim, New York, **1998**, p.468.

[57] Hien, O.; Eschbaumer, C.; Schubert, U. S. *Macromol. Rapid Commun*., **2000**, 21, 1156.

[58] Schubert, U. S.; Hochwimmer, G.; *Macromol. Rapid Commun.,* **2001**, 22, 274.

[59] Gohy, J. F.; Lohmeijer, B. G. G.; Schubert, U. S. *Macromolecules,* **2002**, 35, 4560.

[60] Schubert, U. S.; Hofmeier, H. *Macromol. Rapid Commun*., **2002**, 23, 561.

[61] Mehrotra, R. C.; Bohra, B.; Gaur, D. P. *Metal β–Diketonates and Allied Derivatives*, Academic Press: New York, **1978**.

[62] (a) Teyssié, P.; Smets, G. *Makromol. Chem.,* **1958** 26, 245. (b) De Wilde-Delvaux, M. C.; Teyssié, P. *Spectrochimica Acta,* **1958**, 12, 280.

[63] Masuda, S.; Sertova, N.; Petkov, I. *J. Polym. Sci. Part A: Polym. Chem.,* **1997**, 35, 3683.

[64] (a) Inn, M.; Gérardin, C.; Lambard, J.; Sanchez, C. *J. Sol-Gel Sci. Tech.,* **1995**, 5, 101. (b) Masuda, S.; Minagawa, K. *Prog. Polym. Sci.***, 1996**, 21, 557. (c) Agarwal, R.; Bell, J. S. *Polym. Eng. Sci.,* **1998**, 38, 299.

[65] Marmor, S.; Kidane, G. *Polym. Bull.,* **1978**, 1, 239.

[66] Hanabusa K.; Suzuki, T.; Koyama, T.; Shirai, H. *Makromol. Chem.,* **1992**, 193, 2149.

[67] Dell' Anna, M. M.; Mastrorilli, P.; Rizzuti, A.; Suranna, G. P.; Nobile, C. F. *Inorganica Chimica Acta,* **2000** 304, 21.

[68] Dell' Anna, M. M.; Gagliardi, M.; Mastrorilli, P.; Suranna, G. P.; Nobile, C. F. *Journal of Molecular Catalysis A: Chemical,* **2000** 158, 515.

[69] Krasia, T.; Soula, R.; Börner, H.; Schlaad, H. *Chem. Commun.,* **2003**, (4) 538.

[70] Schlaad, H.; Kilz, P. *Anal. Chem*., **2003**, 75 (6), 1548.

[71] Pasch, H.; Trathnigg, B. *HPLC of Polymers*, Springer: Berlin, **1997**.

[72] G.C Berry, P.M. Cotts, *Static and Dynamic Light Scattering,* **1997**.

[73] Ed. A. H. Fawcett, *Polymer Spectroscopy*, John Wiley and Sons, UK, **1996**.

[74] Albert Einstein, *Investigations of the Theory of Brownian Movement,* Dover Publications, ISBN: 0486603040.

[75] Wenz E. *PhD Thesis*, Freie Universität Berlin, **1996.**

[76] J. W. Strutt Rayleigh, *Philos. Mag.*, 47, 375, **1899.**

[77] Y. Geerts, D. Muscat, K. Mullen*, Macromol. Chem. Phys.,* 196, **1995**, 3425.

[78] S. Menzer, A. J. P. White, D. J. Williams, M. Belohradsky, C. Hamers, F. M. Raymo, A. N. Shipway, J. F. Stoddart, *Macromolecules*, 31, **1998**, 295.

[79] S. I. Stupp, V. LeBonheur, K. Walker, L. S. Li, K. E. Huggins, M. Keser, A. Amstutz, *Science*, 276, **1997**, 384.

[80] T. H. Mourey, S. R. Turner, M. Rubistein, J. M. J. Frechet, C. J. Hawker, K. L. Wooley, *Macromolecules,* 25, **1992**, 2401.

[81] C. L. Jackson, H. D. Chanzy, F. P. Booy, B. J. Drake, D. A. Tomalia, B. J. Bauer, E. J. Amis, *Macromolecules*, 31, **1998**, 6259.

[82] G. Binning, C. Quate, C. Gerber. *Phys. Rev. Lett.*, 56, **1986**, 930.

[83] McLean, R. S.; Sauer, B. B. *Macromolecules,* **1997**, 30, 8314.

[84] Hansma, H. G. *et al. Science*, **1992**, 256, 1180; Hoh, J. H.; Lal, R.; John, S. A.; Revel, J.-P.; Arnsdorf, M. F. *Science*, **1991**, 253, 1405; Radmacher, M.; Tillmann, R. W.; Fritz, M.; Gaub, H. E. *Science*, **1992**, 257, 1900.

[85] O'Reilly, M.; McDonnell, L; O'Mullane, J. *Ultramicroscopy*, 86, **2001**, 107.

[86] Chescoe, D.; Goodhew, J. *The operation of Transmission and Scanning Electron Microscopes*, Oxford University Press, Royal Microscopical Society, **1990.**

[87] Yu, S. H.; Cölfen, H.; Hartmann, J.; Antonietti, *Adv. Funct. Mater.,* **2002**, 12, 541.

[88] Ralston, G. *Introduction to Analytical Ultracentrifugation,* Beckman Instruments, Fullerton, California, **1993**.

[89] Cölfen, H., *Polymer News*, **1998**, 23 (5), 152.

[90] Matijevic, E.; *Current Option in Colloid Interface Science,* **1996**, *1*, 176.

[91] Sedlák, M; Antonietti, M.; Cölfen, H.; *Macromol. Chem. Phys.*, **1998**, *199*, 247.

[92] Witzeman, J. S.; Nottingham, W. D. *J. Org. Chem.,* **1991**, 56, 1713.

[93] Ramakrishnan, S. *Macromolecules*, **1991**, 24, 3753.

[94] Matyjaszewski, K.; Xia, J. *Chem. Rev.,* **2001**, 101, 2921.

[95] (a) Cornelissen, J. J. L. M.; Fischer, M.; Sommerdijk, N. A. J. M.; Nolte, R. J. M. *Science*, **1998**, 289, 1427. (b) Sommerdijk, N. A. J. M.; Holder, S. J.; Hiorns, R. C.; Jones, R. G. J.; Nolte, R. J. M. *Macromolecules*, **2000**, 33, 8289.

[96] (a) Zhang, L.; Eisenberg, A. *Science*, **1995**, 268, 1728. (b) Zhang, L.; Yu, K.; Eisenberg, A. *Science*, **1996**, 272, 1777.

[97] (a) Selb, J.; Gallot, Y. *Makromol. Chem*., **1980**, 181, 2605. (b) Selb, J.; Gallot, Y. *Makromol. Chem*., **1981**, 182, 1491. (c) Selb, J.; Gallot, Y. *Makromol. Chem*., **1981**, 182, 1775.

[98] Hesse, M.; Meier, H.; Zeeh, B. *Spektroskopische Methoden in der Organischen Chemie*, 5th Ed.; **1995**, 95.

[99] Jeffrey, G. A. *An Introduction to Hydrogen Bonding*, Oxford University Press, **1997**, 100, 118.

[100] Polymer Handbook, VII, 519.

[101] Lindman, R.; Olsson, U.; Söderman, O. *Dynamics of solutions and fluid mixtures by NMR*, Delpuech, J.-J., Ed.; John Wiley: New York, **1995**, 345.

[102] Brereton, M. G. *Macromolecules*, **1989**, 22, 3667.

[103] Brereton, M. G. *Macromolecules*, **1990**, 23, 1119.

[104] Lipari, G.; Szabo, A. *J. Am. Chem. Soc.*, **1982**, 104, 4546.

[104] Lipari, G.; Szabo, A. *J. Am. Chem. Soc.*, **1982**, 104, 4559.

[106] Heald, C. R.; Stolnik, S.; Kujawinski, K. S.; De Matteis, C.; Garnett, M. C.; Illum, L.; Davis, S. S.; Purkiss, S. C.; Barlow, R. J.; Gellert, P. R. *Langmuir*, **2002**, 18, 3669.

[107] Liu, Y.; Wang, L.; Pan, C. *Macromolecules*, **1999**, 32, 8301.

[108] Burchard, W. *Statische Lichtstreuung*, Insitute of Macromolecular Chemistry, University of Freiburg.

[109] Price, C. *Pure Appl. Chem.*, **1983**, 55, 1563.

[110] Price, C.; Chan, E. K. M.; Hudd, A. L.; Stubbersfield, R. B. *Polym. Commun*. **1986**, 27, 196.

[111] Canham, P.A.; Lally, T. P.; Price, C.; Stubbersfield, R. B. *J. Chem. Soc. Faraday Trans*., **1980**, 76, 1857.

[112] Quadrifoglio, F.; Urry, D. W. *J. Phys. Chem*., **1967**, 71, 2364.

[112a] Matsui, H.; Douberly, G. E. *Langmuir*, **2001**, 17, 7918.

[113] (a) Ikada, E.; Sugimura, T.; Aoyama, T.; Watanabe, T. *Polymer*, **1975**, 16, 101.
(b) Hol, W. G. J.; van Duijnen, P. T.; Berendsen, H. J. C. *Nature*, **1978**, 273, 443.

[114] Veeraraj, A.; Sami, P.; Raman, N. *Proc. Indian Acad. Sci. (Chem. Sci.),* **2000**, (112), 515.

[115] Mastrorilli, P.; Nobile, C. F.; Suranna, G. P.; Taurino, M. R.; Latronico, M. *Inorganica Chimica Acta*, **2002**, 335 107.

[116] Kodolov, V. I.; Tchirkova, E. I.; Bystrova, S. G.; Shabanova, I. N.; Popova, O. V.; Babushkina, S. N. *Journal of Electron Spectroscopy and Related Phenomena,* **1998**, 88-91, 977.

[117] Corain, B.; Zecca, M.; Mastrorilli, P.; Lora, S.; Palma, G. *Makromol. Chem. Rapid Commun*., **1993**, 14, 799.

[118] Chernyshov, D. M.; Bronstein, L. M.; Börner, H.; Berton, B.; Antonietti, M. *Chem. Mater*. **2000**, 12, 114.

[119] Graham, T. W. *Organic Chemistry*, 5th Ed., John Wiley & Sons, Inc., **1992**.

[120] Hentze, H.-P.; Krämer, E.; Berton, B.; Förster, S.; Antonietti, M. *Macromolecules*, **1999**, 32, 5803.

[121] Mann, S. *J. Chem. Soc. Dalton Trans.,* **1993**, 1.

[122] Mann, S.; Hannington, J. P.; Williams, R. J. P *Nature*, **1986**, 324, 565.

[123] Meyer, M.; Wallberg, C.; Kurihara, K.; Fendler, J. H. *J. Chem. Soc. Chem. Commun*., **1984**, 90.

[124] Roman, J.-P., *et al*. *Colloid Interface Sci.,* **1991**, 144, 324.

[125] Kasparova, P.; *PhD Thesis*, University of Potsdam, **2002.**

[126] Bianconi, P.A.; Lin, J.; Strzelecki, A. R. *Nature* (London), **1991**, 349, 315.

[127] Dalas, E.; *J. Mater. Chem.,* **1991**, 1, 473.

[128] Mann, S. *Biomimetric Materials Chemistry*, VCH **1996**, Cambridge, U.K.

[129] Antonietti, M.; Gröhn, F.; Hartmann, J.; Bronstein, L. *Angew. Chem*., **1997**, 109, 2170.

[130] Cölfen, H. unpublished results.

[131] Schnablegger, H.; Glatter, O. *Appl. Opt.* **1991**, *30*, 4889.

[132] Dicker, I.B.; Cohen, G. M.; Farnham, W. B.; Hertler, W. R.; Laganis, E.D.; Sogah, D.Y. *Macromolecules,* **1990**, 23, 4034.

[133] Beers, K. L.; Gaynor, S. G.; Matjyjaszewski, K.; Sheiko, S. S.; Möller, M. *Macromolecules*, **1998**, 31 (26) 9413.

[134] E. Krämer; *PhD Thesis*, University of Potsdam, **1999**.

[135] Becke, F.; Hagen, H. Ger. 1,274,121,**1968**; *Chem. Abstr.* 70: 3573v.